STUDY OF DRIFT WAVE INSTABILITY IN RF PRODUCED MAGNETIZED PLASMA

by

Abhijit Ghosh

(Enrolment No. : PHYS05201104006)

Saha Institute of Nuclear Physics, Kolkata

A thesis submitted to the
Board of Studies in Physical Sciences

In partial fulfillment of the requirements
for the degree of

DOCTOR OF PHILOSOPHY
of

HOMI BHABHA NATIONAL INSTITUTE

July, 2017

Homi Bhabha National Institute

Recommendations of the Viva Voce Committee

As members of the Viva Voce Committee, we certify that we have read the dissertation prepared by Abhijit Ghosh entitled *"Study of Drift Wave Instability in RF Produced Magnetized Plasma"* and recommend that it may be accepted as fulfilling the thesis requirement for the award of Degree of Doctor of Philosophy.

Chairman - Prof. Nikhil Chakrabarti	N Chakrabarti	**Date:**	20.12.17.
Guide / Convener - Prof. M.S. Janaki	M.S. Janaki	**Date:**	20.12.17
Examiner - Prof. Ashish Ganguli	[illegible]	**Date:**	20.12.2017
Member 1- Prof. Samita Basu	Samita Basu	**Date:**	20/12/17
Member 2- Prof. Munshi Golam Mustafa	Munshi	**Date:**	20/12/17

Final approval and acceptance of this thesis is contingent upon the candidate's submission of the final copies of the thesis to HBNI.

I/We hereby certify that I/we have read this thesis prepared under my/our direction and recommend that it may be accepted as fulfilling the thesis requirement.

Date: 20.12.2017

Place: KOLKATA.

M.S. Janaki

Guide M.S. JANAKI

STATEMENT BY THE AUTHOR

Abhijit Ghosh

DECLARATION

I, hereby declare that the investigation presented in the thesis has been carried out by me. The work is original and has not been submitted earlier as a whole or in part for a degree/diploma at this or any other Institution/University.

Abhijit Ghosh

List of publications arising from the thesis

1. *Plasma density accumulation on a conical surface for diffusion along a diverging magnetic field.*
   S.K. Saha, S. Chowdhury, M.S. Janaki, **A. Ghosh**, A.K. Hui, and S. Raychaudhuri, Phys. Plasmas 21, 043502 (2014).

2. *Observation of upper drift modes in RF produced magnetized plasmas with frequency above ion cyclotron frequency.*
   Abhijit Ghosh, S. K. Saha, S. Chowdhury and M. S. Janaki, Phys. Plasmas 22, 122111 (2015).

3. *Dual upper drift waves in RF produced magnetized helium plasma.*
   Abhijit Ghosh, S. K. Saha, S. Chowdhury and M. S. Janaki, Phys. Plasmas 24, 012104 (2017).

Abhijit Ghosh

Acknowledgements

First of all, I would like to express my sincere gratitude to my supervisors, Sitadi (Prof. M.S. Janaki) and Sujitda (Prof. Sujit K. Saha), for their careful guidance, encouragement and moral support for the last five years. Special mention must be made of Shantanuda (Mr. Shantanu Chowdhury) for his critical comments and suggestions during many discussions and Dipankarda (Mr. Dipankar Das) for his technical help. It has been a great pleasure to work with them at Saha Institute of Nuclear Physics.

I would like to acknowledge Sekarda (Prof. A. N. S. Iyenger), Rabinda (Prof. Rabindranath Pal), Nikhilda (Prof. Nikhil Chakrabarti), Santwanadi (Prof. Santwana Raychaudhuri), and Amitda (Prof. A.K. Hui) for their fruitful comments and discussions.

I would like to take this opportunity to thank the other members of the PPD, Subir da, Chandan da, Sudip da, Debu da, Avik da, Anwesha di, Sourav, Alpha, Satyajit, Pankaj, Debajyoti, Sabuj, Sayanee, Mithun and Subha, for their cooperation and encouragements. One must be very lucky to have such colleagues. I extend my words of appreciation to Partha da, Monobir da, Subhasish da, and many other colleagues in SINP.

This journey would not have been possible without my friends, Anisurda, Bhaijan, Ujjwalda, Lama, Prasanta, Abdul, Goutam, Ashish, Santanu, Raja, Arka, Sabya, Mithun, Debaleen, Kuntal and many others. I would like to specially mention the names of the hostel staffs, Sureshda, Shaktida, Kartikda, Hemantada, Uttamda, Somnathda, and all the boarders, who have joined or left the students' hostel within these years. Thanks to one and all!

Contents

Synopsis

Drift waves in a plasma in the presence of an external magnetic field in the axial direction have been described in the literature to be low frequency waves which are localized in the regions where the plasma density (or temperature) gradient in the radial direction is maximum. The study of such waves find its importance in the magnetically confined inhomogeneous plasmas in devices such as Q-machines, helicon discharges, tokamaks, and other fusion devices due to the role played by the low frequency unstable drift waves in anomalous transport phenomena which causes a loss of plasma density in the radial direction. Drift waves have been studied extensively since it was first discovered in the laboratory plasmas [1] and the important roles played by the factors such as electron-ion, electron-neutral collisions, parallel currents or $\mathbf{E} \times \mathbf{B}$ rotation in the dynamics of such waves have been demonstrated in [2, 3, 4]. Most of these earlier investigations are concerned with the observation of drift waves in the low frequency domain $\omega << \omega_{ci}$ (where ω is the mode frequency and ω_{ci} is the ion cyclotron frequency) since all these experiments have been carried out under high magnetic field (usually $B_z \sim 1$ kG or higher where the low frequency relationship is valid). However, if the magnetic field is low ($\sim$ 100 G), there arises the possibility of having $\omega_{ci} \sim \omega$. Theoretical studies in such cases [5] have predicted an instability of a non-uniform plasma in a uniform external magnetic field at frequencies that are multiples of the ion cyclotron frequency. Ion-cyclotron drift waves (ICDW) ($\omega \geq \omega_{ci}$) were experimentally identified by Hendel and Yamada [6] long ago with discrete and continuous spectra and have been shown to exist in plasmas that are ion-sound stable. An example of such an instability to solar plasma has been discussed [7] in the context of a coupled unstable drift cyclotron mode with the instability driven by the plasma density gradient. The study of the drift waves in presence of the finite density gradient as well as magnetic shear has been carried out by Vranjes and Poedts [8] to obtain global drift and oppositely propagating ion cyclotron waves for a plasma with Gaussian density distribution. However, detailed experimental studies of the drift waves for $\omega \sim \omega_{ci}$ are still lacking in the literature.

The present experiments have been carried out in the Double Layer Experimental (DLX) device [9]. A RF signal of 13.56 MHz has been used to ionize a gas through inductive coupling in the narrower source tube. Two water cooled Helmholtz coils have been placed around this source tube to produce a magnetic field that diverges into a bigger expansion chamber made of stainless steel (SS). All the measurements have been performed in this expansion chamber. S. K. Saha et. al. [9] have reported the existence of a 2-D electric double layer in such a device.

The experimental studies described in this thesis consist of three parts: (a) As a precusrsor to the studies of the instability, a detailed characterization of the time averaged 2-D plasma density and potential profiles have been carried out for plasma diffusing through an aperture in a diverging magnetic field [10]. The radial density profile near the source is peaked on the axis but gradually evolves into a hollow profile away from the source. The plasma potential is peaked on the axis with secondary lobes at the radial locations through which the last magnetic field line (i.e. the last magnetic field line emerging from the edge of the source tube) passes. We observe a slow increase of the peak density along a hollow conical surface and correlate with the 2-D potential measurement reported in [9]. It is also shown that the formation of 2-D structures with similar features are observed whenever

a plasma is allowed to diffuse through a physical aperture in such a diverging magnetic field configuration, with or without the presence of an electric double layer.
(b) In a RF produced magnetized argon plasma expanding into a larger expansion chamber, self-excited electrostatic modes propagating azimuthally in the direction of the electron diamagnetic drift and frequency ($\sim$ 18 kHz) greater than the ion cyclotron frequency ($\sim$ 6 kHz) have been observed [11]. The mode exhibits a weak axial propagation. In the radial direction, the mode amplitude peaks at a location where the radial density gradient is maximum. The modes are detected at axial locations up to 16 cm away from the entrance aperture. For fixed values of the neutral gas pressure and magnetic field, the mode frequency is found to be independent of the location at which it is measured suggesting that it is a global mode. The modes exhibit electrostatic drift wave characteristics revealing a radial structure with the azimuthal mode number $m = 1$ at the lower radial locations ($r \sim 3.0$ cm) while the $m = 2$ mode is located in the outer region. Theoretical modeling using a local dispersion relation based on the fluid equations predicts destabilization of a mode with frequency greater than the ion-cyclotron frequency by electron-neutral collisions and exhibiting other drift wave features. Conventional drift waves reported in the existing literature are low frequency ($\omega << \omega_{ci}$) modes. Since the drift modes observed here have frequencies higher than the conventional drift waves, they have been termed 'upper drift modes' for a clear distinction. Such upper drift modes have been interpreted as high frequency drift modes driven unstable by the collisional mechanism.

For this kind of high frequency drift waves, the ion-cyclotron radius (ρ_i) plays an important role. In this experiment, the wavelength of the drift wave has been found to be greater than ρ_i. These results in argon plasma warrants a further investigation of the characteristics of such modes when the ion Larmor radius is further reduced. The same set of experiments have therefore been repeated in helium plasma for which the ion Larmor radius is smaller than that of argon and therefore $k_{\perp}\rho_i$ is expected to be smaller. Subsequently in helium plasma, two simultaneous modes have been obsereved with frequencies 31 kHz and 52 kHz and mode numbers $m = 1$ and $m = 2$, respectively [12]. They coexist over a wide range of radial and axial locations; propagate azimuthally in the electron diamagnetic drift with a weak axial propagation. A local dispersion relation obtained from the fluid description of the plasma predicts simultanous existence of two modes having mode numbers $m = 1$ and $m = 2$ (with different frequencies) over a range of radial locations.

(c) Two more frequency peaks (viz. 62 kHz with $m = 2$ and 84 kHz with $m = 3$) have been observed in helium plasma over a narrow radial regions ($r \sim 3.2 - 4.5$ cm). The bicoherence analysis for these frequencies suggest that they have been generated via nonlinear interactions of the two primary drift modes (i.e. 31 kHz and 52 kHz) and satisfy the frequency and wave number matching conditions viz. $\omega_3 = \omega_1 + \omega_2$ and $m_3 = m_1 + m_2$. Similar results have been reported in [13, 14] for conventional ($\omega << \omega_{ci}$) drift modes.

These kind of studies assume significance in the experimental situations where the magnetic field is low and have configuration like ours observed in space plasmas.

Bibliography

[1] N. D'Angelo and N. Rynn, Phys. Fluids 4, 275 (1961).

[2] H. W. Hendel, T. K. Chu, and P. A. Politzer, Phys. Fluids 11, 2426 (1968).

[3] R. F. Ellis, E. Marden-Marshall, and R. Majeski, Plasma Phys. 22, 113 (1980); E. Marden-Marshall, R. F. Ellis, and J. E. Walsh, Plasma Phys. Control. Fusion 28, 1461 (1986).

[4] C. Schröder, O. Grulke, T. Klinger, and V. Naulin, Phys. Plasmas 12, 042103 (2005).

[5] A. B. Mikhailovskii and A. V. Timofeev, Sov. Phys. JETP 17, 626 (1963).

[6] H. W. Hendel and M. Yamada, Phys. Rev. Lett. 33, 1076 (1974).

[7] J. Vranjes and S. Poedts, Mon. Not. R. Astron. Soc. 398, 918 (2009).

[8] J. Vranjes and S. Poedts, Phys. Plasmas 11, 891 (2004); J. Vranjes and S. Poedts, Phys. Plasmas, 12, 064501 (2005).

[9] S. K. Saha, S. Raychaudhuri, S. Chowdhury, M. S. Janaki, and A. K. Hui, Phys. Plasmas 19, 092502 (2012).

[10] S.K. Saha, S. Chowdhury, M.S. Janaki, A. Ghosh, A.K. Hui, and S. Raychaudhuri, Phys. Plasmas 21, 043502 (2014).

[11] Abhijit Ghosh, S. K. Saha, S. Chowdhury and M. S. Janaki, Phys. Plasmas 22, 122111 (2015).

[12] Abhijit Ghosh, S. K. Saha, S. Chowdhury and M. S. Janaki, Phys. Plasmas 24, 012104 (2017).

[13] T. Yamada, S. Itoh, T. Maruta, S. Shinohara, N. Kasuya, Y. Nagashima, M. Yagi, K. Terasaka, M. Kawaguchi, S. Inagaki, Y. Kawai, M. Fukao, A. Fujisawa, and K. Itoh, Plasma and Fusion Research: Rapid Communications 2, 051 (2007).

[14] T. Yamada, S. Itoh, T. Maruta, N. Kasuya, S. Shinohara, Y. Nagashima, M. Yagi, K. Terasaka, S. Inagaki, Y. Kawai, M. Fukao, A. Fujisawa, and K. Itoh, Plasma and Fusion Research: Regular Articles 3, 044 (2008).

List of Figures

List of Tables

Chapter 1

Introduction

1.1 Basic Principles of Plasma Waves, Instabilities and Drift Waves

The question of the confinement of the charged particles are given the utmost importance in fusion research. This important question of confinement is generally tackled by applying an external magnetic field. This externally applied magnetic field restricts the random thermal motion of the charged particles in which case they are no longer "free" in their movements. However, a magnetized plasma is seldom in equillibrium condition, i.e. the free energy of the plasma is not minimum in such cases. The plasma can release this free energy through various mechanisms such as a disruption. When it occurs, the plasma acts violently, releasing the whole of the plasma energy. Another process of releasing free energy is called an instability in plasma. In such cases, a wave with growing amplitude can be generated. Obviously, the study of such waves and instabilities and their effects on the stability and confinement of the plasma are of utmost importance to the plasma physics community for the purpose of building fusion devices.

The phenomena of instabilities have been studied theoretically by considering both the aspects: fluid and kinetic theory. When the wavelength (λ) of the resulting wave is sufficiently large compared to the gyroradii (ρ_s where '$s' = e, i$) such that the condition $k\rho_s << 1$ (where $k = 2\pi/\lambda$ is the wavenumber) is satisfied, then the fluid picture is employed and in such cases the instability has been termed as the macroinstability. On the other hand, if we have cases where $k\rho_s >> 1$, then the gyrations of the individual charged particles can no longer be neglected. In such cases, the isotropic fluid model can not be applied. They have to be treated by means of models which take into account the details of the distribution function incorporating the anistropy in velocity space. This second type of instabilities where kinetic theory has to be applied have been termed as microinstabilities. As Lenhert [1] has argued, this distinction between macro- and micro-instabilities is not sharp. There are cases where anisotropy in plasma temperature and finite ion Larmor radius effects have been incorporated in advanced fluid models, giving rise to theoretical models lying in the borderline. Also, depending on the fluctuations of the electric field, both macro- and micro-instabilities can either be an electrostatic wave (where the electric field E is derivable from an electrostatic potential i.e. where $\nabla \times \mathbf{E} = 0$ is satisfied) or an electromagnetic wave where we have $\nabla \times \mathbf{E} \neq 0$.

As noted earlier, a magnetically confined inhomogeneous plasma is usually not in equilibrium. Physically, let us suppose that the external magnetic field

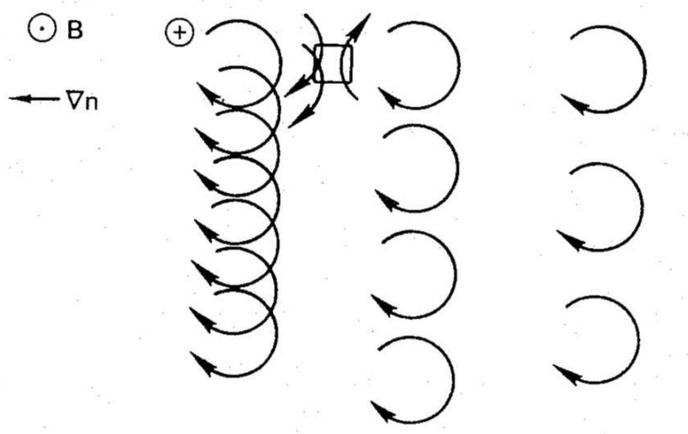

(a)

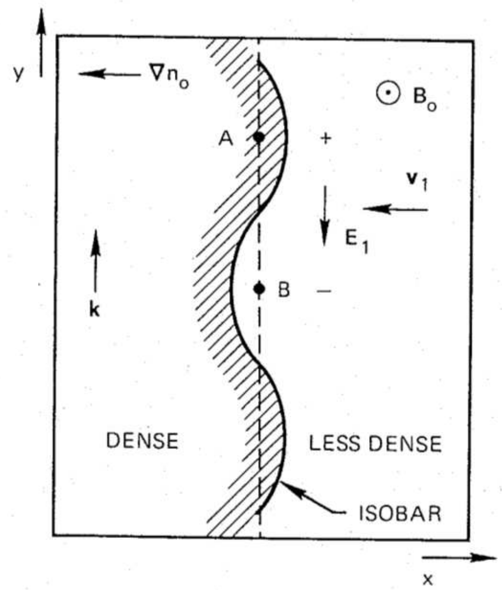

(b)

Figure 1.1: **Origin of the diamagnetic drift (a), and the propagation of the drift wave (b), both in the slab geometry. Both the figures have been reproduced from *Introduction to Plasma Physics and Controlled Fusion* (2nd *ed.)* by F.F. Chen.**

B is in the z direction and the pressure gradient is in the x-direction (along $\mathbf{r}$ in a cylindrical geometry). Since the charged particles rotate around the field lines, due to the inhomogeneities present in pressure between two adjacent layers of the plasma, there will be a net drift of the charged particles in y-direction (along the azimuthal direction in the cylindrical geometry) as has been depicted in Fig. 1.1a. Obviously, the direction of the drifts of the electrons and the ions are in opposite direction. Since the magnetic field generated by this self-developed current opposes the external magnetic field, this drift in the poloidal direction has been termed as the diamagnetic drift. This diamagnetic current is necessary to balance the pressure of the magnetic field. In such a configuration, when the instability appears, it dissipates the diamagnetic currents and reduces the strength of the radial density gradient, which ultimately affects plasma confinements. Clearly, the diamagnetic drifts are universal phenomena because they may develop in a confined plasma without requiring any external driving mechanisms.

1.2 Earlier Works on Low Frequency Drift Waves

Drift waves are instances of an electrostatic macro-instability which occur in the presence of the density or temperature gradients. They have been found to be low frequency waves which propagate predominantly in the poloidal direction with long parallel wavelengths. The amplitude of the fluctuations are maximum in the region where the density (temperature) gradient is strongest, suggesting that they are driven by the density (temperature) gradient. Historically, it was David Bohm [2], who in 1949, found experimentally that for the magnetized plasmas, the cross field transport of the plasma particles exceeded from the value predicted by the classical diffusion theory. Bohm found that the diffusion coefficient for such cases varies as $1/B$ rather than $1/B^2$ as predicted by the classical diffusion theory. He proposed that this anomaly in cross field particle transport was due to an instability whose origin was still unknown to the plasma physics community. Inspired by such an observation, the stability of a collisionless, fully ionized plasma in a strong magnetic field was considered theoretically by Tserkovnikov [3], Rudakov and Sagdeev [4], Moiseev and Sagdeev [5], Silin [6] and others. Using cylindrical coordinates [3, 4] or a local slab model [5, 6] and Vlasov-Maxwell equations with proper boundary conditions, a low frequency (i.e. $\omega << \omega_{ci}$ where ω is the mode frequency and ω_{ci} is the ion-cyclotron frequency) instability has been predicted which exists only in the presence of a density gradient. Experimentally, Garvin et al. [7], Luke and Jamerson [8] and D'Angelo [9] reported low frequency oscillations in fully ionized Cesium thermionic converters. These low frquency oscillations were observed only in the presence of an ion sheath in the plasma. D'Angelo argued that these oscillations originated when the electrons gain a directed kinetic energy while accelerated due to the presence of the ion sheath. Consequently, the oscillations were termed as ion waves as they are absent in the presence of an electron sheath. Garvin et al. [7] highlighted the role of these oscillations in generating alternating current in Cesium cells. In continuation of their studies on these low frquency oscillations, for the first time, D'Angelo and Motley [10] characterized these oscillations in details in similar type of experiments performed with straight magnetic field configuration. Particularly, they highlighted the role played by the existence of the density gradients. By measuring the phase relations at different positions, they found that the density fluctuations are propagating azimuthally in the direction of the electron diamagnetic drift with finite axial component (i.e. the axial wavenumber, $k_{||} \neq 0$). Also, with a local slab model, they successfully explained part of the experimental results. Buchelnikova [11] reported similar kind of experimental results in straight magnetic fields. For fully ionized thermal plasma in Q-machine, Lashinsky [12] reported the effect of the plasma length and the stabilization of drift waves by Landau damping. All the above experimental findings stressed that, for a straight magnetic field, the wave is excited only in the presence of an ion sheath. However, even if the magnetic field lines are curved, D'Angelo et al. [13] reported that the same kind of electrostatic drift waves are excited. In all these cases, the observed frequency has been found to be close to the one predicted by the theory:

$$\omega = -k_{\perp}\frac{k_B T_e}{eBL_n} \tag{1.1}$$

where $k_{\perp}$ is the wavenumber perpendicular to the magnetic field line, k_B is the Boltzmann constant, T_e is the elctron temerature, e is the electronic charge, B is the magnetic field and L_n is the density gradient scale length.

In a series of articles, F.F. Chen [14] has shown theoretically the important roles played by various factors such as sheaths, finite plasma β (i.e. the ratio of the plasma pressure and the magnetic pressure), resistive & viscous damping and finite ion-Larmor radius on this low frequency instability. In these articles, Chen gives a detailed physical mechanism of how this instability occurs. J.D. Jukes [15] has shown that the electrostatic short-wavelength drift waves are a special type of micro-instabilities by employing a phase-integral method incorporating the finite ion-Larmor radius in the model. T.K. Chu and co-workers [16] have considered theoretically the effects of ion-transverse collisional viscosity, electron parallel resistivity, ion-parallel motion and radial electric field on the electrostatic drift waves in a uniformly rotating plasma cylinder. In reviewing the various theories of the stability of a low pressure (small β) plasma, A.A. Galeev et al. [17] have shown that the dissipative effects, in particular the effect of the finite electrical conductivity plays an important role in the stability of the plasma for the case of electrostatic drift instability. Subsequent theoretical and experimental works established [18, 19, 20, 21, 22, 23, 24, 25] the nature and various causes of this instability. Out of these important works, the first non-local analysis in cylindrical geometry has been considered by Chen[19] where numerical computations have been given for the resulting eigenvalue equation in cylindrical geometry when the waves are not localized radially by shear in the drift velocity. Similar non-local effects have been considered by Midzuno [25] for the Gaussian type equilibrium density profiles. A detailed comparison of local and non-local models with experimentally determined density profiles and a varying radial electric field in weakly ionized plasmas has been carried out by R.F. Ellis and co-workers [26, 27, 28].

A.J. Anastassiades and C.L. Xaplanteris [29] have reported drift wave instability in the presence of an RF-field in partially ionized magnetized plasma, where the instability has been destabilized by the additional RF-field drift of the electrons. They explained the experimental data with a theoretical model which predicts a strong dependence of the growth rate for the drift waves on the electron drift velocities due to the radial density and RF-field gradients. More recently, the quiescent nature of helicon plasma has been reported by F.F. Chen [30] and M. Light et al. [31]. Low frequency relaxation oscillations in helicon plasmas have been observed in transition between a low-density, inductive discharge and a high-density, helicon-wave discharge in WOMBAT experiment [32], but the authors have not characterized these oscillations. In a high density helicon discharge producing quiescent plasmas, M. Light and co-workers [31, 33] have explained the decrease in equilibrium density as the magnetic field strength is increased to be caused by a hybrid mode of resistive drift waves and Kelvin-Helmholtz instability. Low frequency resistive drift waves in helicon plasmas has been reported for the first time by G.R. Tynan and co-workers [34]. C. Schroeder and co-workers [35] have reported detailed mode structures of electrostatic resistive drift waves on a poloidal plane in high density cylindrical helicon plasmas. Using a non-local cylindrical model following R.F. Ellis et al. [27] and considering radial profiles for collisional frequencies (which has been ignored so far), they have explained the experimental results to be the resistive drift waves.

Concerning the question of the role of these low frequency drift waves on the overall stability of the plasma, Moiseev and Sagdeev [5] showed that the departure of the perpendicular diffusion coefficient $D_\perp$ for the magnetized plasmas from the classical diffusion theory can be acounted for by the cross field particle transport caused due to this low frequency instability and the corresponding turbulence arising from it. Since then, the role played by this low frequency instability in anomalous diffusion and turbulence phenomena have been highlighted by numerous works [19, 21, 36, 37, 38, 39, 40, 41, 42, 43, 44, 5, 46].

1.3 Drift Like Waves Near Ion Cyclotron Frequency

All the experimental works we discussed above have been done in sufficiently high magnetic field ($\sim kG$) where the plasma β is low. As a result, the wave that has been generated is electrostatic in nature and the low frequency condition $\omega << \omega_{ci}$ is easily satisfied. Hence, the theoretical models that have been developed have either completely neglected the ion-gyration or the finite ion-Larmor radius (ρ_i) effects entered into the model as a small correction parameter. But, even at the higher magnetic fields, in the presence of density inhomogeneity, instabilities near the ion-cyclotron frequency are excited. They are hybrid modes, coupled with the low frequency drift waves. They occur in the velocity space due to the deviation of the distribution function from the equilibrium Maxwellian velocity distribution i.e. these are instances of microinstabilities. These are described only in the kinetic theory where the finite ρ_i effects are important. Two such modes are Ion Cyclotron Drift Waves (ICDW) and Drift Cyclotron Loss Cone (DCLC) instability.

Mikhailovsky and Timofeev [47] have shown theoretically the possibility of the coupling between the cyclotron modes and the drift waves in the magnetized plasma in presence of a strong density gradient when the mode frequency becomes comparable to ω_{ci}. In that case they predicted an instability with frequencies $\omega = n\omega_{ci}$ where n is an integer. The first experimental verification of this mode can be found in the work of Hendel and Yamada [48]. In the Princeton Q-1 thermally ionized potassium plasma, they found a mode with both discrete and continuous spectra in presence of a parallel electron current. By measuring ω and the wavenumber $\mathbf{k}$ experimentally and comparing the resulting dispersion relation with the theory, the mode was identified with the ion cyclotron drift waves predicted by Mikhailovsky and Timofeev. Maekawa et. al. (1977) [49] and Maekawa and Tanaka(1978) [50] reported the excitation of ICDW by cross field current which is the electron drift current resulting from $\mathbf{E}_r \times \mathbf{B}$ velocity. Later experimental observations and theoretical explanations firmly established the role of ICDW in the ion heating and anomalous resistivity [52, 53, 54, 55, 56, 51]. As noted earlier, unlike the low frequency drift waves, ICDWs are microinstabilities.

A different type of electrostatic micro-instability in the same frequency range of $\omega \sim \omega_{ci}$ in the mirror type magnetic field configurations has been predicted in the early '60s by Mikhailovsky [57], Rosenbluth and Post [58] and Post and Rosenbluth [59]. Post and Rosenbluth [59] predicted the possibility of having three types of instabilities in mirror-confined plasmas termed as DCLC: One is of convective type which are characterized by small but finite parallel wavelength (i.e. $k_\perp >> k_\parallel$ but $k_\parallel \neq 0$), destabilization mechanism of this does not depend on the existence of a finite radial density gradient. Also, it occurs at high frequencies i.e. $\omega >> \omega_{ci}$. This type of instability requires the plasma to be larger than a critical length (L_0). The value of L_0 is generally very large for mirror confined plasmas even at higher densities. Hence, this convective type of instabilities are generally not observed in laboratory plasmas. Another kind of instability in the same frequency range is predicted which is similar to the above one i.e. not depending on the radial density gradients but for this case we have $k_\parallel = 0$. A third non-convective (i.e. $k_\parallel = 0$) type instability is also predicted which requires the existence of a finite radial density gradient and the plasma to be larger than a critical radius. This third category of the instabilities fall in the frequency regime of our interest i.e. $\omega \sim \omega_{ci}$. The critical condition predicted for this instabilitiy to occur is easily met in the laboratory plasmas. In the years that followed, both theoretical and experimental works [60, 61, 62, 63, 64, 65, 66] established the DCLC as one of the most dangerous type of instability in confined plasmas in mirror-devices.

1.4 Motivation of the Present Study

As has been noted in the above discussions, low frequency drift waves or its coupled type (i.e. ICDW or DCLC) play an important role in the stability of the magnetically confined inhomogeneous plasma. Of particular interest is its role in ion heating, anomalous resistivity and anomalous cross field transport. Since the magnetic field used in all those experiments has always been relatively higher (i.e. $\sim$ kG), the condition $\omega << \omega_{ci}$ has always been satisfied for drift waves. If we decrease the magnetic field, apparently, equation (1.1) suggests that the mode frequency should increase. If we change the magnetic field, the complete equilibrium profiles of the plasma density and temperature also get modified. Hence, the density gradient scale length L_n also changes with the magnetic field. For this reason, any definite parametric scaling of the mode frequency with the magnetic field is difficult to predict. We have seen that the drift waves have usually been found to be in the range of few kHz. So, if we lower ω_{ci} by decreasing the magnetic field, we could then arrive at the possibility of having drift waves at $\omega \sim \omega_{ci}$. In a recent publication by A.M. DuBois et al. [67], with experiments conducted in the Auburn Linear EXperiment for Instability Studies (ALEXIS), the authors reported the excitation of drift waves in a range of available magnetic fields from lower limit ($\sim 300G$) to higher ($\sim 900G$) limits. At the lower magnetic fields where the high frequency limit $\omega \sim \omega_{ci}$ is satisfied, the amplitudes of the drift waves have been found to be very small, suggesting that the possibility of excitation of drift waves at $\omega \sim \omega_{ci}$ in their experiment is very low. In fact, they found the amplitudes of the drift waves to be strongest only at the higher magnetic fields where the low frequency limit is satisfied. Consequently, the authors have used the quadratic dispersion relation suitable for the low frequency drift waves.

This thesis contains experimental study of self-excited drift waves observed in a RF-produced magnetized argon plasma in the high frequency regime i.e. drift waves in the range $\omega \gtrsim \omega_{ci}$. Theoretical analysis predicts the destabilization of such modes due to the electron-neutral collisions. Contrary to the other high frequency coupled kinetic modes (such as ICDW or DCLC) where the condition $k_{\perp}^2 \rho_i^2 >> 1$ (i.e. the ion-Larmor radius is much larger than the perpendicular or the azimuthal wavelength) is satisfied, this is resistive drift mode where the azimuthal wavelength is larger than the ion-Larmor radius i.e. we have for this case: $k_{\perp}^2 \rho_i^2 < 1$. Since the drift modes observed here have frequencies greater than the conventional (i.e. $\omega << \omega_{ci}$) drift waves, they have been termed as "upper drift modes" for a clear distinction. These results in argon plasma warrant a further investigation of the characteristics of such modes when the ion-Larmor radius is further reduced. Hence, the same set of experiments with suitable parameters have been repeated in helium plasma.

1.5 Organization of the Thesis

The thesis has been organized as follows. A brief review of earlier works on the waves with frequencies $\omega \sim \omega_{ci}$ has been presented in the introductory chapter. The experimental device and the diagnostic tools used have been described in detail in Chapter 2. Chapter 3 contains the detail study of the steady state profiles of the basic plasma parameters such as density, temperature and plasma potential with experiments performed in argon plasma. It also contains identification of the frequency peak observed in the density or in floating potential fluctuations. In Chapter 4, we present experimental and theoretical study of the fluactuations with experiments performed in helium plasma. We summarise our works contained in this thesis in Chapter 5. In this concluding chapter, the scope of possible future works that can be done in DLX have also been pointed out.

Bibliography

[1] B. Lenhert, Plasma Phys. 9, 301(1967).

[2] D. Bohm, E. H. S. Burhop, H. S. W. Masseyand R. W. Williams, in The Characteristics of Electrical Discharges in Magnetic Fields (A. Guthrie and R. K. Wakerling, eds.), p. 173, McGraw-Hill, New York, 1949.

[3] I.A. Tserkovnikov, Soviet Phys. JETP 5, 58 (1957).

[4] L.I. Rudakov and R.Z. Sagdeev, Soviet Phys. JETP 37, 952 (1960).

[5] S.S. Moiseev and R.Z. Sagdeev, Soviet Phys. JETP 44, 763 (1962).

[6] V.P. Silin, Soviet Phys. JETP 17, 857 (1963).

[7] H. L. Garvin, W. B. Teutsch, and R. W. Pidd, J. Appl. Physics 31, 1508 (1960).

[8] K. P. Luke and F. E. Jamerson, J. Appl. Physics 32, 321 (1961).

[9] N. D'Angelo, Phys. Fluids 4, 1054 (1961).

[10] D'Angelo and Motley, Phys. Fluids 6, 422 (1963).

[11] N.S. Buchelnikova, Soviet Phys. JETP 19, 175 (1964); Nucl. Fusion 4, 165 (1964).

[12] H. Lashinsky, Phys. Rev. Lett. 12, 121 (1964); 13, 47 (1964).

[13] N. D'Angelo, D. Eckhartt, G. Grieger, E. Guilino, and M. Hashmi, Phys. Rev. Letters 11, 525 (1963).

[14] F.F. Chen, Phys. Fluids 7, 949 (1964); 8, 752 (1964); 8, 912 (1965); 8, 1323 (1965).

[15] J. D. Jukes, Phys. Fluids 7, 1468 (1964).

[16] T.K. Chu, B. Coppi, H.W. Hendel, and F.W. Perkins, Phys. Fluids 12, 203 (1969).

[17] A.A. Galeev, S.S. Moiseev, and R.Z. Sagdeev, Plasma Physics (J. Nucl. Energy, Part C) 6, 645 (1964).

[18] N. D'Angelo and S. von Goeler, Nucl. Fusion 6, 135 (1966).

[19] F. F. Chen, Phys. Fluids 10, 1647 (1967).

[20] L. Enriques, A.M. Levine, and G.B. Righetti, Plasma Physics 10, 641 (1968).

[21] H.W. Hendel, T.K. Chu, and P.A. Politzer, Phys. Fluids 11, 2426 (1968).

[22] A.A. Rukhadze and V.P. Silin, Sov. Phys. Usp. 11, 659 (1969).

[23] H.W. Hendel and T.K. Chu, 1971, *9. Collisional Drift Instabilities*, Plasma Physics, 345-394. (https://doi.org/10.1016/S0076-695X(08)60846-7).

[24] R.F. Ellis and R.W. Motley, Phys. Rev. Letters 27, 1496 (1971).

[25] Y. Midzuno, J. Phys. Soc. Japan 33, 502 (1972).

[26] R.F. Ellis and E. Marden-Marshall, Phys. Fluids 22, 2137 (1979).

[27] R. F. Ellis, E. Marden-Marshall, and R. Majeski, Plasma Phys. 22, 113 (1980).

[28] E. Marden-Marshall, R. F. Ellis, and J. E. Walsh, Plasma Phys. **28**, 1461 (1986).

[29] A.J. Anastassiades and C.L. Xaplanteris, J. Phys. Soc. Japan 52, 492 (1983).

[30] F. F. Chen, in *High Density Plasma Sources*, edited by O. A. Popov (Noyes, New Jersey, 1995) (https://doi.org/10.1016/B978-081551377-3.50003-7).

[31] M. Light, F. F. Chen, and P. L. Colestock, Phys. Plasmas 8, 4675 (2001).

[32] A. W. Degeling, T. E. Sheridan, and R. W. Boswell, Phys. Plasmas 6, 1641 (1999); 6, 3664 (1999).

[33] M. Light, F. F. Chen, and P. L. Colestock, Plasma Sources Sci. Technology 11, 273 (2002).

[34] G. R. Tynan et al., Bull. Am. Phys. Society 46, BM1.13 & LP1.134 (2001).

[35] C. Schroeder, O. Grulke, and E. Scime, Phys. Plasmas 11, 04249 (2004); Phys. Plasmas 12, 042103 (2005).

[36] F. C. Hoh, Revs. Modern Phys. 34, 267 (1962).

[37] F. Boeschten, Plasma Physics 6, 339 (1964).

[38] B.J. Eastlund, Phys. Fluids 9, 594 (1966).

[39] B. J. Eastlund, K. Josephy, R. F. Leheny, and T. C. Marshall, Phys. Fluids 9, 2400 (1966).

[40] A.A. Ivanov, Ya. R. Rakhimbabaev, and V.D. Rusanov, Soviet Phys. JETP 25, 545 (1967).

[41] T. K. Chu, H. W. Hendel, and P.A. Politzer, Phys. Rev. Letters 19, 1110 (1967).

[42] H.L. Pecseli, Physica Scripta T2/1, 147 (1982).

[43] A Latten et al., Review of Scientific Instruments 66, 3254 (1995).

[44] T. Klinger, A. Latten, A. Piel, G. Bonhomme, T. Pierre, and T. Dudok de Wit, Phys. Rev. Letters 79, 3913 (1997).

[45] W. Horton, Rev. Mod. Physics, Vol. 71, No. 3, April 1999.

[46] T. Windisch, O. Grulke, and T. Klinger, Phys. Plasmas 13, 122303 (2006).

[47] A.B. Mikhailovsky and A.V. Timofeev, Soviet Phys. JETP 17, 626 (1963); A.B. Mikhailovsky, Nucl. Fusion 5, 125 (1965).

[48] H.W. Hendel and M. Yamada, Phys. Rev. Letters 33, 1076 (1974).

[49] T. Maekawa, M. Sando, and S. Tanaka, Phys. Letters 60A, 199 (1977).

[50] T. Maekawa and S. Tanaka, J. Phys. Soc. Japan 44, 1354 (1978).

[51] M. Yamada, H.W. Hendel, S. Seiler, and S. Ichimaru, Phy. Rev. Letters 34, 650 (1975).

[52] P. Massmann, P.H. De Haan, A.P.H. Goede, and H.J. Hopman, Plasma Physics 20, 633 (1978).

[53] M. Yamada and H.W. Hendel, Phys. Fluids 21, 1555 (1978).

[54] K. Matsunaga, Physics Letters 76A, 245 (1980).

[55] R. Hatakeyama, M. Oertl, E. Mrk, and R. Schrittwieser, Phys. Fluids 23, 1774 (1980).

[56] R.W. Boswell, Adv. Space Res. 1, 331 (1981).

[57] A.B. Mikhailovsky, Nucl. Fusion 5, 125 (1965).

[58] M.N. Rosenbluth, and R.F. Post, Phys. Fluids 8, 547 (1965).

[59] R.F. Post and M.N. Rosenbluth, Phys. Fluids 9, 730 (1966).

[60] J.G. Cordey, L.G. Kuo-Petravic, and M. Petravic, Nucl. Fusion 8, 153 (1968).

[61] I.G. Brown, M.A. Rothman, and R.M. Sinclair, Phys. of Fluids 12, 1318 (1969).

[62] A.V. Timofeev, Atomnaya Energiya 30, 270 (1971).

[63] S. Kishimoto, H. Akimune, and T. Suita, J. Phys. Soc. Japan 32, 796 (1972).

[64] T.C. Simonen, Phys. Fluids 19, 1365 (1976).

[65] H. Akiyama and S. Takeda, J. Phys. Soc. Japan 43, 1739 (1977).

[66] W.J. Turner, E.J. Powers, and T.C. Simonen, Phys. Rev. Letters 39, 1087 (1977).

[67] A. M. DuBois, A.C. Eadon, and E. Thomas Jr., Phys. Plasmas 19, 072102 (2012).

Chapter 2

The Experimental Device and Diagnostics

2.1 Experimental Device

An electric double layer is a region within the plasma where a local electric field exists due to the creation of two oppositely charged layers. It has been found that a DL is generated when there is an abrupt change in the diameter of the chamber containing a magnetized plasma [1, 2, 3, 4, 5]. In such cases, a DL is created at the junction between the two chambers or where the divergence of the magnetic field is maximum, and a low energy ion beam is generally observed in the downstream region because of the accelaration of the plasma ions by the strong electric field existing near the junction. The study of DLs in such systems draws a lot of attention due to its potential applicability in producing mechanical thrust by the ion beam for the space propulson devices. To study the physics of such phenomena associated with DLs, a device has been developed at SINP by S.K. Saha et al. [6] which will be called as Double Layer eXperiment (DLX) device. Apart from the study of DLs, a detailed investigation has been done on the waves and instabilities in the RF magnetized plasma in this device and this study is the subject of the present thesis.

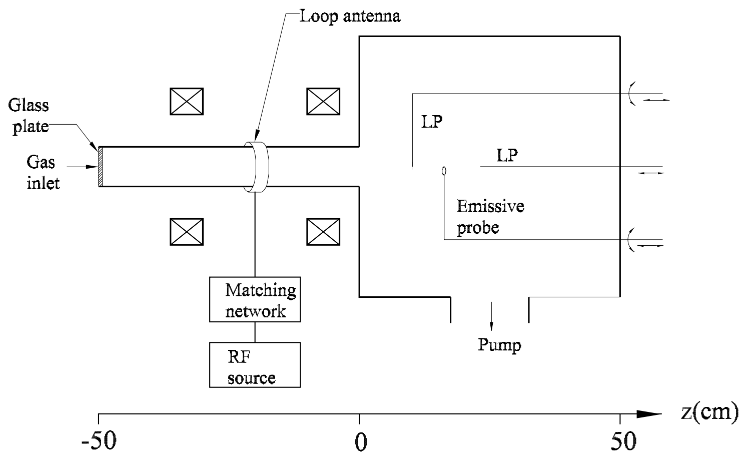

Figure 2.1: **The Schematic diagram of the experimental set up DLX.**

A schematic of the set up has been shown in Fig. 2.1. This device consists of a quartz tube whose diameter is 7.5 cm and length 50 cm and one end of this tube is connected co-axially to a bigger chamber made of stainless steel (SS). The diameter and length of this bigger chamber are both 50 cm. Neutral gas is fed into the quartz tube through the other end. This end has been terminated by a glass plate to make the plasma current free. Since plasma is produced in this quartz tube, it has been termed as the source tube. A single turn loop antenna made out of 2.5 cm wide and 0.3 cm thick copper strip, has been placed around this source tube. An air cooled Radio Frequency (RF) generator operating at 13.56 MHz has been connected to the loop antenna through a $\pi-$type matching network (Fig. 2.2). The power of the RF source can be varied over a range of $0-1250$ W. A copper mesh surrounds the quartz tube. It acts as a Faraday shield i.e. it prevents the strong RF field from leaking into the environment and affecting other measuring instruments. The plasma is produced by the inductive discharge of the gas by the RF field. Two water cooled solenoidal coils have been placed coaxially around the source tube. A current source (EPS Power Source $0-360$ V, $0-15$ A, $0-1500$ W) supplies a direct current (in the range $0-10$ A) through the solenoid coils. The typical axial variation of the magnetid field has been shown in Fig. 2.3a when a current of 8 A passes through the coils. As can be seen

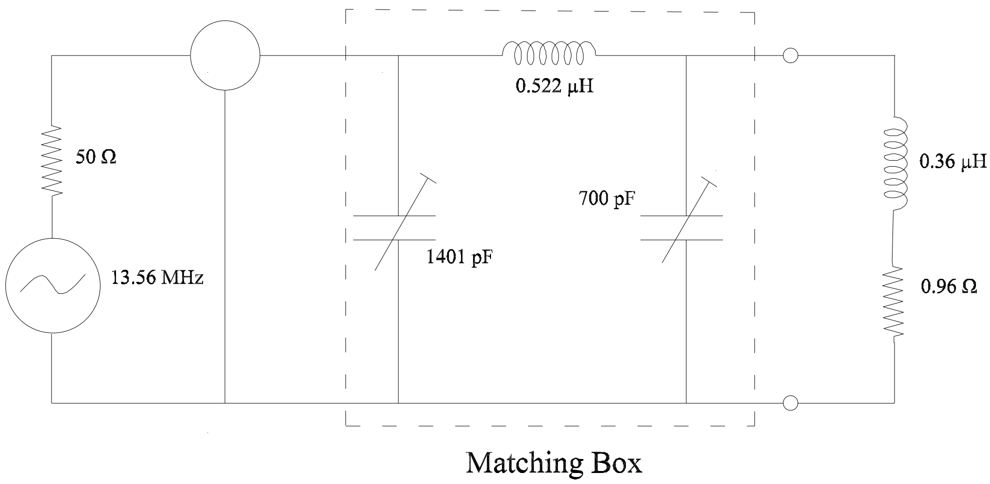

Figure 2.2: **The circuit diagram of the π-type matching network.**

from Fig. 2.3a, the magnetic field has two maxima at the positions of the

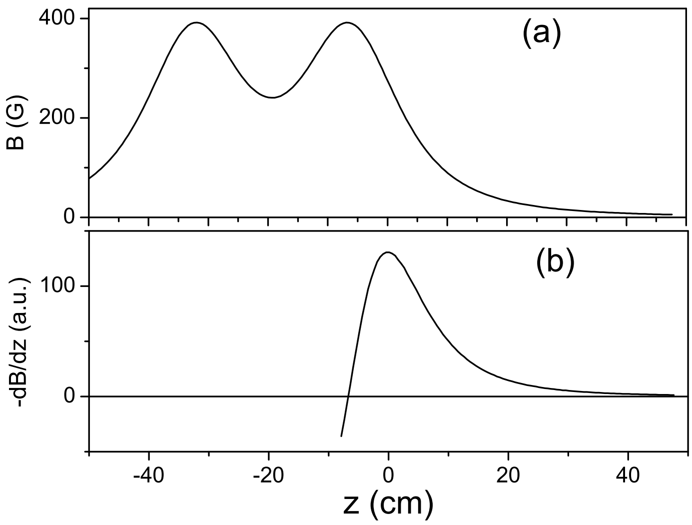

Figure 2.3: **(a) Axial variation of the magnetic field. This profile has been generated when a constant current of 8 A passes through the Helmholtz coils, and (b) the axial variation of the spatial gradient -dBz/dz in the plasma expansion region.**

two coils and decreases monotonically into the expansion chamber. As a result, plasma produced in the source tube also expands into the SS chamber (henceforth, expansion chamber) following the divergent magnetic field lines. The variation of the axial gradient of the magnetic field has been shown in Fig. 2.3b. Clearly, the spatial gradient (i.e. dB_z/dz) is maximum at $z = 0$ cm.

A rotary pump (pumping speed of which is 200 l/min) in combination with a turbomolecular pump (pumping speed of which is 520 l/s) have been connected to the expansion chamber through a pneumatic valve. The expansion chamber can be pumped down to a base pressure of $\sim 1.5 \times 10^{-6}$ Torr by this pump systems. The pressure in this region is monitored by a wide range

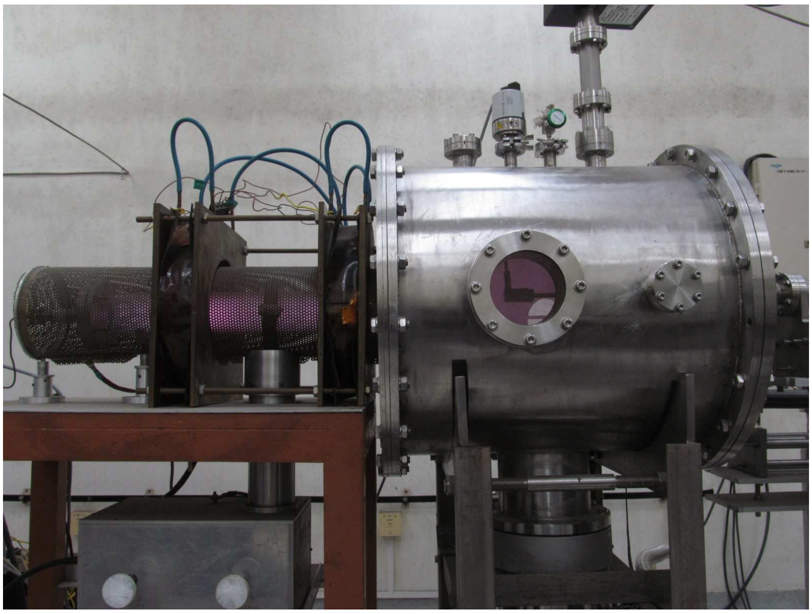

Figure 2.4: **Phtograph of the source tube and the expansion chamber containing helium plasma produced inside the source tube under the condition:** $p = 0.4$ **mTorr, RF power** $200W$ **and magnetic field as has been shown in Fig. 2.3a.**

inverted magnetron gauge. One port each on the both sides of the cylindrical body of the grounded SS chamber act as viewing windows through which we can peek at the plasma body and the movements of several probes inside the expansion chamber. Figure 4 shows a photograph of the device with helium plasma produced inside the source tube.

Also, there are five ports at the end flange of the SS chamber to facilitate the mounting of various types of Langmuir probes (LP), an emissive probe and a retarding field energy analyzer (RFEA). The working principles of these three diagnostics and their constructions have been discussed below.

2.2 Diagnostics

2.2.1 The Compensated LP

The Langmuir probe characteristics is obtained when the current (I) collected by the LP is plotted against the potential difference between the probe tip and the plasma across the plasma sheath created around the probe tip. In a RF environment, due to the fluctuations in plasma potential, this potential difference between the probe tip and the plasma also fluctuates since the voltage of the probe tip is fixed externally [8]. Hence, the current measured by the LP is an average for a range of sheath voltages, and due to the nonlinear behaviour of the sheath, the $I - V$ curve becomes distorted. As a result, the density and electron temperature that are determined from such probe characterisrtics are erroneous.

One way to minimize the effects of the RF fluctuations in LP measurements is to make the voltage of the probe tip to follow the fluctuating potential of the plasma such that the voltage difference between the tip and the plasma across the sheath remains constant all the time. The method developed by A.E. Wendt [8] is based on this principle. The same method has been used here. A passive external RF filter has been used to force the probe tip to follow the plasma potential fluctuations. Physically, if we consider the fluctuating potential of the plasma as an alternating volatage source ($\tilde{V_p}$), then the sheath surrounding the probe and the filter circuit act as a voltage divider responding to $\tilde{V_p}$. So, if the impedance offered by the RF filter circuit

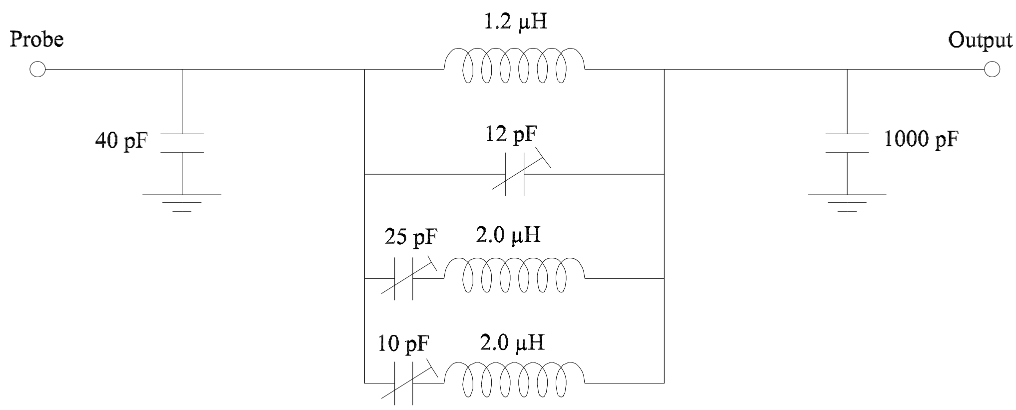

Figure 2.5: **The diagram of the the RF compensation circuit consisting of the parallel LC combinations.**

Frequency at which resonance occurs (MHz)	$\lvert z\rvert(k\Omega)$	Q
13.56	9.38	56.5
27.12	1.33	51.3
40.68	1.28	58.3

Table 2.1: **Performance of the filter circuit.**

is $Z(\omega)$, then we have:

$$\tilde{V}_{probe} = \frac{\tilde{V}_p Z(\omega)}{Z(\omega) + Z_{sh}}$$

where $\tilde{V}_{probe}$ and Z_{sh} are potential of the probe and the impedance of the sheath, respectively. Clearly, for the correct determination of the probe characterictics, the filter circuit should provide high impedances (i.e. high $Z(\omega)$) from the probe tip to the ground at the RF frequency of 13.56 MHz and its second and third harmonics.

The compensation circuit based on Wendt's method described above, has been shown in Fig. 2.5. Parallel lumped-component (LC) combinations have been used, giving high impedances and high-Q resonances at 13.56 MHz and its harmonics, details of which have been shown in Table-2.1. This compensated LP consists of a 3 mm diameter molybdenum rod, whose entire cylindrical surface is covered by a thin snugly fitting glass tubing. The end face, which is kept uncovered, acts as a circular disc probe. The normal direction to the disc surface is kept perpendicular to the magnetic field so that it collects only the plasma ions and not the beam ions, while measuring the ion saturation current.

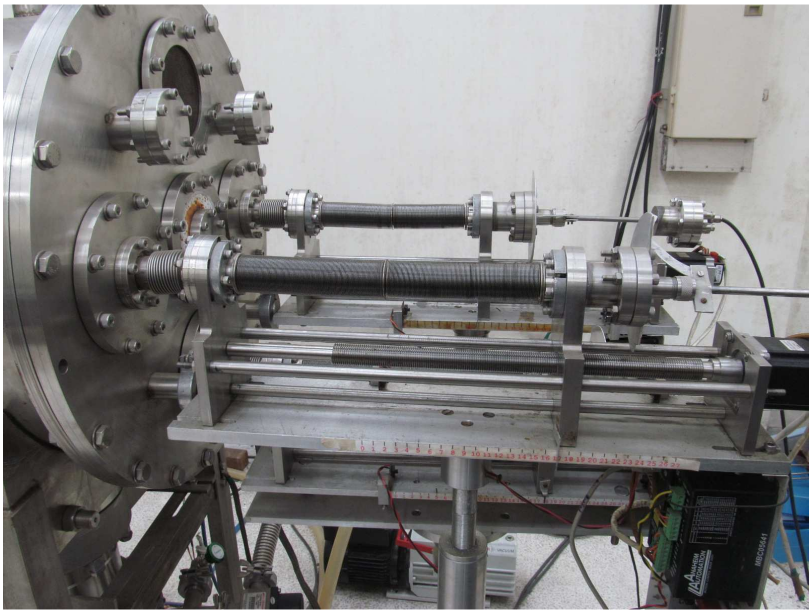

Figure 2.6: **Photograph of the vacuum bellow and the guide-rail system.**

This diagnostic is mounted in L-shaped configuration to enable two-dimensional scans of the plasma parameters, the radial scan being done by rotating the shafts. The axial movements are done by vacuum bellows and precision guide-rail systems (Fig. 2.6). The carriages are moved by lead screw arrangements driven by stepper motors, which can be controlled from a computer for precise movements. The 2-D equilibrium plasma density and temperature profiles obtained from this compensated probe has been reported in Refs. [6, 7] and have been discussed in Chapter 3.

2.2.2 The Uncompensated LP

The compensated LP (which has a large capacitance to the plasma) is, however, not suitable for measuring the density or potential fluctuations arising due to instabilities. Also, to measure the velocity or the direction of propagation of the wave, it is essential to record the the fluctuations at two different locations simultaneously. To measure the propagations of the waves in the radial, axial or poloidal directions, various set of uncompensated LPs have been designed. All the uncompensated LPs are made of 0.7 mm diameter tungsten wires with the exposed tip protruding 3.0 mm from a ceramic tube covering the rest of the wire.

Firstly, to measure the propagations of the waves in the azimuthal direction, three L-shaped Langmuir probes with different shaft lengths have been mounted on a single and axially movable arrangement (Fig. 2.7). It has been observed that the amplitude of the fluctuations is maximum around $r \sim 3.0$ cm (see Figures 3.11 and 4.5). Hence, one probe has been placed at $r = 3.0$ cm. Since the RF fluctuations are stronger in the the region $r < 3.0$ cm and the azimuthal propagation of a mode is expected to exist at radial locations away from the axis, the shaft lengths of the two other LPs have been chosen to be 5.9 and 7.1 cm, respectively. The LPs are at right angle to the axis and they make an azimuthal angle of about 20^0 with each other such that no LP is shadowed by the others. These probes are axially movable and can be rotated along the azimuthal direction at the above mentioned radii. Both the axial and azimuthal movements are performed manually. This three-LP system has been inserted through the central port in the end flange.

Figure 2.7: **Photograph of the three LPs at different radii.**

One L-shaped LP is inserted through one of the off-axis ports in the end flange. The radial distance of the LP from the shaft is 16.5 cm, and the LP can be placed at any desired radial location by rotating the shaft manually. Unlike the previous case, its axial movements are performed by a motor-controlled axially movable arrangement in an L-type configuration similar to the movements of the compensated probe. To measure the azimuthal propagation, the density or potential fluctuations have been recorded simultaneously using this single LP as the reference probe and any of the above mentioned three-probes as the azimuthally moving probe.

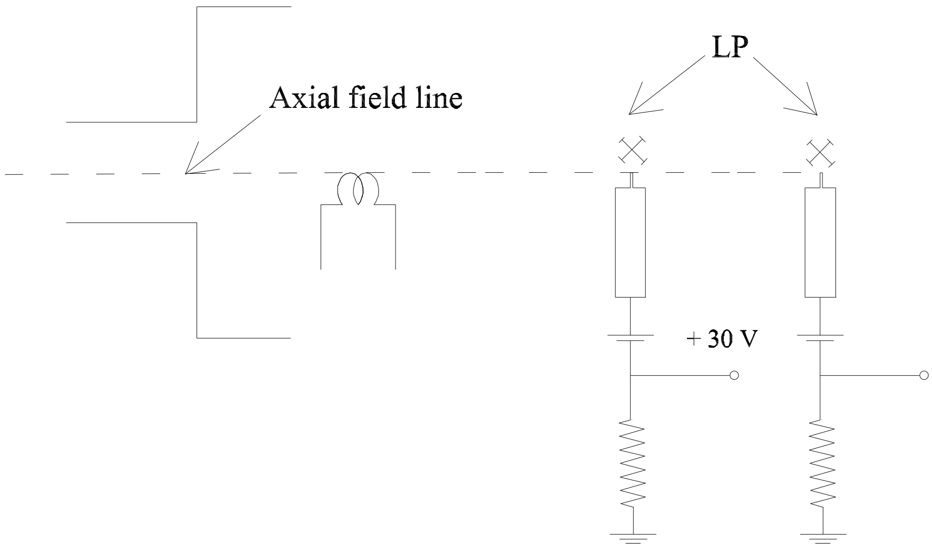

Figure 2.8: **Schematic of the procedure that has been followed to align the two un-compensated Langmuir probes electrically so that both the LPs lie approximately on the axial magnetic field line. The heated EP has been biased at $+40$ V and both the LPs have been biased at -30 V.**

Secondly, to measure the axial propagation of the wave, another single LP (similar both in construction and movements to the above case) has been inserted through a second off-axis port available at the right end of the expansion chamber. In this case, it is important that the the two LPs which are being used simultaneously, are on the axis i.e. are on the same straight magnetic field line emanating from theaxis of the source. For the drift waves, we have $k_z << k_\theta$ where k_z the axial or parallel wave number and k_θ is the azimuthal or perpendicular wavenumber (see Sections 3.3.2 and 4.3.2). Hence, a slight misalignment of the probes on the field line causes a small azimuthal separation and the consequent phase difference can mask the small phase difference due to the axial separation. For this reason, it is crucial that the two uncompensated LPs are aligned electrically so that they lie exactly on the same axial magnetic field line. The two LPs are first brought to the axis approximately but at different axial distances. To align them electrically, first the vacuum chamber has been evacuated to the base pressure and then the hot emissive probe (EP, details of which are discussed below), the tip of which has been placed on the axis, has been biased at -30 V so that the emitted electrons are repelled from it. The two LPs has been biased at $+40$ V each so that they can collect electrons. By moving the LPs slightly in the transverse direction, the electron currents drawn by the LPs are maximised, which happens only when both of them are on the axis, i.e the LPs lie along the same straight magnetic field line with the EP. This procedure has been shown schematically in Fig. 2.8. Once the two LPs have been aligned electrically, their azimuthal positions have not been disturbed any further, they are moved only axially by the motor arrangement.

This same arrangement has been used to measure any radial propagation. For this, one LP has been kept fixed on the axis while the second was moved at various radial locations. By measuring the potential fluctuations simultaneously, the informations about the radial propagation has been obtained.

2.2.3 The Four-LP System

It has been shown that there exists a phase difference between the density and potential fluctuations for resistive drift waves (see equation 3.15). This phase difference is caused by the the elctron-neutral collisions for our case. To measure this phase difference, a four-LP system (Fig. 2.9) has been developed. These four LPs have been arranged in a diamond configuration. Two LPs along a diagonal (aligned along $\mathbf{B}_z$) are used as the floating double probe and are biased into the ion-saturation region by a floating power supply. This double-LP is used to record the density fluctuations. The potential drop across a resistor (measuring the Isat fluctuations $\tilde{n}$) is optically isolated and taken as the density fluctuation signal.

Figure 2.9: **Photograph of the four-LP system.**

The other two probes along the diagonal (aligned perpendicular to B_z) have been used to measure the floating potential fluctuations, $\tilde{\phi}_{f1}$ and $\tilde{\phi}_{f2}$.

These two $\tilde{\phi}_f$s have been averaged over to get a single $\tilde{\phi}_f(t)$. This arrangement has been done to ensure that the fluctuations in the density and the floating potential are measured at virtually the same location in the plasma.

2.2.4 Emissive Probe

Unlike a Langmuir probe, the working principle of which is based on the collection of charged particles, the emissive probe (EP), as the name suggests, is a filament which emits an electron current into the plasma when the probe voltage V_{pr} is lower than or equal to the space or plasma potential (V_p), i.e. when we have $V_{pr} \leq V_p$. For the case of $V_{pr} > V_p$, the emission current decreases exponentially, and the probe current starts to be dominated by the electron collection. Now, the temperature of these emitted electrons is generally much smaller than the plasma electrons, and hence the exponetial drop is very sharp for the case of $V_{pr} > V_p$. Clearly, the potebtial at this inflection point on the $I-V$ curve can be considered as the plasma potential. Physically, if voltage in the filament is gradually increased from the lower to the higher values, the emission first increases, then it comes to a saturated value which is the electron saturation current. At this point the floating potential of the EP is taken as equal to the plasma potential. The emission at this point is termed as the strong emission. The EP is known to give a robust measurement of the plasma potential.

The present arrangement consists of two independent half-turn loops (one used at a time) of 100 μm diameter tungsten wires placed on a four-hole ceramic tube 6 mm in diameter (Fig. 2.10a). For making electrical contacts to the filaments, four PTFE-insulated multistrand copper wires are taken and about 5 cm of the insulator is peeled off. More strands are added to the exposed strands, which are then tightly pushed from the rear end into the holes in the ceramic tube, thus completely filling up the space inside the holes. The protruding parts of the strands are cut-off from the front end. A 100 μm diameter tungsten wire, about 2.5 cm long, is taken and its two ends are carefully pushed into the copper strands in two adjacent ceramic holes, leaving open a half-turn loop (about 4 mm diameter) of the tungsten wire. This arrangement gives a good electrical contact between the tungsten and the copper wires without using any connector or spot-welding. The other filament is mounted in the same way into the other two ceramic holes. The ceramic tube is then mounted on the motor movement arrangement in a L-type configuration (Fig. 2.6).

The emissive probe has been heated by an electrically isolated 30 V, 3 A, 0.1% regulated power supply. The condition of strong emission has been achieved with a typical heating current of ~ 2 A. The floating potential of the electrical mid-point of the two ends of the filament (obtained by a potential divider consisting of two equal resistors, Fig. 2.10b) has been measured by an attenuator probe having an impedance of 10 MΩ. This floating potential has been taken as the time-averaged plasma potential. E.Y. Wang and co-workers [8] have pointed out that the accuracy of this method is dependent

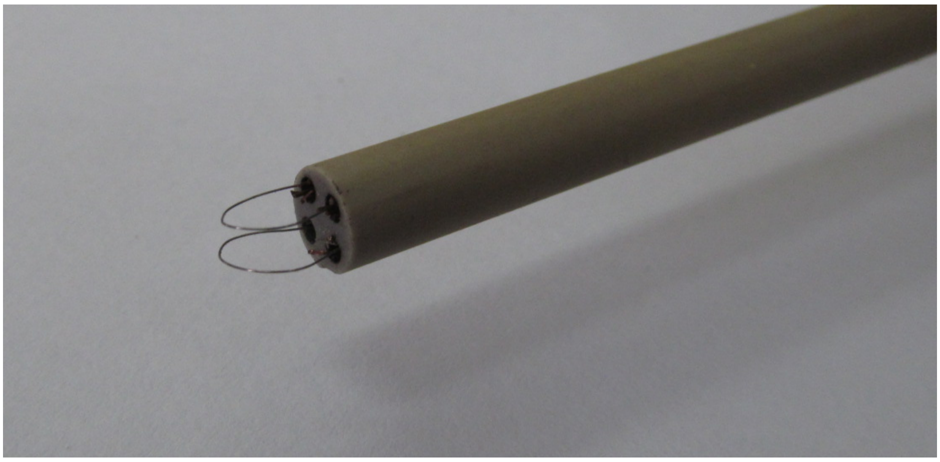

(a)

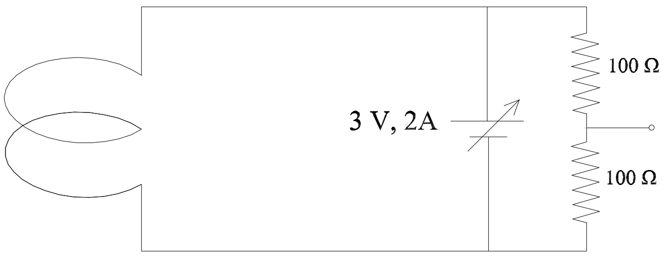

(b)

Figure 2.10: **(a) Phtotogragh of the two filaments, and (b) The schematic of the heating arrangement of the EP.**

on the fluctuatons in V_p in a RF plasma environment. They employed the swept emissive probe or the inflection point method of differential emitting probes for such cases. A comparison of the values of V_p obtained from the floating point method of the singly-emitting probe (employed here) and the inflection point method of the differential emitting probes will be discussed in Sec. 3.2.2.

2.2.5 Retarding Field Energy Analyzer (RFEA)

The RFEA (Fig. 2.11) has been used to measure the ion energy distribution function of the plasma and is of the conventional design having four grids [10]. It consists of a thin-walled hollow cylindrical alumina ceramic cup, having a 5 mm diameter entrance aperture at the front end and a stack of several grids and insulator rings. The first grid G_1 consists of a stainless steel (SS) mesh (250 wires per in., hole size 76 μm, and 57% transparency), which is kept floating to minimize perturbation to the plasma. The first grid is in contact with a 0.25 mm thick SS ring having a 6 mm diameter hole, providing mechanical support to the thin mesh. This is followed by a 0.5 mm thick insulating spacer ring having a 7 mm diameter hole. The next three grids $G_2 - G_4$ are mounted by repeating the sequence of SS mesh, SS ring, and spacer ring three times. The collector is a 0.25 mm thick SS disc. The entire stack is mounted inside the ceramic cup and then the rear end is sealed by a 2 mm thick ceramic disc, which keeps the entire grid assembly under pressure to ensure good electrical contacts. Thin electrical leads, spot-welded to the SS rings to provide electrical contact to the grids, come out through a side slot of the ceramic cup on to a hollow ceramic tube, which can be clamped to the motor movement arrangement in a L-type configuration. The entire RFA assembly is very compact, 12 mm diameter and 7 mm thick, so as to produce minimal perturbation to the plasma.

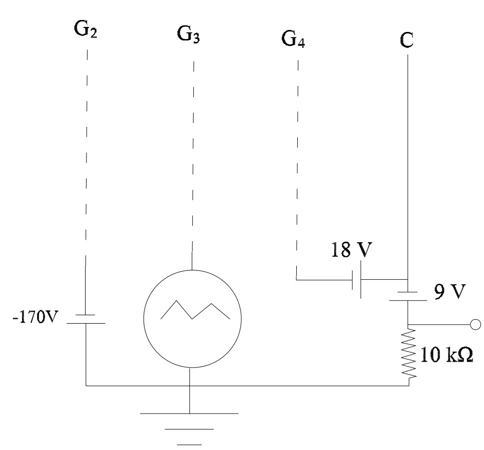

Figure 2.11: **Schematic of the RFEA.**

To find the ion energy distribution function (IEDF), the voltages applied to the various grids with respect to the chamber ground are as follow: (1) the entrance grid G_1 is kept floating, (2) the electron repeller grid G_2 is usually kept at -170 V to stop the highest energy electrons coming from the source, (3) the discriminator grid G_3 is swept at 3 Hz from 0 to 120 V, much above the maximum ion beam energy of 85 eV at $p = 0.1$ mTorr, (4) the secondary electron suppressor grid G_4 is kept at -27 V (i.e., -18 V with respect to the collector), and (5) the collector is biased at -9 V through a $10k\Omega$ resistor to ground. The collector bias and the suppressor grid bias are provided by batteries kept in a shielded enclosure to minimize noise pickup. The linear voltage sweep of the discriminator grid is provided by a bipolar power operational amplifier with a fixed gain of 10, whose input is supplied from a function generator. The sweep voltage V_d and the collector current I_c (measured by the potential drop across the $10k\Omega$ resistor) are digitally averaged over 32 swept measurements to obtain the collector $I_c - V_d$ characteristic, which can be differentiated to obtain the IEDF.

Bibliography

[1] C. Charles and R. Boswell, Appl. Phys. Lett. 82, 1356 (2003).

[2] O. Sutherland, C. Charles, N. Plihon, and R. W. Boswell, Phys. Rev. Lett. 95, 205002 (2005).

[3] N. Plihon, C. S. Corr, and P. Chabert, Appl. Phys. Lett. 86, 091501(2005).

[4] N. Plihon, P. Chabert, and C. S. Corr, Phys. Plasmas 14, 013506 (2007).

[5] X. Sun, S. A. Cohen, E. E. Scime, and M. Miah, Phys. Plasmas 12, 103509 (2005).

[6] S.K. Saha, S. Raychaudhuri, S. Chowdhury, M.S. Janaki, and A.K. Hui, Phys. Plasmas 19, 092502 (2012).

[7] S.K. Saha, S. Chowdhury, M.S. Janaki, A. Ghosh, A.K. Hui, and S. Raychaudhuri, Phys. Plasmas 21, 043502 (2014).

[8] A.E. Wendt, Rev. Sci. Instrum. 72, 2926 (2001).

[9] E. Y. Wang, N. Hershkowitz, T. Intrator, and C. Forest, Rev. Sci. Instrum. 57, 2425 (1986).

[10] G. D. Conway, A. J. Perry, and R. W. Boswell, Plasma Sources Sci. Technol. 7, 337 (1998).

Chapter 3

Studies of Steady State and Fluctuations in Argon Plasma : Experimental and Theoretical Results

3.1 Introduction

As discussed earlier in Chapter 1, a magnetized plasma often is not in equillibrium. In such cases, an instability can grow availing of free energy from various sources (a review of various experimental study on instabilities can be found in Ref. [1]). A thorough study of the instabilities (i.e. knowing the source of free energy, the possibility of having strong growth rate, identification of the instability etc.) requires that we have detailed informations about the equillibrium characteristics of the plasma. These include knowing the detailed equillibrium profiles of plasma density, potential, both electron and ion temperatures, the energy distribution function of the charged particles etc.

Some of the diagnostics that have been described in the previous chapter will facilitate us to study the equillibrium properties of plasma in DLX. S.K. Saha et el. [2] have reported the spontaneous development of a DL which exists only at low neutral pressures ($\sim 0.08 - 0.2$ mTorr) in DLX. The DL exists in this device within $z = 0-6$ cm as confirmed by the measurements of the axial plasma potential profile. The presence of an accelerated ion beam in the downstream region has been detected within $z = 0 - 13$ cm. The 2-D nature of the ion energy distribution function of the downstream plasma has been studied by a movable ion energy analyser (i.e. RFEA described in the previous chapter), which shows that the beam radius increases along the axial distance. The 2-D structure of the plasma potential has been studied by a movable emissive probe.

In this chapter, we will discuss the 2-D nature of the plasma density when the argon plasma diffuses through an aperture in the diverging magnetic field. We will see that the radial density profile near the source is peaked on the axis but gradually evolves into a hollow profile away from the source. We observe a slow increase of the peak density along a hollow conical surface and correlate with the 2-D potential measurement reported earlier [2]. It is also shown that the formation of the 2-D structures with similar features are observed whenever the plasma is allowed to diffuse through a physical aperture in such a diverging magnetic field configuration, with or without the presence of the electric double layer, i.e., the phenomenon is *generic* in nature.

A closer look at the density profiles reveals that strong density gradient in the radial direction exists for both higher (0.4 mTorr) as well as lower (0.1 mTorr) pressures. Also, as stated earlier, at lower pressures, the DL accelerates an ion beam in the downstream region. Both the density gradient and the ion beam act as a source of free energy. They can excite drift waves or the ion acoustic waves, respectively. This chapter (which is based on the two published reports [3, 2]) has been concluded with the identification of the observed fluctuations to be the resistive drift instability.

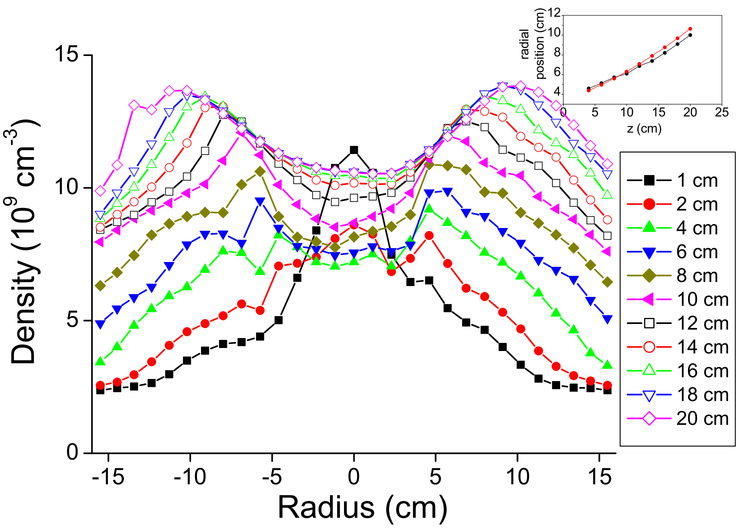

Figure 3.1: **The radial profiles of the plasma density measured by the RF-compensated LP at $p = 0.1$ mTorr, RF power $= 200$ W and magnetic field as in Fig. 2.3a at different axial distances as shown in the legend. The error bar in the density from several measurements is $\pm 2\%$. The inset shows the radial positions of the density peaks (solid black circles) and the MDMFL (solid red circles) plotted against axial distance.**

3.2 Steady State Profiles

3.2.1 Time Averaged Density Profiles

We present here the 2-D profile of the density (Fig. 3.1) measured by the RF-compensated LP under the following conditions: p = 0.1 mTorr, RF power = 200 W and axial magnetic field B_z = 272 G (at z = 0 cm which corresponds to a current of 8 A in the Helmholtz coils). Data are recorded for $z = 1 - 20$ cm in steps of 1 cm and the radius from -15.5 to 15.5 cm by rotating the probe shaft in steps of 4^0 on both sides, corresponding to a radial displacement of 1.15 cm at each step. Very near the source ($z = 1$ cm), the radial density profile exhibits a sharp peak on the axis, reminiscent of that inside the source tube. The density on the axis decreases at further axial distances but simultaneously two off-axis maxima begin to develop ($z = 2-6$ cm). For $z \geq 7$ cm, the central peak disappears and all the subsequent density profiles are hollow. It is noticed that the peak densities at these off-axis maxima continue to increase for increasing z till z = 18 cm (after which the peak density remains the same, z = 20 cm being the maximum possible travel of the LP) and the radial positions of the peaks also shift outward. The density therefore has a hollow conical structure (similar to that reported in Ref. [5]) but the slow increase of the peak density along the conical surface in the present case is in contrast to the previous observation [5]. It is also observed that the density on the axis increases slowly with z for $z \geq 6$ cm, consistent with the axial density profile reported earlier [2] using a

1-D movable LP. The typical Debye length is $\lambda_D = 0.3$ mm on the axis near the source.

The importance of the the maximum diverging magnetic field lines (MDMFL), i.e., the field lines passing through the radial edge of the exit aperture has been highlighted by experiment [2, 5] and numerical simulation [6]. With experiments performed under the same conditions ($p = 0.1$ mTorr, RF power 200 W) in DLX, S.K. Saha et al. [2] reported that the minima of the radial profiles of V_p lie on this MDMFL. In the inset shown in Fig. 3.1, the radial positions of the density peaks and the MDMFL at different z have been plotted, showing that *the maxima of the radial profiles of density also lie on this field line, which defines a conical structure.*

In Fig. 3.2, we present the contour plot of the density ($\times 10^9$ cm^{-3}) in the r-z plane. The contours have a convex structure in the axial region, being closely spaced near the source, corresponding to a rapid fall of density on the axis. The radial profiles are clearly hollow in nature for $z > 6$ cm. The MDMFL has been plotted by a red line on this figure. It clearly shows that the maximum of density occurs on the MDMFL and the peak density increases along the MDMFL as in Fig. 3.1. No subsidiary peak of density beyond the first off-axis peak could clearly be discerned, unlike the case of V_p under the same conditions reported in Ref. [2] (Fig. 2 of Ref. [2]), although there is some indication of it for $r < 0$ cm and $z \leq 8$ cm (see also Fig. 3.1).

Recent numerical particle-in-cell simulation by Rao and Singh [6] has given some understanding of the physics of the above 2-D features. Con-

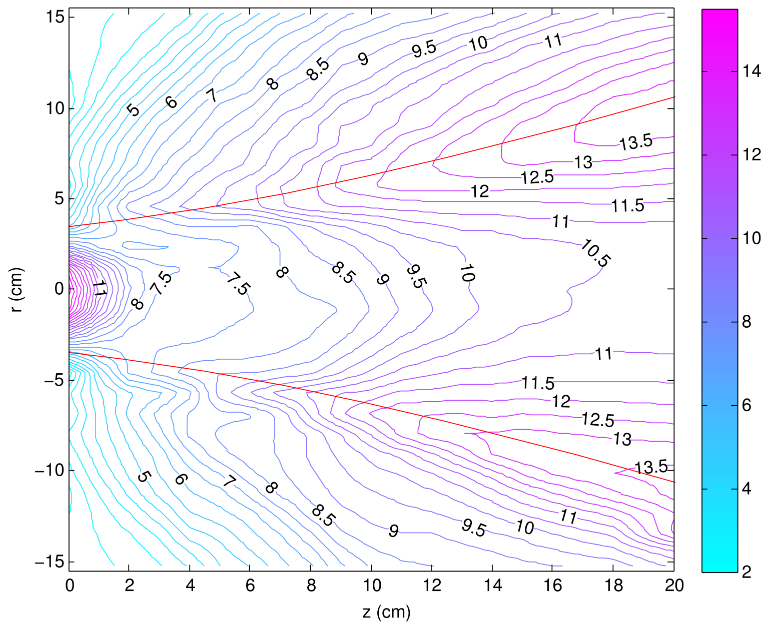

Figure 3.2: **The 2-D contours of the plasma density obtained under the same plasma conditions as in Fig. 3.1. The labels of the contours are in unit of $10^9 cm^{-3}$. The two most diverging magnetic field lines passing through the radial edge of the source tube are also shown.**

sidering the electrons as magnetized, while the ions as weakly magnetised (which is true in the present experiment for $z = 0 - 20$ cm, the region of observation), a strong radial electric field $\mathbf{E}_r$ is generated at the radial boundary of the exit aperture of the source. It creates a $\mathbf{E}_r \times \mathbf{B}$ drift of the electrons, constituting an azimuthal current and a consequent radially outward $\mathbf{J} \times \mathbf{B}$ force on the electrons. The ions also feel the radially outward $\mathbf{E}_r$. Since the electrons and the ions are electrostatically tied together, both move radially outward towards the conical surface. This explains the depletion of the plasma in the axial region and the consequent creation of a hollow profile.

The radially transported ions are electrostatically confined on the MDMFL in the potential well there (see next section) and the electrons follow them, producing a density peak on the conical surface. Such radial electric field has been demonstrated from experimental measurements [13]. The existence of a potential well on the MDMFL has also been experimentally confirmed [2].

In DLX, the axial density initially decreases fairly rapidly with increasing z (Fig. 3.2 here and Fig. 3 of Ref. [2]), which cannot be explained by the diverging nature of the magnetic field alone. This loss is not a collisional one too since the electron-ion collisional mean free path greatly exceeds the dimensions of the expansion chamber. The rapid axial density decrease should therefore be accounted for by the above mechanism of radially outward transport of the plasma. This point will be discussed in more details in Sec. 3.2.4. The decrease of the central density peak along with the appearance of the off-axis peaks with increasing z (Fig. 3.1) is consistent with the above. A recent experiment on helicon plasma thruster [7] has also shown such hollow density profile near the exit aperture of the source.

To elucidate the role of the DL in the formation of the above 2-D structures, the above measurements of the density and V_p (discussed in the next section) have been done at a pressure of 0.4 mTorr, where a DL does not exist. The 2-D structure and the contour of density at $p = 0.4$ mTorr is shown in Figures 3.3a and 3.3b, respectively. They are seen to exhibit broadly the same features as that of Figures 3.1 and 3.2 for $p = 0.1$ mTorr, respectively. The radial density profile is peaked on the axis near the source ($z = 1$ cm),

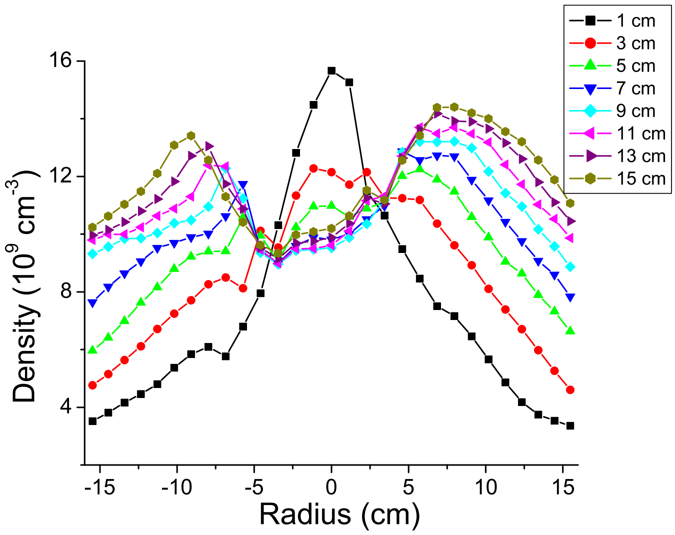

(a)

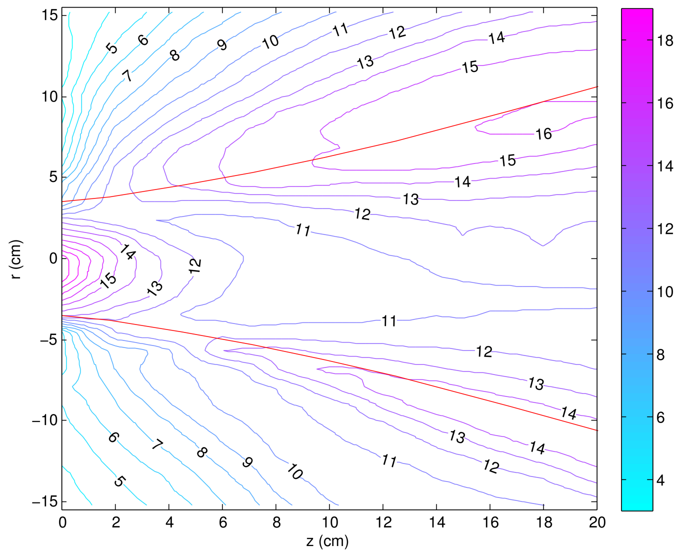

(b)

Figure 3.3: **(a) The radial profiles of the plasma density measured by the RF-compensated LP at different axial distances as shown in the legend. The error bar in the density from several measurements is** $\pm 2\%$**, (b) The 2-D contours of the plasma density. The labels of the contours are in unit of** $10^9\ cm^{-3}$**. The two most diverging magnetic field lines passing through the radial edge of the source tube are also shown. Both the profiles have been obtained at** $p = 0.4$ **mTorr, RF power** $= 200$ **W and magnetic field as in Fig. 2.3a.**

which decreases in height for higher z and gradually evolves into a hollow profile. The initial axial peak, however, decreases faster than that at $p = 0.1$ mTorr. The density contours are U-shaped near the source. The off-axis density peaks still lie on the MDMFL as in the case of $p = 0.1$ mTorr (Fig. 3.2) and the density decreases monotonically radially outward from the MDMFL. The above features of the 2-D density structure are, therefore, generic in nature for a diverging magnetic field configuration, independent of the existence of a DL.

The same experiment has been repeated by using the RFEA for the plasma density measurement. The RFEA, in this case, is mounted to face the side wall so that it collects only the plasma ions and not the axially moving beam ions. The 2-D profile of the collector current (Fig. 3.4) by this method agrees fairly well with that obtained by the RF-compensated LP (Fig. 3.3a).

3.2.2 Time Averaged Plasma Potential Profiles

A 2-D mapping of the plasma potential V_p has been carried out in the expansion chamber by using the off-axis rotatable emissive probe. Both sides of the axis have been scanned without assuming symmetry. The results have been reported by S.K. Saha et al. [2] with experiments performed under conditions where an electric DL exists (i.e. at $p = 0.1$ mTorr and RF power of 200 W). It was shown that the plasma equipotential contours have a U-shaped structure near the axis (central major lobe) and also a secondary lobe

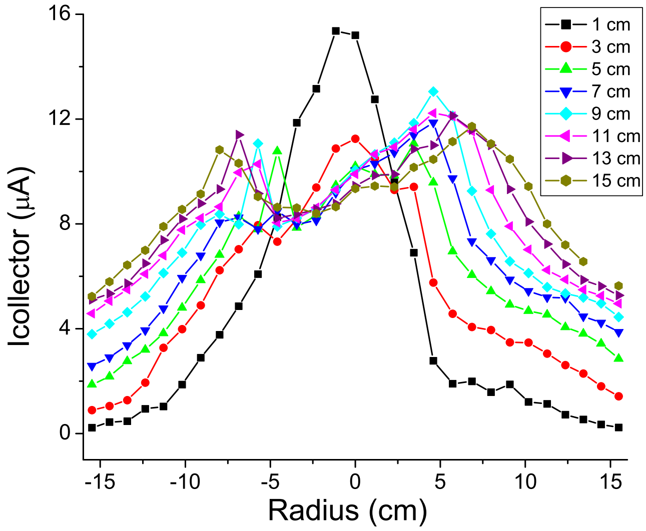

Figure 3.4: **The radial profiles of the collector current (which is directly proportional to the plasma density) measured by the RFEA under the same plasma conditions as in Fig. 3.3 at different axial distances as shown in the legend.**

on either side. The minimum of the radial profile of V_p was shown to lie on the MDMFL.

The existence of these secondary lobes in the 2-D potential structure has also got an explanation from the numerical simulation [6] discussed earlier. The radially accelerated ions overshoot the MDMFL due to inertia. They are, however, pulled back electrostatically by the electrons, which are strongly magnetized and confined on the MDMFL. The ions oscillate about this field line and the resulting positive space charge creates the minima of V_p on the MDMFL and the next maxima of V_p (secondary lobe), a little radially away from it.

Again, to elucidate the role of the DL in the formations of the 2-D struc-

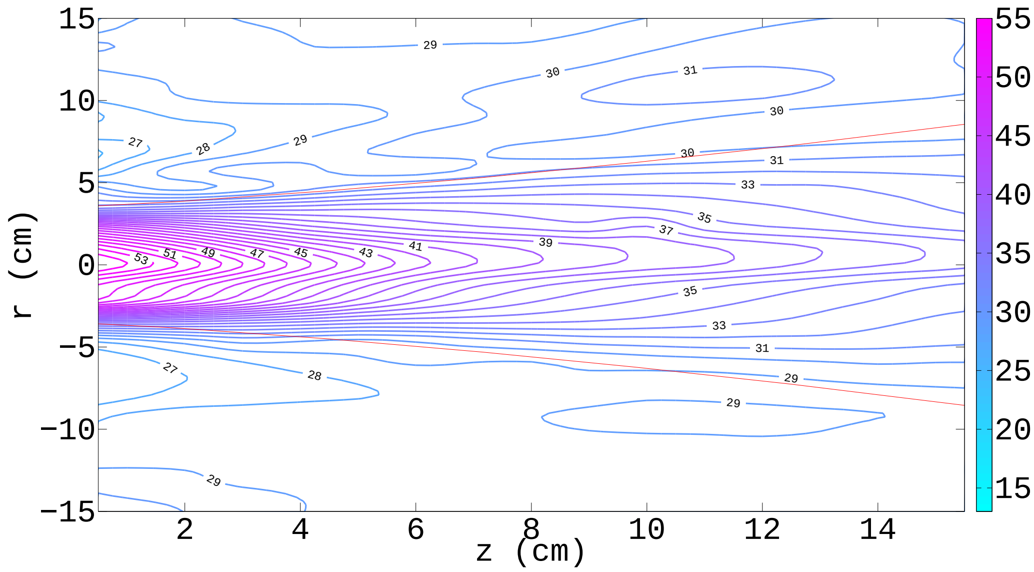

(a)

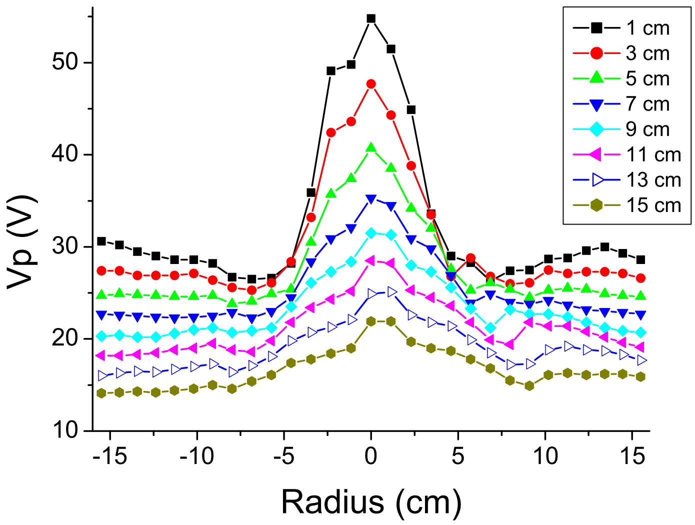

(b)

Figure 3.5: **(a) The 2-D contours plots of the plasma equipotential. The labels (in V) of some of the contours have been shown, and (b) The radial profile of the plasma potential for different axial distances as indicated in the legend. In this figure (i.e. Fig. b), the radial profile for $z = 1$ cm has been plotted on the scales shown but the other plots have been successively shifted by 2 V in the downward direction to make the weak secondary lobes clearly visible. For both cases, the plasma conditions are: $p = 0.4$ mTorr, RF power $= 200$ W and the magnetic field as in Fig. 2.3a. The error bar in the plasma potential is ± 0.5 V from several measurements.**

tures of the plasma potential, the experiments have been repeated at $p = 0.4$ mTorr where the DL vanishes. The plasma equipotential contours at $p = 0.4$ mTorr (Fig. 3.5a), drawn with a 1 V difference between the consecutive contour levels shows the same broad features as for $p = 0.1$ mtorr, showing that the features of the 2-D plasma potential structure are again generic in nature to the diverging magnetic field configuration and independent of the existence of the DL. It shows that the minima of V_p lie on the MDMFL and there is only a U-shaped lobe on the axis, confined within the cone defined by the MDMFL. Outside the cone, V_p decreases monotonically radially outward, apparently showing no secondary lobes of V_p in the contour plot. However, plotting the radial profiles of V_p at different z (Fig. 3.5b) reveals, on closer scrutiny, that weak secondary lobes do exist (for example, the first off-axis peak for $z = 11$ cm occurs at $r = 9.1$ cm). In this figure (Fig. 3.5b), the radial profile for $z = 1$ cm has been plotted on the scales shown but the other plots have been successively shifted by 2 V in the downward direction to make the weak secondary lobes clearly visible. The difference between the first radial minimum and the next maximum (secondary lobe) is, however, ~ 1.5 V only. This explains why the secondary lobes, which become less pronounced at higher collisionality, could not be discerned in the contour plot of V_p (Fig. 3.5a) at $p = 0.4$ mTorr.

In all the above cases, the floating potential of the emissive probe under strong emission has been taken as the plasma potential. But, as mentioned in the previous chapter, the accuracy of this method is dependent on the fluctuatons in V_p in a RF plasma environment. We have compared the previous measurements of V_p with the swept emissive probe or the inflection point method of calculating the plasma potential as described by E. Y. Wang and co-workers [8] at several positions and different pressures. Emissive probe characteristics are digitally averaged over several measurements and recorded for several different low emission currents below 500 μA. The derivative dI_{probe}/dV_{probe} is calculated numerically and smoothed, yielding the value of V_p from the two peaks of the derivative. A systematic difference of up to 15 V between the two methods is found, although the accuracy of this difference is not good because of the broad nature of the peaks of the derivative. The agreement is much better at higher pressure, large axial distances, and off-axis points, where the fluctuations of plasma potential are lower.

These experimental results indicate that the above features of the 2-D structures of density and potential remain similar whenever a plasma is allowed to diffuse through a physical aperture along a diverging magnetic field, with or without the existence of a DL, i.e., the effects appear to be generic in nature. With increasing pressure, however, collisionality plays a role. The radial ion oscillation about the MDMFL is impeded by collisional effects at higher pressures, thus suppressing the occurrence of the secondary lobe of V_p as observed.

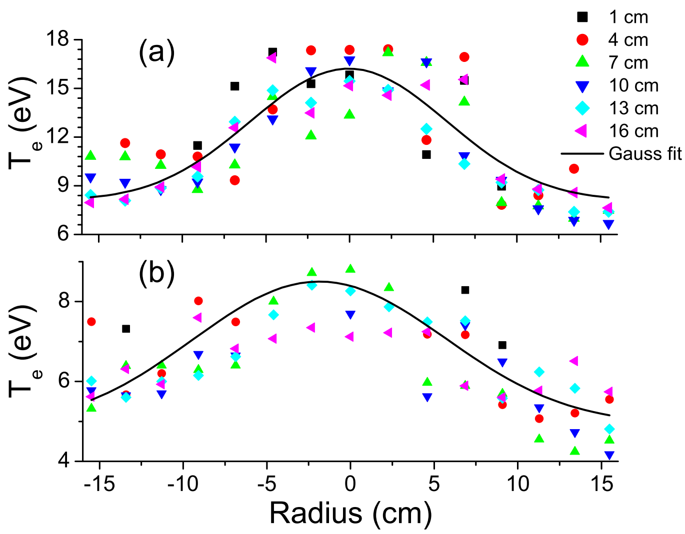

Figure 3.6: **The radial profiles of the electron temperature obtained from the probe characteristics of the RF-compensated LP at RF power** $= 200$ **W and (a)** $p = 0.1$ **mTorr and (b)** $p = 0.4$ **mTorr at different axial distances as shown in the legend.**

3.2.3 Radial Profile of the Electron Temperature

The electron temperature (T_e) has been obtained from the $I-V$ characteristics of the compensated LP in the expansion chamber. The transition region of the $I-V$ curve has been chosen carefully and fitted the same region to an exponential curve. The electron temperature is then calculated from the slope of the $\ln(I)-V$ graph of the exponential fit. The experiments have been conducted under the following conditions: $p = 0.1$ and 0.4 mTorr, RF power $= 200$ W and axial magnetic field $B_z = 272$ G (at $z = 0$ cm which corresponds to a current of 8 A in the Helmholtz coils). Data have been recorded for $z = 1-16$ cm in steps of 3 cm and the radius from -15.5 to

15.5 cm by rotating the probe shaft in steps of 8° on both sides, corresponding to a radial displacement of 2.3 cm at each step. The results has been shown in Fig. 3.6. Very near the source ($z = 1$ cm), at both pressures, the values of T_e are highly scattered due to the presence of strong RF fluctuations in this region. As we go axially outwards, we see a flattening of T_e in the central region (within $\sim r = \pm 3.0$ cm). These scattered data points have been fitted to a Gaussian curve. The temperature gradient calculated from this fit and its relative strength compared to the density gradient has been discussed later in the chapter (see Fig. 3.12, Sec. 3.3.2). For the present experiment, the average T_e has been taken to be ~ 12 eV at $p = 0.1$ mTorr and ~ 8 eV at $p = 0.4$ mTorr.

3.2.4 Further Discussion about the Density and Potential Profiles

The numerical simulation [6] discussed earlier assumes a radially uniform density (also radially uniform T_e) distribution at the exit aperture of the plasma source, not a realistic radially peaked density distribution as observed in the present experiment. It has been shown that this initial radial density profile at the exit aperture evolves into a hollow profile, whose peak density can even exceed that at the source. The initial increase of the peak density along the conical surface (in Ref. [6]) is similar to our observation. We, however, observe a continuous increase of the peak density along the conical surface and do not observe any decrease up to $z = 20$ cm. The rate of increase of the peak density decreases for increasing z and becomes zero at $z = 20$ cm. Since, however, $z = 20$ cm is the maximum distance the probe can travel, it could not be verified whether the peak density decreases thereafter. A simulation done with the experimentally observed radial density profile at the exit aperture may be needed for a better comparison with the observed results.

All the experimental set ups and numerical simulations, where the formation of the conical structures has been observed, have a common configuration, viz., the expansion of the plasma through a physical aperture into a grounded chamber along a diverging magnetic field. A physical aperture is necessary because it is a boundary, which creates a strong radial electric field $\mathbf{E}_r$ because of the difference in magnetization of the electrons and ions. This $\mathbf{E}_r$ is strongest at the radial boundary of the exit aperture and slowly decreases (but still has appreciable value) in the axial region away from the source (see below). The conical structure is formed as a result of the radial transport of the electrons induced by the $\mathbf{J}_\theta \times \mathbf{B}$ force and confinement of the ions in the potential well on the MDMFL as explained in Sec. 3.2.2. The presence of a grounded expansion chamber does not, however, seem essential for the formation of the conical structure because the above mechanism of the creation of $\mathbf{E}_r$ should work even without any physical boundary after expansion (for example, a helicon plasma thruster operating in a space simulation chamber, where the boundary is far away from the aperture). The effect of the grounded expansion chamber will be to anchor the floating potential near the wall to $\sim 5Te/e$. So the values of V_p in the expansion region will be different from that without a boundary but the conical structure will still be formed as has been observed. The radial density profiles near the exit aperture of a plasma thruster operating in a space simulation chamber need to be examined for ascertaining of the role of a grounded chamber.

The slow increase of the plasma density on the axis for $z \geq 6$ cm (Fig. 3.1) has been reported by S.K. Saha et al. [2] earlier and was also seen by several authors [11, 12] but no explanation for the same is available as yet. The particles near the axial region will also drift radially outward, causing a slow increase of the peak density along the MDMFL. This is possible because the $\mathbf{E}_r$ is still appreciable away from the source (for example, at $r = 4.9$ cm, $E_{r,z=6cm}/E_{r,z=15cm} = 3$). This is in agreement with previous measurements [13] that $\mathbf{E}_r$ is a slowly decreasing function of the axial distance. Due to good confinement of the ions in the potential well on the MDMFL in the absence of collision, the continuous radial flow of the ions can lead to density accumulation and several-fold increase in the total number of particles per unit axial length in the steady state. It is interesting to note that the slow increase of the axial density comes to a halt at $z = 20$ cm and the peak density on the MDMFL also exhibits the same behavior.

The experimental observation that the total number of particles per unit axial length integrated over a circular cross-section of the cone increases as we move axially away from the source is contrary to expectation. Before the numerical simulation [6] was published, it was suggested by earlier works that the peak of the density on the MDMFL could be due to the ionization by high energy electrons coming out from the source or by a hot electron population existing on the MDMFL. Both the possibilities of generation of new particles by ionization has been considered in the present case. There is experimental evidence in DLX that high energy electrons (of energy up to $\sim$ 160 eV in the tail of the distribution) are present in the expansion chamber. These electrons, generated in the plasma source tube, acquire high energy from the electric field of the capacitive coupling with the antenna and enter the expansion chamber overcoming the potential hill of the DL. It was suggested in a similar experiment [9] that these hot electrons travel along the MDMFL from the peripheral region of the source tube and produce additional ionization downstream, causing the maximum of the radial density profile on the MDMFL. No corroborating radial profile of the current density of these hot electrons was, however, presented.

We present here our measurement of the radial profile of the current density J_e of the energetic electrons of energy $E = 100 - 160$ eV using the RFEA. In this case, the RFEA is kept facing the source and the electron repeller grid is first kept at -170 V. The discriminator grid is swept up to 135 V at which all beam ions are found to be stopped. The collector current is then truly zero, showing that all the electrons and ions are prevented from reaching the collector (black curve A in Fig. 3.7). The electron repeller bias is now adjusted to -100 V, so that all the electrons having energy greater than 100 eV and up to a maximum of $E_{max} \sim 160$ eV reach the collector,

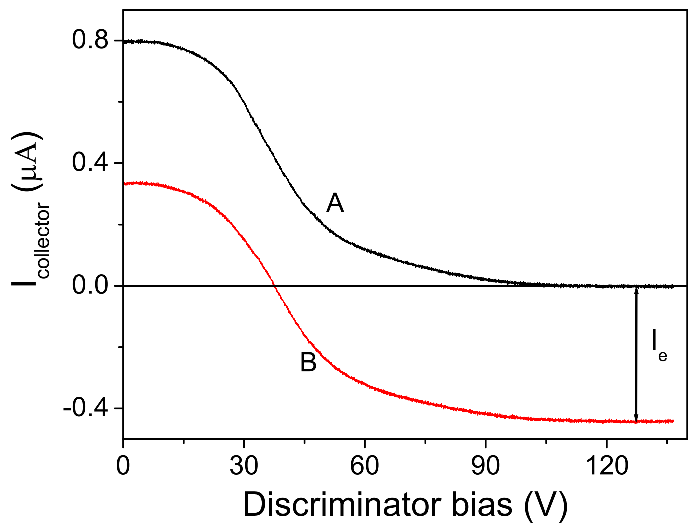

Figure 3.7: **The collector current characteristics of the RFEA facing the source for the electron repeller bias of** -170 **V (black curve A) and** -100 **V (red curve B).** I_e **is the high-energy electron current for energy** $E = 100160$ **eV. Conditions:** $z = 8$ **cm,** $r = 2.9$ **cm,** $p = 0.1$ **mTorr, and RF power** $= 200$ **W**

giving a negative collector current (red curve B in Fig. 3.7). This high-energy electron current can be recorded from the collector $I_c - V_d$ characteristic for the discriminator bias of $120 - 135$ V. The result of such measurement at $z = 8 - 16$ cm downstream is shown in Fig. 3.8. At $z = 8$ cm, the MDMFL is at $r = \pm 5.6$ cm, where J_e has no peak corresponding to the high energy electrons coming from the peripheral region of the source. Instead, J_e is peaked on the axis, decreases radially outward and is much lower at $r = \pm 5.6$ cm. However, the density of these energetic electrons being far too small and the mean free path of ionization by electron impact at $p = 0.1$ mTorr being 132 cm (much larger than the axial extent of the observation region

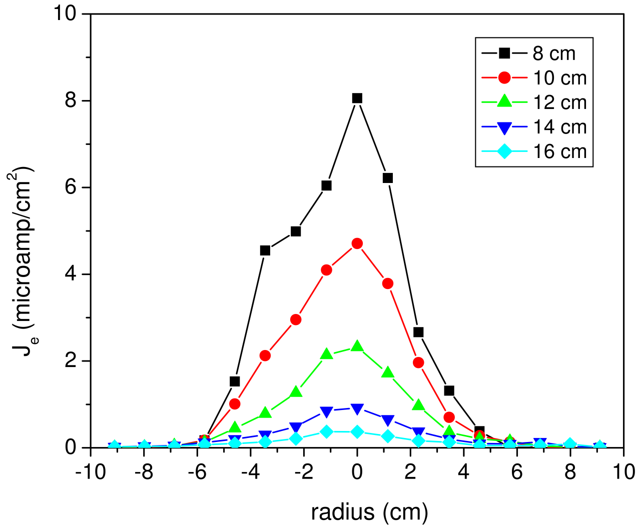

Figure 3.8: **The radial profile of the current density J_e of high energy electrons coming from the source, measured by the RFEA at $z = 8, 10, 12, 14$, and 16 cm. The error bar in J_e from several measurements is $\pm 0.2\mu A/cm^2$ for the curve corresponding to $z = 8$ cm and is much less for the other curves. Conditions: $p = 0.1$ mTorr and RF power $= 200$ W.**

of 20 cm in this experiment), their possible role in producing the plasma density peak on the MDMFL or in increasing the total number of particles to a significant extent by ionisation is ruled out. The axially peaked radial profile of J_e shown in Fig. 3.8 further indicates that ionization by these high energy electrons is not responsible for producing the hollow plasma density profile in this experiment, unlike that in Ref. [9]. Also, if ionization by these high energy electrons streaming along the MDMFL had been the cause of the radial density peak (as stated in Ref. [9]), the ionization should have decreased with z, contrary to the peak density increasing with z along the conical surface as observed in the present experiment.

Incidentally, we find from Fig. 3.8 that the number of these energetic electrons decreases very rapidly with z, with a e-folding length of ~ 5 cm, much less than the mean free path of ionizing collision. Some non-classical phenomenon like instability [10] may need to be invoked to explain this observation and may be partly responsible for the initial rapid fall of the density with z on the axis.

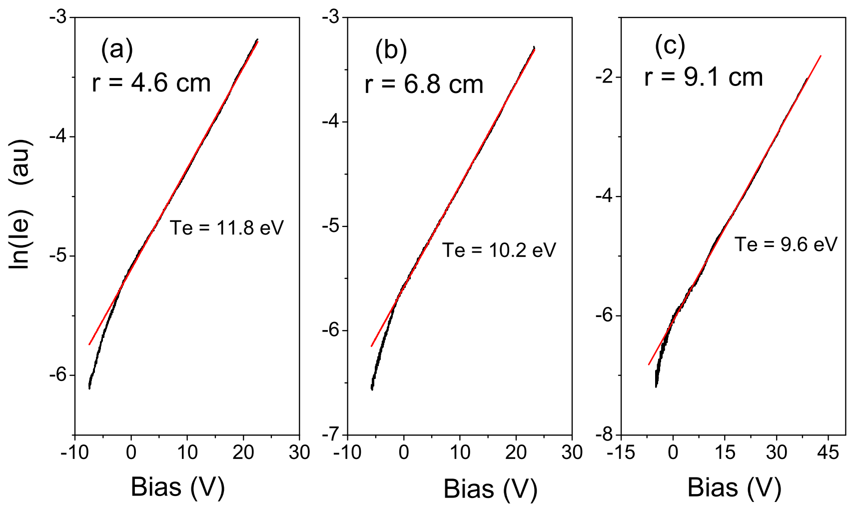

Figure 3.9: $\ln(I_e)$, **measured by the RF-compensated LP, plotted against probe bias at** $z = 10$ **cm and at three different radial locations:** $r = 4.6$ **cm (inside the MDMFL),** 6.8 **cm (on the MDMFL), and** 9.1 **cm (outside the MDMFL). The linear fits are shown by the red lines along with the corresponding** T_e**.**

A bi-Maxwellian electron energy distribution (with a $T_{e,bulk}$ and a $T_{e,tail}$) has been observed near the MDMFL in the earlier experiment [9]. It was suggested that the radial density peak on the MDMFL is likely to be caused due to enhanced ionization by the electron population with the higher T_e.

To investigate this possibility, probe characteristics have been measured by the RF-compensated LP at three different radial locations at $z = 10$ cm viz. $r = 4.6$ cm (inside the MDMFL), 6.8 cm (on the MDMFL), and 9.1 cm (outside the MDMFL). The natural logarithms of the electron current I_e (absolute value) have been plotted against the probe bias in Figures 3.9a-3.9c. It can be clearly seen that single Maxwellian populations exist in all the three cases (with $Te = 11.8, 10.2$, and 9.6 eV, respectively, decreasing a little at higher radii), with no evidence of any higher-T_e group. This shows that the radial density peak on the MDMFL is not being caused by any higher-T_e electron population in the present case, in contrast with that in Ref. [9].

In summary, an initial radial density profile peaked on the axis is found to evolve into a hollow profile as the plasma diffuses away from the source in a diverging magnetic field. The result has been explained by the radial drift of the plasma on the basis of a published simplified simulation model. We also observe a slow increase of the peak density along a hollow conical surface defined by the MDMFL, in contrast to an earlier observation. Further, the features of the 2-D conical structures of the density and the potential remain similar with or without the presence of a DL, exhibiting a generic behavior when a plasma expands through a physical aperture along a diverging magnetic field.

3.3 Study of Instabilities

3.3.1 General Observations

Fluctuations in the range $\sim$ 20 kHz in the floating potential as well as in the ion saturation current have been observed in the DLX in a wide range of pressures ($0.1 - 0.6$ mTorr). The time series data of these fluctuations have been recorded using Yokogawa DL 1640 oscilloscope in a time span of 100 ms and the data has been sampled at 1 MHz giving a data length of 100k. The time series has been analysed by a MATLAB programme which divides the total data length into 100 blocks, each containing 1k data points. The FFT has been taken in each block, then the real and imaginary parts have been averaged over the 100 blocks. This averaging over the blocks effectively suppreses any noise in the data. Standard tool for calculating the phase difference between two signals is also available in MATLAB. The values of the coherence between the two signals has been calculated using the standard formula for the normalised cross-correlation function of two signals. A typical analysis of the floating potential fluctuations ($\tilde{\phi_f}$) recorded simultaneously using two uncompensated LPs separated in the azimuthal direction has been shown in Fig. 3.10. A peak with a frequency of $f = 18$ kHz can be seen in the power spectrum of $\tilde{\phi_f}$ (Fig. 3.10a) indicating an instability which exists throughout the whole axial region. All measurements of the wave characteristics using Langmuir probes have been made in the expansion chamber mainly for $z \geq 8$ cm, thereby avoiding the zone where the

RF interference is likely to influence the fluctuation measurements. Figure 3.10b shows the variation of the phase angle between the two signals with frequency. This variation is linear with frequency up to ∼ 100 kHz, showing that it is a mode propagating in the azimuthal direction. The direction of propagation coincides with the direction of the electron diamagnetic drift (see next section and Sec. 3.4.3). Figure 3.10c shows that the two simultaneously recorded fluctuations are strongly correlated at the fequency where the power is maximum, i.e. a coherent mode exists.

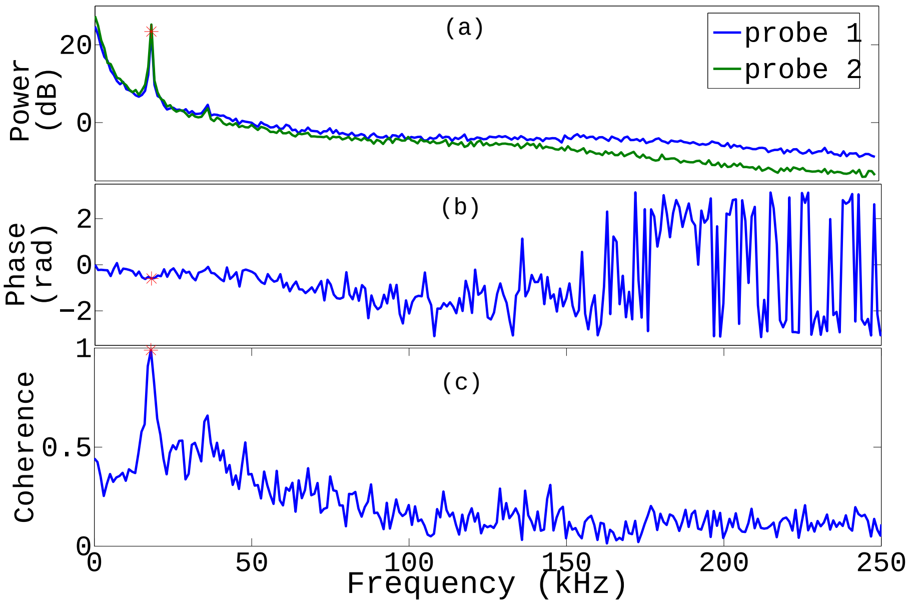

Figure 3.10: **Frequency spectra of the fluctuation power (a), the phase difference (b) between the signals from the two azimuthally separated probes and the coherence (c) between them. The two signals have been recorded at $z = 8$ cm, $r = 3.0$ cm, $p = 0.4$ mtorr, RF power $= 200$ W. The dominant frequency from the top panel is 18 kHz (marked by the red star).**

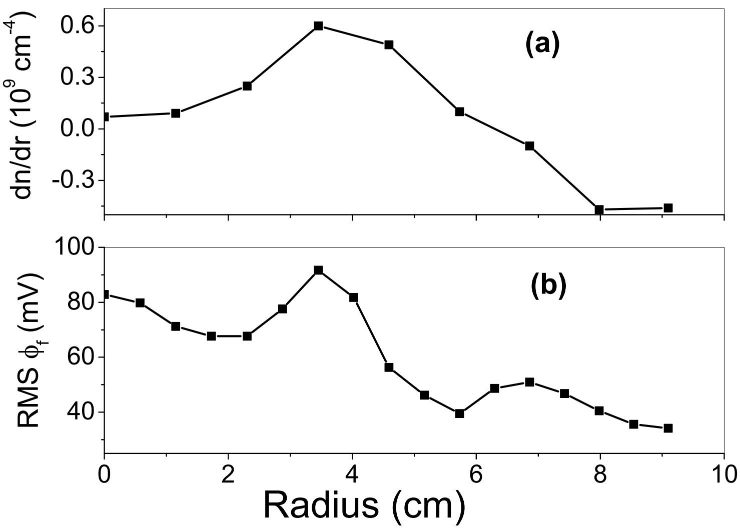

Figure 3.11: **The density gradient $\frac{dn}{dr}$ (a) obtained from Fig. 3.3a and the RMS values of $\tilde{\phi}_f$ (b). Both the profiles have been obtained at $p = 0.4$ mtorr, RF power $= 200$ W, and $z = 8$ cm.**

3.3.2 Identification of the Instability

To identify this mode, the following measurements have been performed.

(i) The radial gradient of the density (obtained from Fig. 3.3a) has been plotted in Fig. 3.11a. It can be seen that the RMS value of the fluctuations in the floating potential, plotted in Fig. 3.11b is maximum around the same region where the radial gradient in density is also maximum. From the Gaussian fit of the electron temperature at $p = 0.4$ mTorr (Fig. 3.6b), it is expected that the radial gradient in T_e is also maximum around the same region of $r \sim 3.0$ cm. To separate the ∇T_e and ∇n regions, we have plotted their relative contribution to the pressure gradient in the radial direction in Fig. 3.12. It can be seen that the contribution of the temperature gradient is almost negligible compared to the density gradient. Hence, the electron temperature has been taken to be varying weakly. This suggests that the fluctuations are density gradient driven.

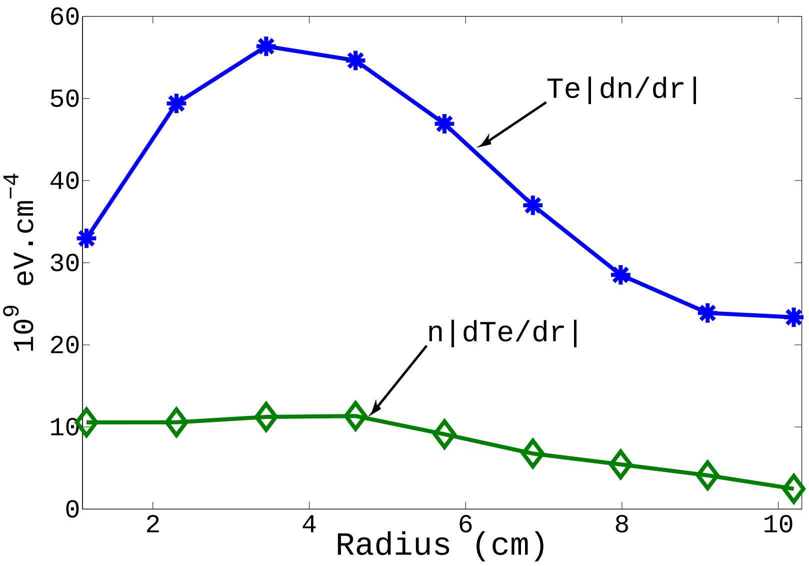

Figure 3.12: **The density gradient has been obtained from the polynomial fit of the density profile at $z = 1$ cm of Fig. 3.3a. The temperature gradient has been obtained from the formula of the Gaussian fit of T_e of Fig. 3.6b.**

The radius at which the fluctuation amplitude is maximum is nearly equal to the radius of the source tube. Such a result has been reported earlier [14]. When the plasma from the source tube diffuses into the expansion chamber, a strong radial density gradient is created near the edge of the entrance aperture. The density gradient-driven instability is most likely to be created at this radius, which then propagates axially with a weak propagation constant $k_z \sim 0.09$ cm^{-1} (see Table-3.1), giving rise to the radial maximum of $\tilde{\phi}_f$ measured at other axial locations, as shown in Fig. 3.11b.

(ii) For mode analysis, floating potential fluctuations have been recorded using two LPs at the same axial position: one LP is kept fixed at a particular radius (here r = 3.0 cm) while the other LP (of radial shaft length = 3.0 cm, Fig. 2.7 of the previous chapter) is rotated along the azimuthal direction at the same radius, thus varying the azimuthal separation between the two LPs. The typical variation of the power spectrum, the phase difference and the coherence with the frequency have been depicted in Fig. 3.10a, b and c respectively at z = 8 cm, r = 3.0 cm and azimuthal separation = 20°. One can see that the dominant frequency is 18 kHz (Fig. 3.10a). The phase difference corresponding to this dominant frequency is then noted. The above procedure is repeated for other azimuthal separations and the phase difference is then plotted against the azimuthal separation. The results have been shown in Fig. 3.13 for four different magnetic fields with the neutral pressure and the RF power remaining the same. The phase difference varies linearly with the azimuthal separation which matches closely with the mode propagating as $m = 1$. The mode number does not change in spite of change in the magnetic field, contrary to earlier observations [3].

From Fig. 3.13, the azimuthal wave number (k_θ) has been calculated using the relation:

$$k_\theta = \frac{180}{\pi}[\frac{\Phi}{r\theta}] \tag{3.1}$$

where Φ, θ and r are the phase difference in radian, the azimuthal separation between the the two LPs in degree and the radius at which the measurements have been performed, respectively, at $B = 270$ G.

Electron Temperature T_e	8.0 eV
Ion Temperature T_i	0.2 eV
Ion Gyrofrequency f_{ci}	9.4 kHz
Electron Gyrofrequency f_{ce}	200 MHz
Ion Larmor Radius ρ_i	1.04 cm
Electron Larmor Radius ρ_e	0.03 cm
Density Gradient Scale Length L_n	$\sim$ 13 cm
Electric Field Scale Length L_E	$\sim$ 3 cm
Ion-Neutral Collision Frequency ν_{in}	4.5 kHz
Electron-Neutral Collision Frequency ν_{en}	16.2 MHz
Electron Diamagnetic Drift Speed v_{de}	2×10^5 cm/s
Ion Sound Speed C_s	5×10^5 cm/s
Wave Phase Velocity (from expt.) v_{phase}	2.3×10^5 cm/s
Azimuthal Wave Number k_θ	0.56 cm^{-1}
Axial Wave Number k_z	0.09 cm^{-1}
Axial Wavelength λ_z	$\sim$ 70 cm

Table 3.1: **Parameters of the plasma for $B = 270$ G (at $z = 0$ cm), $p = 0.4$ mTorr, and RF power = 200 W.**

The typical values of the azimuthal wave number (k_θ) and the azimuthal phase velocity of the wave (calculated from $\omega = k_\theta v_{phase}$) have been shown in Table-3.1. Also shown in this table is the electron diamagnetic drift speed (v_{de}) calculated from $v_{de} = \frac{T_e}{eBL_n}$ where T_e is the electron temperature in eV, L_n is the density gradient scale length and e is the electronic charge. It can be seen that the two velocities are nearly equal. Also, the wave propagates (for all z) in the same direction as v_{de} calculated for the peaked density profile (i.e. at $z = 1$ cm).

(iii) It has been observed that the frequency of the mode remains constant at all radial positions and the radial variation of the azumuthal phase velocity of the wave is negligible. Now, since $\omega = k_\theta v_{phase}$, to keep $k_\theta = \frac{m}{r}$ constant, we should get higher mode numbers as we go radially outwards. Figure 3.14 shows the experimental verification of this argument. In this figure, the phase difference is plotted against the azimuthal separation at two radial locations viz. $r = 3.0$ and 5.9 cm. It can be seen that, at $r = 3.0$ cm, we mainly have the $m = 1$ mode of propagation both for positive and negative angles with respect to the reference probe. At $r = 5.9$ cm, the negative angles show clearly the presence of the $m = 2$ mode, although for the positive angles there is some discrepancy, possibly due to the co-existence of both the $m = 1$ and $m = 2$ modes. This occurence of higher mode numbers at higher radii is a well known result from the existing theoretical models [3, 16].

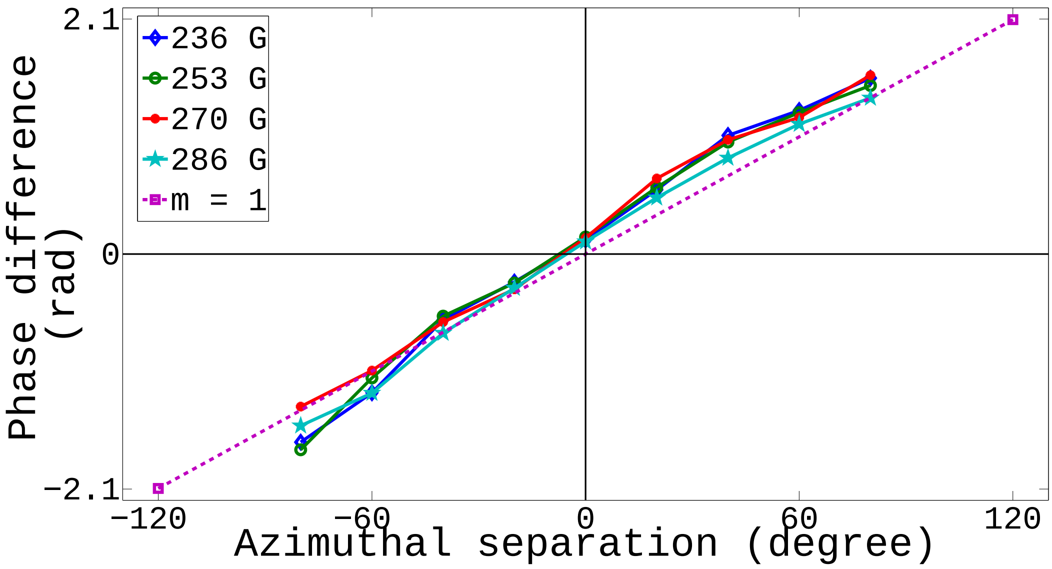

Figure 3.13: **The phase difference plotted against the azimuthal separation for four different magnetic fields with other plasma conditions as in Fig. 3.10. The values of B shown here are at $z = 0$ and correspond to different currents in the Helmholtz coils. The plot for the ideal $m = 1$ line has been shown by the dashed line.**

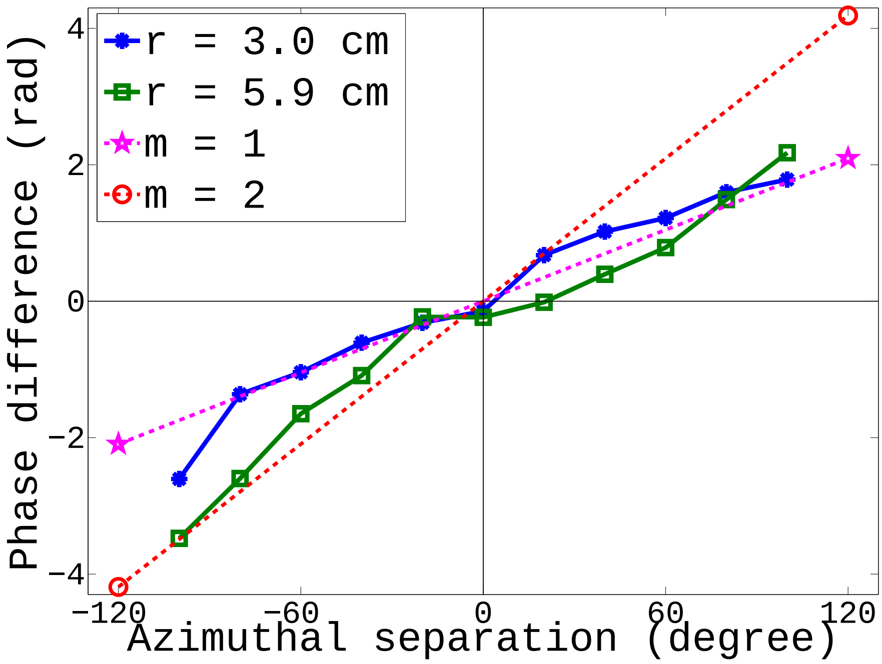

Figure 3.14: **The phase difference plotted against the azimuthal separation, showing the variation of the mode number with radius at** $z = 8$ **cm and** $r = 3.0$ **cm (blue line),** 5.9 **cm (green line) for same plasma conditions as in Fig. 3.10. The ideal** $m = 1$ **and** $m = 2$ **propagation plots have also been shown.**

(iv) To measure the phase difference between $\tilde{n}$ and $\tilde{\phi}_f$, the four-LP system has been employed. The working principle of the four-LP system has already been described in Sec. 2.2.3. This arrangement has been done to ensure that the fluctuations in the density and the floating potential are measured at virtually the same point in the plasma. The phase difference is then obtained following the method explained above (as in Fig. 3.10). It varies between 0.5^c and 1.3^c at different radii with the density fluctuations leading in phase as expected for drift waves. As has been shown by the theoretical models [3], the existence of a finite phase difference between $\tilde{n}$ and

$\tilde{\phi}_f$ is a characteristic of resistive drift waves. We will see in Sec. 3.4.3, that for our case, this phase difference results from the electron-neutral collisions.

(v) To measure the axial wave propagation, two uncompensated LPs have been aligned electrically so that they lie exactly on the same axial magnetic field line. The importance and the procedure of the electric alignment of two LPs have already been described in Sec. 2.2.2 (Fig. 2.8 of the previous chapter). One of these two electrically aligned LPs has been fixed at $z = 7$ cm, while the other was moved axially outwards in steps of 3 cm. At each axial separation, $\tilde{\phi}_f$ from both the two LPs are measured simultaneously and following similar kind of analysis (case(ii) above), the axial phase difference ($\Delta\phi$) corresponding to each axial separation (Δz) is obtained. The results have been shown in Fig. 3.15.

The parallel wavelength (λ_z) is obtained from the slope of the $\Delta\phi$ vs Δz graph, i.e. $\lambda_z = 2\pi \times \frac{\Delta z}{\Delta\phi}$. The typical value of λ_z (and hence k_z) is shown in Table-3.1. It can be seen that $\lambda_z \sim 1.5 \times L$ (where L is the length of the expansion chamber) and $k_\theta \sim 6 \times k_z$ i.e the wave is propagating strongly along the azimuthal direction with a weak component along the axial direction. This is an important feature of the gradient driven drift waves. It differentiates drift waves from the other kind of waves propagating azimuthally viz. the flute modes or the K-H instability which must have $k_z = 0$ [17, 18].

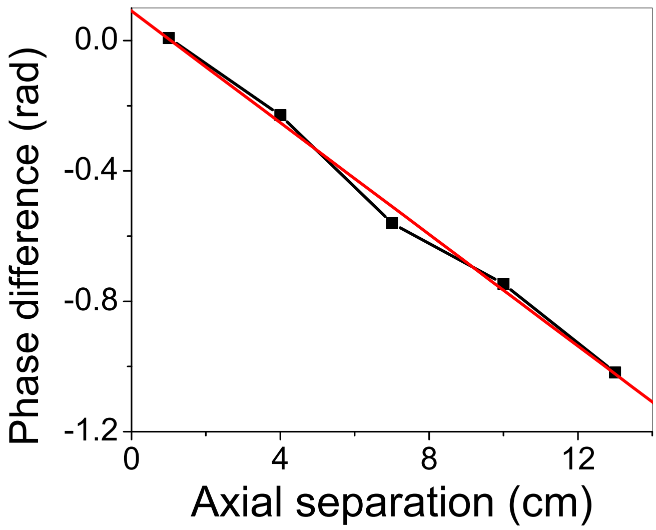

Figure 3.15: **The axial phase difference plotted against the axial separation (black line) for $r = 0$ cm and the same plasma conditions as in Fig. 3.10. The axial wave number has been calculated from the slope of the best straight line fit (red line).**

3.3.3 Summary and Discussion

Experimental observations presented in the earlier sections reveal the existence of an azimuthally propagating mode with a frequency that is fixed for a given set of values of the neutral pressure, magnetic field and RF power and does not vary with the local parameters. The plasma diffusing into the expansion chamber displays a peaked density profile in the region close to the entrance aperture (up to $z = 3$ cm) and evolves slowly into a hollow density profile flanked by two radial peaks (Fig. 3.1 and 3.3a). Calculation of the density gradient in this device show that in the radial direction, the density gradient is maximum on a plasma column of radius around 3.0 cm whose diameter coincides with that of the entrance aperture. The amplitude of the the fluctuations is maximum at the location where the radial density gradient is maximum (Fig. 3.11). Correlation measurements show that the density fluctuations lead the potential fluctuations by 0.5^c to 1.3^c. The modes have been observed to propagate predominantly in the azimuthal direction (along the electron diamagnetic drift corresponding to the peaked density profile) that remains the same as we go axially outward from the entrance aperture. The mode has a weak propagation along the axial direction. Since the mode is propagating predominantly in the azimuthal direction, the possibility of it being an ion acoustic wave (which has no component perpendicular to the magnetic field) is ruled out. The weak axial propagation indicates that the mode is not a K-H or other flute type instability.

As has been mentioned in Sec. 1.3, an instability in the frequency range $0 < \omega < \omega_{ci}$ has been predicted by Post and Rosenbluth [22] in the magnetic mirror devices. This instability occurs in an inhomogeneous plasma for the mirror type magnetic field configuration. They have predicted the following characteristics for the DCLC mode:

(a) The mode is non-convective (i.e. $k_{||} = 0$), propagating azimuthally in the direction of the *ion* diamagnetic drift.

(b) At high densities ($\sim 10^{14} cm^{-3}$), it has shown that the density gradient scale length, L_n, satisfies a critical condition $L_{ncritical} \sim 0.01\rho_i$ for the instability to occur. For the low densities, $L_{ncritical}$ is negligibly small.

(c) For this type of instabilities to occur, the plasma needs to be larger in radius than a critical radius, r_{min}. This r_{min} has been shown to follow the relationship: $\frac{r_{min}}{\rho_i} \sim 300$. The mirror ratio ($R$) in such type of instability has been found to be $R \sim 3.0$.

Also, as has been found experimentally by Akiyama and Takeda [23], the DCLC mode exists only within the region of the mirror field.

Now, for the present experiment, it can be seen from Fig. 2.3a that the mirror field exists within $\sim z = -40$ to -5 cm. The fluctuations have been recorded up to $z = -7$ cm inside the source with a single LP at $r = 1.5$ cm. Measurements could not be performed beyond that distance due to the disturbance of the source plasma by the insertion of the LP. However, no new peak in the power spectrum of the time series data has been observed in the region $z = 0$ to -7 cm. As has been discussed in the earlier sections, the present mode detected in the expansion chamber is convective type, propagating azimuthally in the direction of the *electron* diamagnetic drift satisfying the relation $k_\theta >> k_z$. It can be seen from Table-3.1, that $L_n \sim 9\rho_i$. The mirror ratio considering the region $z = -40$ to -5 cm is $\sim R = 1.5$. These characteristics of the present mode strongly suggest that it is not the electrostatic DCLC mode, as predicted by Post and Rosenbluth [22].

All the characteristics of the mode, in fact, suggest that the mode is the electrostatic (the plasma $\beta \sim 10^{-4}$) resistive drift wave instability. Measurements of the mode frequency using LP has been made starting from $z = 1$ cm at various radial locations and the waves have been observed to propagate with a constant frequency of ~ 18 kHz to a distance of $z = 16$ cm, the maximum distance where the measurements have been performed. In the region close to the edge of the entrance aperture, the gradient of the density and the amplitude of the fluctuation are highest which lead to the possibility that the gradient-driven drift like modes are excited there.

3.4 Theory: Dispersion Relation and Growth Rate

In the expansion chamber, due to the divergence of the magnetic field, the field strength varies from 270 G (at $z = 0$ cm) to 47 G (at $z = 16$ cm) leading to a variation in the ion cyclotron frequency from 9.4 kHz to 1.7 kHz. The observed frequency is therefore greater than ω_{ci} at the point of excitation as well as at all locations throughout the expansion chamber. Although the observed mode shows all the characteristics of a conventional drift mode, it falls under a different frequency regime i.e. unlike conventional drift modes, we have here $\omega > \omega_{ci}$. All the existing theoretical models for the drift waves follow the low frequency limit. Hence, in order to understand the characteristics of these high frequency drift modes, the existing theoretical models need to be extrapolated to frequencies $\omega > \omega_{ci}$.

3.4.1 Kinetic Model

A.B. Mikhailovskii and A.V. Timofeev [19] have shown that, as the frequency of the drift wave is increased towards ω_{ci}, a coupling between the ion cyclotron modes and the drift modes occurs in the magnetized inhomogeneous plasma. The extra free energy in the spatial inhomogeneity of the plasma is generally fed to the ion Bernstein mode, resulting in a coupled mode with frequency $\omega = n\omega_{ci}$ where n is an integer. For such an instability with frequency $\omega \sim \omega_{ci}$, S. Ichimaru [20] has shown that the dielectric response function has the following form:

$$\epsilon(k,0,\omega) = 1+\frac{1}{k^2\lambda_{De}^2}[\frac{\omega_e^*}{\omega}+1-\Lambda_0(\beta_e)]+\frac{1}{k^2\lambda_{Di}^2}1-(\omega-\omega_i^*)[\frac{\Lambda_0(\beta_i)}{\omega}+\frac{\Lambda_1(\beta_i)}{\omega-\omega_{ci}}] = 0 \tag{3.2}$$

where

$$k_e^2 = \frac{4\pi e^2 n}{T_e}, \omega_e^* = \mathbf{k}.\mathbf{v_d} = \frac{k_B T_e}{m_i \omega_{ci} L_n} k_y$$

and $\lambda_{D\alpha} = \frac{T_\alpha}{4\pi n q_\alpha^2}$ $(\alpha = e, i)$ is the Debye length. Here, we have assumed that all the equillibrium quantities are varying in the $x-$direction, while the mode is propagating in the $y-$direction. For this type of coupled modes, we also have,

$$\beta_e = k^2(\frac{T_e}{T_i})(\frac{m_e}{m_i})\rho_i^2 < 1 \tag{3.3}$$

and

$$\beta_i = k^2\rho_i^2 >> 1 \tag{3.4}$$

.

Here ρ_i is the ion Lrmor radius. The last condition (equation 3.4) suggests that the wavelength of the coupled mode is much smaller than the ion Larmor radius. With the help of the above mentioned assumptions, we have,

$$\Lambda_0(\beta_e) \cong 1 - \beta_e,$$

$$\Lambda_0(\beta_i) \cong \Lambda_1(\beta_i) \cong [(2\pi)^{1/2} k\rho_i]^{-1} \equiv \Delta$$

Using these approximations in the above dispersion relation, where it is expected that $\Delta << 1$, we arrive at the following quadratic relation:

$$1 + k^2\lambda^2 - \frac{\omega_i^*}{\omega} = \frac{\omega - \omega_i^*}{\omega - \omega_{ci}}\Delta \tag{3.5}$$

where

$$\lambda^2 = \lambda_{Di}^2 + \frac{m_e}{m_i}\rho_i^2.$$

From equation (3.5), we have two solutions corresponding to the following two limits:

(i) $\omega_1 = \frac{\omega_i^*}{1+k^2\lambda^2}$ when $\omega << \omega_{ci}$. This corresponds to the conventional drift waves. And,

(ii) $\omega_2 = \omega_{ci}(1 + \frac{\Delta}{1+k^2\lambda^2})$ when $\omega \sim \omega_{ci}$. This branch corresponds to the ion cyclotron mode.

So, the coupled mode may appear at a region of intersection between the above two branches. Considering a wide range of parameters such as density, temperature, magnetic field, density gradient scale length and wavelength in hot solar atmosphere, J. Vranjes and S. Poedts [21] found that the coupling may occur only at narrow range of wavelengths when it becomes comparable to the ion gyroradius i.e when the condition $\lambda \sim \rho_i$ is satisfied.

Unlike the above case, as can be seen from Table-3.1, we have $\lambda >> \rho_i$. As a result, the equations (3.3) and (3.4) become:

$$\beta_e = k^2(\frac{T_e}{T_i})(\frac{m_e}{m_i})\rho_i^2 << 1 \tag{3.6}$$

and

$$\beta_i = k^2\rho_i^2 << 1 \tag{3.7}$$

.

Assuming the elctrons to follow the Boltzmann distribution, we have for the ions,

$$\Lambda_0(\beta_i) \cong 1 - \beta_i, \Lambda_1(\beta_i) \cong \frac{\beta_i}{2}$$

Using these approximations in equation (3.2), we have,

$$1 + \frac{1}{k^2\lambda_{De}^2} + \frac{1}{k^2\lambda_{Di}^2}[1 - (\omega - \omega_i^*)(\frac{1-\beta_i}{\omega} + \frac{\omega\beta_i}{\omega^2 - \omega_{ci}^2})] = 0$$

Simplifying the above equation, we get the following dispersion relation:

$$\omega^3 - \omega(\omega_{ci}^2 + k^2c_s^2) + \omega_e^*\omega^2 - \omega_e^*\omega_{ci}^2 = 0 \tag{3.8}$$

Again, from equation (3.8) we have two solutions corresponding to the following two limits:

(i) $\omega_1 = \frac{\omega_i^*}{1+k^2\rho^2}$ when $\omega << \omega_{ci}$. This corresponds to the conventional drift waves. And,

(ii) $\omega_2 = \pm\sqrt{(\omega_{ci}^2 + k^2c_s^2)}$ when $\omega \sim \omega_{ci}$. This branch corresponds to the ion cyclotron mode and occurs in absense of any inhomogeneity in density.

As noted earlier, the coupling between these two modes occurs only when the criterion $\lambda \sim \rho_i$ is satisfied. Since we are far removed from this regime, hence, the coupling between these two modes is not expected to occur in the present case. On the other hand, the experimental results suggest that the present mode has all the characteristics of a conventional resistive drift wave. The driving mechanism of resistive drift waves can be explained and the growth rates can be calculated from the two fluid model incorporating the collisional effetcs.

3.4.2 Fluid Model

We attempt to obtain a general dispersion relation for drift waves in the linear, local slab model in the two fluid picture by ignoring the low frequency approximation ($\omega << \omega_{ci}$ as usually considered). To develop this model, we have made the following assumptions which are consistent with our experimental observations:

(a) The magnetic field, $\mathbf{B}$, is in the axial direction and the axial variation of B_z has not been considered for simplicity.

(b) For the characteristic frequencies applicable to our experiment, from Table-3.1, we can see that $\omega_{ce} >> \omega > \omega_{ci}$.

(c) Equilibrium plasma densities vary in the x-direction. However, density gradient scale length, L_n is taken to be more or less constant.

(d) From Table-3.1, $T_i = 0.2$ eV and $T_e = 10$ eV. So only electron diamagnetic drifts have been considered.

(e) Since $\rho_e << L_E \sim \rho_i$, during one complete gyration, ions will feel the $\mathbf{E} \times \mathbf{B}$ drift very weakly and therefore not considered. Hence, $\mathbf{E} \times \mathbf{B}$ drift has been considered only for the electron fluid.

The general two fluid equations for the charged particles are the continuity and the momentum equations, namely:

$$\frac{\partial n_\alpha}{\partial t} + \nabla \cdot (n V_\alpha) = 0 \tag{3.9}$$

and

$$n_\alpha m_\alpha \frac{dV_\alpha}{dt} = -k_B T_\alpha \nabla n_\alpha + q_\alpha n_\alpha (E + v \times B) - m_\alpha n_\alpha \nu_\alpha V_\alpha. \tag{3.10}$$

where $\alpha = e, i$; k_B is the Botzmann constant, V_α is the velocity of the charged particles. The last term on the RHS of equation (3.10) is the resistive term arising due to the collisions of the charged particles with the neutrals where ν_α stands for the collisional frequency. The Coulomb collisions have been ignored (the mean free path of the ionizing collision is 132 cm which is almost 2.5 times the dimension of the expansion chamber). The equilibrium situation is described by the following conditions:

(i) The equilibrium ion velocity, $V_i = 0$,

(ii) The equlibrium parallel velocity of the elctrons, $V_{ez} = u_0$, is constant,

(iii) The perpendicular drift i.e. the diamagnetic drift of the electron fluid is in the $y-$ direction and has the standard form,

$$V_d = \frac{k_B T_e}{eB} \frac{1}{n} \frac{dn}{dx} = \frac{k_B T_e}{eBL_n} = \frac{k_B T_e}{m_i \omega_{ci} L_n}$$

where $L_n = (\frac{1}{n}\frac{dn}{dx})^{-1}$ is the density gradient scale length.

Linearizing the continuity equation (3.9) for the elctrons, imposing the above mentioned assumptions (a)-(e), and assuming all perturbed quantities varying as $\sim exp(-i\omega t + i\mathbf{k}.\mathbf{r})$, we get,

$$\bar{\omega}\frac{\tilde{n}_e}{n} - (k_x\tilde{v}_{ex} + k_y\tilde{v}_{ey} + k_z\tilde{v}_{ez}) + \frac{i}{L_n}\tilde{v}_{ex} = 0 \tag{3.11}$$

Where $\bar{\omega} = \omega - k_yV_d - k_zu_0$.

Similarly, from the z-component of the momentum equation for the electrons,

$$0 = -k_BT_e\frac{\partial\tilde{n}_e}{\partial z} + en\frac{\partial\tilde{\phi}}{\partial z} - m_en\nu_e\tilde{v}_{ez}$$

or,

$$ik_BT_ek_z\frac{\tilde{n}_e}{n} - iek_z\tilde{\phi} = -m_e\nu_e\tilde{v}_{ez}$$

or,

$$\tilde{v}_{ez} = \frac{k_BT_e}{m_e\nu_e}(ik_z)\frac{\tilde{n}_e}{n} - \frac{iek_z}{m_e\nu_e}\tilde{\phi} \tag{3.12}$$

Similarly, for the $x-$ and $y-$components, we have,

$$\tilde{v}_{ex} = \frac{k_BT_e}{enB}\frac{\partial\tilde{n}_e}{\partial y} - \frac{1}{B}\frac{\partial\tilde{\phi}}{\partial y} = \frac{k_BT_e}{eB}(ik_y)\frac{\tilde{n}_e}{n} - \frac{iek_y}{B}\tilde{\phi} \tag{3.13}$$

$$\tilde{v}_{ey} = -\frac{k_BT_e}{enB}\frac{\partial\tilde{n}_e}{\partial x} + \frac{1}{B}\frac{\partial\tilde{\phi}}{\partial x} = -\frac{k_BT_e}{eB}(ik_x)\frac{\tilde{n}_e}{n} - \frac{iek_x}{B}\tilde{\phi} \tag{3.14}$$

Substituting the above expressions for $\tilde{v}_{ex}$, $\tilde{v}_{ey}$ and $\tilde{v}_{ez}$ in equation (3.11), we get,

$$[\bar{\omega} - \frac{k_y}{L_n}\frac{k_BT_e}{enB} + ik_z^2\frac{k_BT_e}{m_e\nu_e}]\frac{\tilde{n}_e}{n} = [-\frac{k_y}{L_nB} + \frac{ik_z^2e}{m_e\nu_e}]\tilde{\phi}$$

or,

$$\frac{\tilde{n_e}}{n} = \frac{-\frac{k_y}{L_n B} + \frac{ik_z^2 e}{m_e \nu_e}}{\bar{\omega} - \frac{k_y}{L_n}\frac{k_B T_e}{enB} + ik_z^2 \frac{k_B T_e}{m_e \nu_e}}\tilde{\phi}$$

or,

$$\frac{\tilde{n_e}}{n} = \frac{-\frac{k_y}{L_n}\frac{k_B T_e}{eB} + ik_z^2 \frac{k_B T_e}{m_e \nu_e}}{\bar{\omega} - \frac{k_y}{L_n}\frac{k_B T_e}{eB} + ik_z^2 \frac{k_B T_e}{m_e \nu_e}} \frac{e\tilde{\phi}}{k_B T_e}$$

Then, finally, we get the following expression for the perturbed density for the electron fluid:

$$\frac{\tilde{n_e}}{n} = \frac{\omega^* + i\nu_{||}}{\bar{\omega} + i\nu_{||}}\tilde{\phi}^* \tag{3.15}$$

Where,

$$\omega^* = k_y V_d = k_y \frac{k_B T_e}{eBL_n}, \nu_{||} = k_z^2 \frac{k_B T_e}{m_e \nu_e}, \tilde{\phi}^* = \frac{e\tilde{\phi}}{k_B T_e}$$

On the other hand, linearizing the momentum equation for the ions, we have,

$$-i(\omega + i\nu_i)\tilde{v}_{ix} - \omega_{ci}\tilde{v}_{iy} = -\frac{e}{m_i}(ik_x)\tilde{\phi}$$

and

$$-i(\omega + i\nu_i)\tilde{v}_{iy} + \omega_{ci}\tilde{v}_{ix} = -\frac{e}{m_i}(ik_y)\tilde{\phi}$$

Let's write, $\omega + i\nu_i = \omega_0$, then the above two equations can be written as,

$$i\omega_0\tilde{v}_{ix} + \omega_{ci}\tilde{v}_{iy} = \frac{e}{m_i}(ik_x)\tilde{\phi}$$

and

$$\omega_{ci}\tilde{v}_{ix} - i\omega_0\tilde{v}_{iy} = -\frac{e}{m_i}(ik_y)\tilde{\phi}$$

Solving the above two equations for $\tilde{v}_{ix}$ and $\tilde{v}_{iy}$, we have,

$$\tilde{v}_{ix} = \frac{e}{m_i}\frac{k_x\omega_0 + ik_y\omega_{ci}}{\omega_0^2 - \omega_{ci}^2}\tilde{\phi} \tag{3.16}$$

and

$$\tilde{v}_{iy} = -\frac{e}{m_i}\frac{-k_y\omega_0 + ik_x\omega_{ci}}{\omega_0^2 - \omega_{ci}^2}\tilde{\phi} \tag{3.17}$$

Linearizing the continuity equation for the ions, we get,

$$-i\omega\frac{\tilde{n}_i}{n} + i(k_x\tilde{v}_{ix} + k_y\tilde{v}_{iy} + k_z\tilde{v}_{iz}) + \frac{1}{n}\frac{dn}{dx}\tilde{v}_{ix} = 0$$

Substituting the expressions for $\tilde{v}_{ix}$ and $\tilde{v}_{iy}$ from equations (3.16) and (3.17) into the above equation, we get,

$$\frac{\tilde{n}_i}{n} = [\frac{\omega_0 c_s^2(k_x^2 + k_y^2)}{\omega(\omega_0^2 - \omega_{ci}^2)} + \frac{k_z^2 c_s^2}{\omega\omega_0} - \frac{i}{L_n}\frac{(k_x\omega_0 + ik_y\omega_{ci})c_s^2}{\omega(\omega_0^2 - \omega_{ci}^2)}]\frac{e\tilde{\phi}}{k_B T_e} \tag{3.18}$$

Here, $c_s^2 = \frac{k_B T_e}{m_i}$, and if we write $k_x^2 + k_y^2 = k_\perp^2$, then we finally have for the ion fluid,

$$\frac{\tilde{n}_i}{n} = [\frac{k_\perp^2 c_s^2}{\omega_0^2 - \omega_{ci}^2}\frac{\omega_0}{\omega} + \frac{k_z^2 c_s^2}{\omega\omega_0} - \frac{ik_x}{L_n}\frac{c_s^2}{\omega_0^2 - \omega_{ci}^2}\frac{\omega_0}{\omega} + \frac{k_y}{L_n}\frac{c_s^2}{\omega_0^2 - \omega_{ci}^2}\frac{\omega_{ci}}{\omega}]\tilde{\phi}^* \tag{3.19}$$

Now, assuming quasi-neutrality condition, we have,

$$\frac{\tilde{n}_i}{n} = \frac{\tilde{n}_e}{n}$$

or,

$$\frac{k_\perp^2 c_s^2}{\omega_0^2 - \omega_{ci}^2}\frac{\omega_0}{\omega} + \frac{k_z^2 c_s^2}{\omega\omega_0} - \frac{ik_x}{L_n}\frac{c_s^2}{\omega_0^2 - \omega_{ci}^2}\frac{\omega_0}{\omega} + \frac{k_y}{L_n}\frac{c_s^2}{\omega_0^2 - \omega_{ci}^2}\frac{\omega_{ci}}{\omega} = \frac{\omega^* + i\nu_{||}}{\bar{\omega} - i\nu_{||}}$$

or,

$$\frac{k_\perp^2 c_s^2/\omega_{ci}^2}{\frac{\omega_0^2}{\omega_{ci}^2}-1}+\frac{k_y c_s^2/\omega_{ci}^2}{L_n}\frac{\omega_{ci}/\omega}{\frac{\omega_0^2}{\omega_{ci}^2}-1}=\frac{\omega^*+i\nu_{||}}{\bar{\omega}-i\nu_{||}}$$

or,

$$\frac{b\omega_0}{\omega}-\frac{\omega^*}{\omega}=\frac{\omega^*+i\nu_{||}}{\omega+i\nu_{||}}(\frac{\omega_0^2}{\omega_{ci}^2}-1) \tag{3.20}$$

Let us remember that $\omega_0 = \omega + i\nu_i$ and $\nu_{||} = k_z^2\frac{k_B T_e}{m_e \nu_e}$. In absense of collisions, $\omega_0 = \omega$ and the value of $\nu_{||}$ is very high. Then, equation (3.20) becomes:

$$b-\frac{\omega^*}{\omega}=\frac{\omega^2}{\omega_{ci}^2}-1$$

or,

$$\omega^3-\omega(\omega_{ci}^2+k^2c_s^2)-\omega_e^*\omega_{ci}^2=0 \tag{3.21}$$

Now, simplifying the algebraic equation (3.20), we finally arrive at the following dispersion relation:

$$(\frac{\omega^*+i\nu_{||}}{\omega_{ci}^2})\omega^3+[\frac{2i\nu_i(\omega^*+i\nu_{||})}{\omega_{ci}^2}-b]\omega^2-[i\nu_{||}(1+b)+i\nu_i b-\omega_1 b+\frac{\nu_i^2(\omega^*+i\nu_{||})}{\omega_{ci}^2}]\omega$$
$$+\nu_{||}(b\nu_i+i\omega^*)-\omega_1(\omega^*-ib\nu_i)=0$$

or,

$$A\omega^3+B\omega^2-C\omega+D=0 \tag{3.22}$$

. where

$$A=\omega^*+i\nu_{||}, B=2i\nu_i(\omega^*+i\nu_{||})$$

$$C=i\nu_{||}(1+b)+i\nu_i b-\omega_1 b+\nu_i^2(\omega^*+i\nu_{||})$$

$$D=(i\nu_{||}-\omega_1)(\omega^*-ib\nu_i)$$

with

$$\nu_{\parallel} = \frac{k_z^2 T_e}{m_e \nu_e}, b = k_{\perp}^2 \rho^2, \omega_1 = k_\theta \frac{E}{B}$$

$$\rho^2 = \frac{k_B T_e}{eB\omega_{ci}}, \omega^* = -k_\theta \frac{k_B T_e}{eBL_n}, k_{\perp} = k_\theta = \frac{m}{r}$$

with ω, ν_i, $\nu_{\parallel}$, ω^* and ω_1 all normalized by ω_{ci}. Here ω is the mode frequency, ν_e and ν_i are the electron-neutral and ion-neutral collision frequency, respectively, ρ is the ion gyroradius at the electron temperature, k_B is the Boltzmann constant, b is a measure of the finite ion inertia effects perpendicular to B, ω_1 is the $\mathbf{E} \times \mathbf{B}$ frequency.

3.4.3 Discussion of the Theoretical Results

Equation (3.22) is a cubic equation that has three roots, only one of which gives the proper real part (the real frequency with the sign indicating the direction of the electron diamagnetic drift) and a positive imaginary part (i.e. the growth rate) which is relevant to our experimental findings. The parameters used to solve the equation have been obtained from the experimentally measured density profiles and the values of B_z. A typical value of frequency obtained from eqn. (22) is $\omega = (-10.13 + i1.95)$ kHz for the input parameters: $\nu_{\parallel} = 32.4$ MHz, $\nu_i = 8$ kHz. The growth rate ω_I varies significantly only with $\nu_{\parallel}$, and negligibly with ν_i and the $\mathbf{E} \times \mathbf{B}$ frequency ω_1. This implies that it is the electron-neutral collisions that drive the mode unstable. Also, since ω_I does not vary with ω_1, it also justifies the argument in assumption (e) above.

Since the density profile evolves from a peaked to a hollow profile with the transition occurring around $z = 3$ cm, the direction of the density gradient changes sign over this region. Experimentally obtained values of phase velocity indicate that the mode propagates azimuthally in the direction of v_{de} (corresponding to the peaked profile) at all the axial locations from $z = 1$ to 16 cm. This observation gives the indication about the location of the mode excitation being close to the entrance aperture. The obtained values of L_n lie in the range of $7 - 12$ cm and do not significantly vary in the radial direction for $z < 3$ cm and $r > 3$ cm. For these values of L_n and the values of B_z lying between $200 - 250$G, the cubic dispersion relation given in equation (3.22) gives one root that has a positive growth rate and the sign of the real frequency indicates that it propagates in the direction of v_{de} when the electron-neutral collisional frequency is assumed to be finite. For $r < 3$ cm, L_n is found to be very high because of the peaked density profiles. Close to the axis (i.e. near $r \sim 0$), this theoretical model then predict negative growth rates, so that the mode excitation is not possible there. These predictions are also consistent with the observation that the large mode amplitudes are obtained for $r \sim 3$ cm as shown in Fig. 3.11b.

It has been seen from the theory that for a given value of B, there is a critical value of L_n, above which ω_I is negative i.e. the mode is not excited for such a case. For $B = 250 - 200$ G (i.e. within the region $z = 1 - 3$ cm),

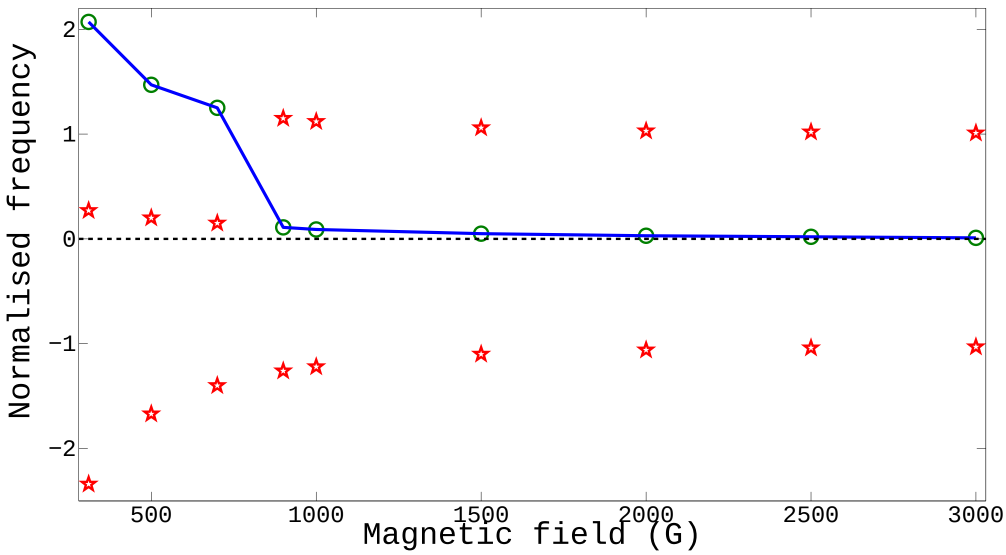

Figure 3.16: **Variation of the mode frequency (normalised by $\omega_{\mathbf{ci}}$) with the magnetic field, obtained from the solutions of equation (3.22) for the argon plasma. The parameters used are as follows: $k_\theta = 0.3$ cm^{-1}, $k_z = 0.1$ cm^{-1}, $L_n = -8$ cm, $T_e = 10$ eV.**

the experimentally obtained value of L_n is below the corresponding critical values (e.g. the critical value of L_n is 10.9 cm for $B = 200$ G), leading to the conclusion that the mode is likely to be excited in this region.

Further, we also attempt to study the variation of the mode frequency with the variation of the system parameters. Now, experimentally, we can vary only two parameters viz. the neutral pressure (and hence ν_e, ν_i) and the magnetic field. If the magnetic field is varied by varying the current in the Helomholtz coils in the source region, the profiles of the plasma density should change and hence the value of L_n also should change. In absence of this data about the variation of L_n for various B, we have assumed L_n to be constant at all the magnetic fields to get the variation of the mode frequency

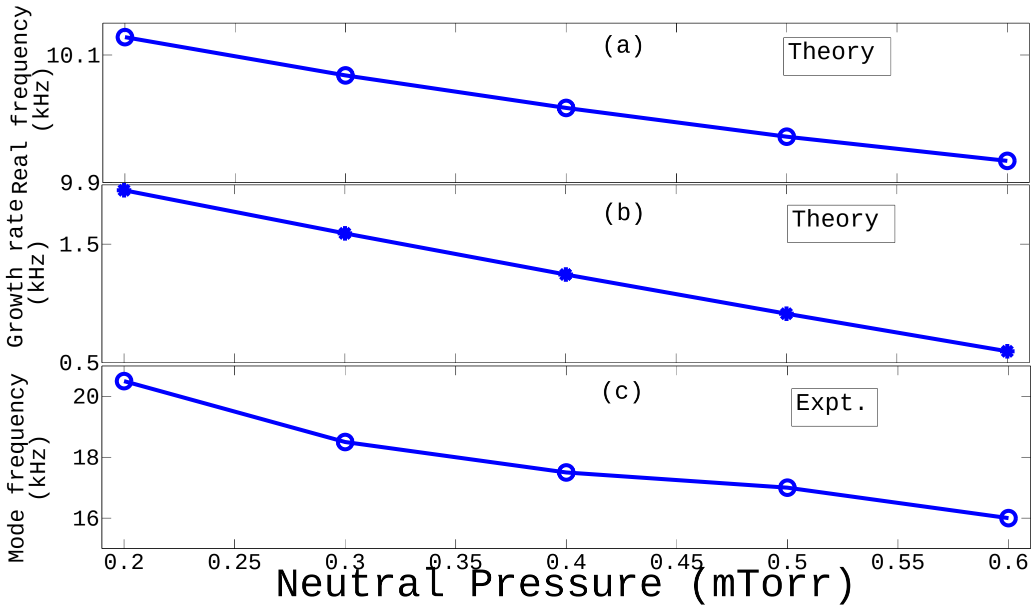

Figure 3.17: **Variation of the mode frequency (a) and the growth rate (b) with neutral pressure as obtained from theory. The experimentally measured mode frequency is shown in panel (c). Parameters used for the theoretical graphs are:** T_e = 10 **eV,** k_θ = 0.5 **cm**$^{-1}$**,** $k_z = 0.1$ **cm**$^{-1}$**,** $B = 200$ **G,** $L_n \sim 10$ **cm.**

with B. Equation (22) has been solved for $B = 300 - 3000$ G and $L_n = -8$ cm. We have found that in the above range of B, only one mode is excited with positive growth rate. The other two branches have negative growth rates and since their real parts are not sensitive to the variation of L_n (for a particular B), we conclude that the two branches with negative growth rates correspond to the ion-cyclotron branch. The mode frequencies (i.e. the real parts of the solutions with positive growth rates, joined by the blue line here) have been plotted against B in Fig. 3.16. It can be seen from this figure that, at the higher magnetic fields ($>$ 800 G), the mode frequencies are much less than ω_{ci} ($\frac{\omega_R}{\omega_{ci}} \sim 0.02 - 0.25$) and these frequencies are sensitive to L_n. It indicates that this branch correspond to the low frequency conventional drift modes. However, as we approach towards the lower magnetic fields (< 600 G), the real parts of the solutions become greater than ω_{ci} ($\frac{\omega_R}{\omega_{ci}} \sim 1.2 - 2.0$). These frequencies are still sensitive to L_n and bear an inverse realtionship with B, showing that they correspond to a new mode of the drift branch which is influenced by the ion-gyro motion. This qualitatively justifies our experimental observations subject to the above assumption of the constancy of L_n.

In Fig. 3.17 we have shown the theoretical results of the variation of the mode frequency and the growth rate with the neutral pressure; also shown in this figure are the experimental findings. It can be seen that the feature that the mode frequency decreases as we increase the neutral pressure is present both in the theory and in the experiments although their numerical values do not have a close correspondence. We believe that this mismatch is due to the use of the local slab model. As has been shown elsewhere [3], a non-local cylindrical model based on the full numerical solution of the drift wave problem in the cylindrical coordinates will give more accurate results on the dependence of the growth rate on various parameters such as the density, magnetic field as well as the azimuthal mode number and also include the effects of the inhomogeneous density profile.

$\mathbf{E} \times \mathbf{B}$ drift of the electrons i.e. ω_1 (~ 1 MHz) term in equation (3.22) is much smaller compared to $\nu_{\parallel}$ (~ 30 MHz) and hence does not play any role in the growth rate. Also, the variation of the growth rate with ν_i (~ 4

kHz) is negligible. So, we conclude that the collisions of the electrons with the neutrals is responsible for driving the mode unstable.

Bibliography

[1] B. Lenhert, Plasma Phys. 9, 301(1967).

[2] S.K. Saha, S. Raychaudhuri, S. Chowdhury, M.S. Janaki, and A.K. Hui, Phys. Plasmas 19, 092502 (2012).

[3] S.K. Saha, S. Chowdhury, M.S. Janaki, A. Ghosh, A.K. Hui, and S. Raychaudhuri, Phys. Plasmas 21, 043502 (2014).

[4] A. Ghosh, S.K. Saha, S. Chowdhury, and M.S. Janaki, Phys. Plasmas 22, 122111 (2015).

[5] C. Charles, Appl. Phys. Lett. 96, 051502 (2010).

[6] S. Rao and N. Singh, Phys. Plasmas 19, 093507 (2012).

[7] K. Takahashi, C. Charles, and R. W. Boswell, Phys. Rev. Lett. 110, 195003 (2013).

[8] E. Y. Wang, N. Hershkowitz, T. Intrator, and C. Forest, Rev. Sci. Instrum. 57, 2425 (1986).

[9] K. Takahashi, C. Charles, R. Boswell, W. Cox, and R. Hatakeyama, Appl. Phys. Lett. 94, 191503 (2009).

[10] N. Singh, S. Rao, and P. Ranganath, Phys. Plasmas 20, 032111 (2013).

[11] C. Charles and R. Boswell, Appl. Phys. Lett. 82, 1356 (2003).

[12] S. L. Cartier and R. L. Merlino, Phys. Fluids 30, 2549 (1987).

[13] K. Takahashi and T. Fujiwara, Appl. Phys. Lett. 94, 061502 (2009).

[14] C. S. Corr, N. Plihon, P. Chabert, O. Sutherland, and R. W. Boswell, Phys. Plasmas 11, 4596 (2004).

[15] R. F. Ellis, E. Marden-Marshall, and R. Majeski, Plasma Phys. 22, 113 (1980); E. Marden-Marshall, R. F. Ellis, and J. E. Walsh, Plasma Phys. Control. Fusion 28, 1461 (1986).

[16] L. Zhang, Plasma Phys. Control. Fusion 34, 501 (1992).

[17] D. L. Jassby, Phys. Fluids 15, 1590 (1972).

[18] C. Schroeder, O. Grulke, T. Klinger, and V. Naulin, Phys. Plasmas 12, 042103 (2005).

[19] A. B. Mikhailovskii and A. V. Timofeev, Sov. Phys. JETP 17, 626 (1963).

[20] S. Ichimaru, Basic Principles of Plasma Physics: A Statistical Approach, Westview Press, 1973.

[21] J. Vranjes and S. Poedts, A & A 482, 653 (2008).

[22] R.F. Post and M.N. Rosenbluth, Phys. Fluids 9, 730 (1966).

[23] H. Akiyama and S. Takeda, J. Phys. Soc. Japan 43, 1739 (1977).

Chapter 4

Experimental and Theoretical Studies of Fluctuations in Helium Plasma

4.1 Introduction

In the previous chapter we have discussed the excitation of resistive upper drift modes in an argon plasma [1] with the modes having $\omega \gtrsim \omega_{ci}$. As has been argued there, these high frequency drift modes are different from the ICDW or DCLC which occur in the same frequency range. It has also been mentioned in the introductory chapter (Sec. 1.3) that the ICDW or DCLC are kinetic modes generated due to the anistropy in the velocity distribution functions and where the condition $k_\perp^2 \rho_i^2 >> 1$ is satisfied (i.e. for these kinetic modes, the ion-Larmor radius is always greater than the wavelength). Unlike these kinetic modes, we have seen that the upper drift modes are resistive drift modes excited in the long wavelength region (i.e. for this case $k_\perp^2 \rho_i^2 < 1$). Conventional drift modes reported in the existing literature have $\omega << \omega_{ci}$. So, the observations of resistive drift waves in the high frequency regime is a novel phenomenon which has not been explored before. These results in argon plasma warrant a further investigation of the characteristics of such modes when the ion Larmor radius is further reduced. For this purpose, a lighter gas, such as helium, has been used. As a result, the ion Larmor radius is smaller than that of argon and therefore $k_{\perp}\rho_i$ is expected to be smaller.

In the present chapter (bulk of which is based on the published article [2]), we will discuss the results obtained from experiments conducted in helium plasma. As noted in the previous chapter, a thorough study of the instabilities requires that we have detailed informations about the equillibrium characteristics of the plasma. A brief discussion of the plasma density and potential profiles has been presented, followed by the detailed study of the simultaneous excitation of two resistive upper drift modes which has been termed as the dual upper drift modes. The chapter has been concluded with a discussion on the non-linear interaction of the dual upper drift modes.

4.2 Time Averaged Plasma Density and Potential Profiles

Since the density and potential profiles in helium plasma show similar characteristics to the argon plasma, we have shown here the radial variation of the plasma potential and density only at some selected axial locations relevant to the studies of the instabilities.

The time averaged radial variation of the plasma density, measured using the RF-compensated LP, has been shown in Fig. 4.1 at three axial positions,

$z = 1, 8$ and 12 cm. The experiments have been conducted under the following conditions: neutral gas pressure $p = 0.4$ mtorr, RF power = 300 W and the magnetic field B_z (at $z = 0$) = 238 G (which corresponds to a current of 7 A through the Helmholtz coils). It has been seen that, near the entrance aperture ($z \sim 1$ cm), the density profile is peaked on the axis. But after $z \geq 5$ cm, it starts becoming hollow with its minimum located on the axis. The off-axis maxima lie on the magnetic field line diverging from the radial edge of the entrance aperture.

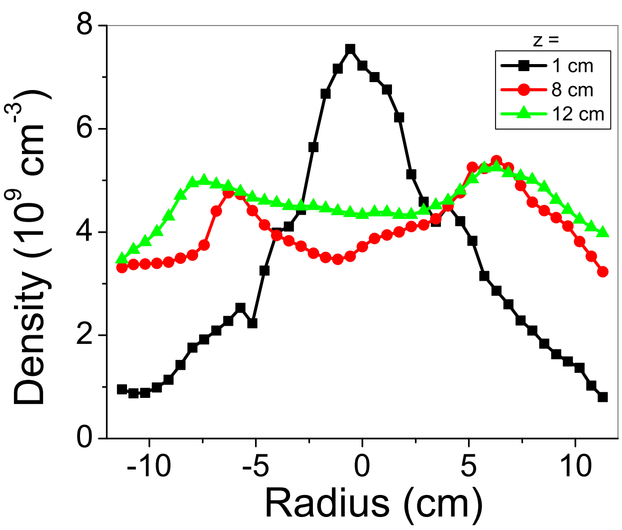

Figure 4.1: **Radial variation of the plasma density measured by a RF-compensated LP at $p = 0.4$ mTorr, $B_z(z = 0) = 238$ G and RF power = 300 W at three axial positions, $z = 1, 8, 12$ cm as indicated by the legends. The error bar in the plasma density is $\pm 2\%$ from several measurements.**

The radial variation of the plasma potential, measured using the emissive probe under the same plasma conditions as above, has been shown at three

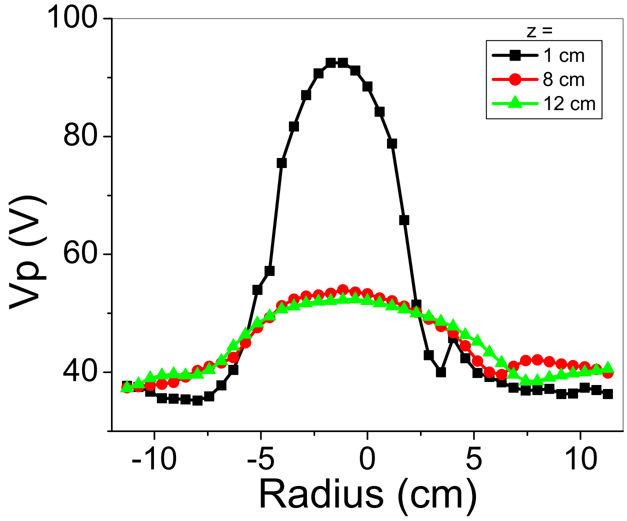

Figure 4.2: **Radial variation of the plasma potential measured by the EP at p = 0.4 mTorr, $B_z(z = 0) = 238$ G and RF power = 300 W at three axial positions, $z = 1, 8, 12$ cm as indicated by the legends. The error bar in the plasma potential is $\pm 0.5\%$ V from several measurements.**

axial locations $z = 1, 8$ and 12 cm (Fig. 4.2). It can be seen that the plasma potential is peaked with the maximum at the centre and it decreases as we go radially outwards with the minima around those radial locations where the density have maxima. The physics behind such density and potential profiles have been already been discussed in the previous chapter (Sections 3.2.1, 3.2.2 and 3.2.4).

4.3 Study of the Instabilities

4.3.1 General Observations

Time series data of the fluctuations in the floating potential and the ion saturation current have been recorded in the expansion chamber of the DLX using the same Yokogawa DL 1640 oscilloscope for a time span of 100 ms and the data has been sampled at 1 MHz giving a data length of 100k. The time series has been analysed by the same MATLAB programme developed for the argon plasma and the dominant peaks in the power spectrum have been detected. Two peaks with frequencies near 30 kHz and 50 kHz, respectively, can be seen in the power spectrum of $\tilde{\phi}_f$ indicating two unstable modes which exist throughout the whole axial and radial regions (Fig. 4.3 and 4.4a). A typical analysis of the floating potential fluctuations ($\tilde{\phi}_f$) recorded simultaneously using two uncompensated LPs separated in the azimuthal direction has been shown in Fig. 4.4. Figure 4.4b shows the variation of the phase angle between the two signals with frequency. This variation is linear with frequency up to ~ 100 kHz, showing that both the peaks are modes propagating in the azimuthal direction. The direction of propagation coincides with the direction of the electron diamagnetic drift (see next section). Figure 4.4c shows that the two simultaneously recorded fluctuations are strongly correlated at the frequencies where the power is maximum, i.e. both of them are coherent modes. Like our previous case, all measurements of the wave characteristics using Langmuir probes have been made in the expansion chamber mainly for $z \geq 8$ cm, thereby avoiding the zone where the RF interference is likely to influence the fluctuation measurements.

In addition to the above two dominant frequencies, two more frequency peaks with low power have been observed in a narrow radial region $r \sim 3.2-4.3$ cm. The bispectrum analysis indicate that these two seconary modes have been generated due to the non-linear inteaction of the two primary modes mentioned above, details of which will be discussed later.

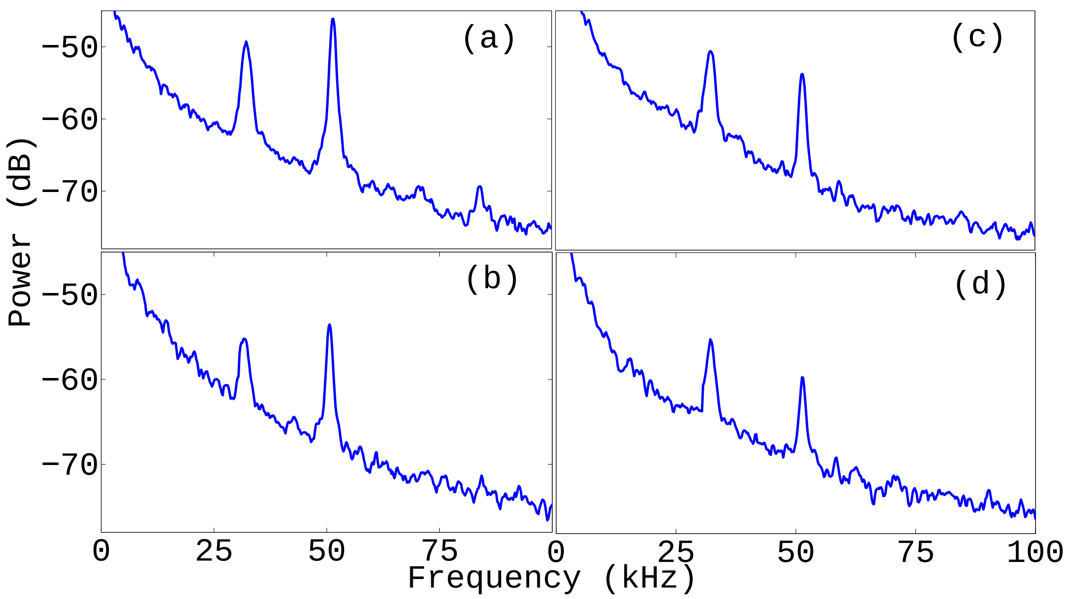

Figure 4.3: **Frequency spectra of the floating potential fluctuations recorded using a single uncompensated LP showing the simultaneous presence of two peak frequencies at positions: (a)** $z = 1$ **cm,** $r = 3.0$ **cm; (b)** $z = 12$ **cm,** $r = 3.0$ **cm; (c)** $z = 4$ **cm,** $r = 2.0$ **cm; (d)** $z = 4$ **cm,** $r = 6.0$ **cm**

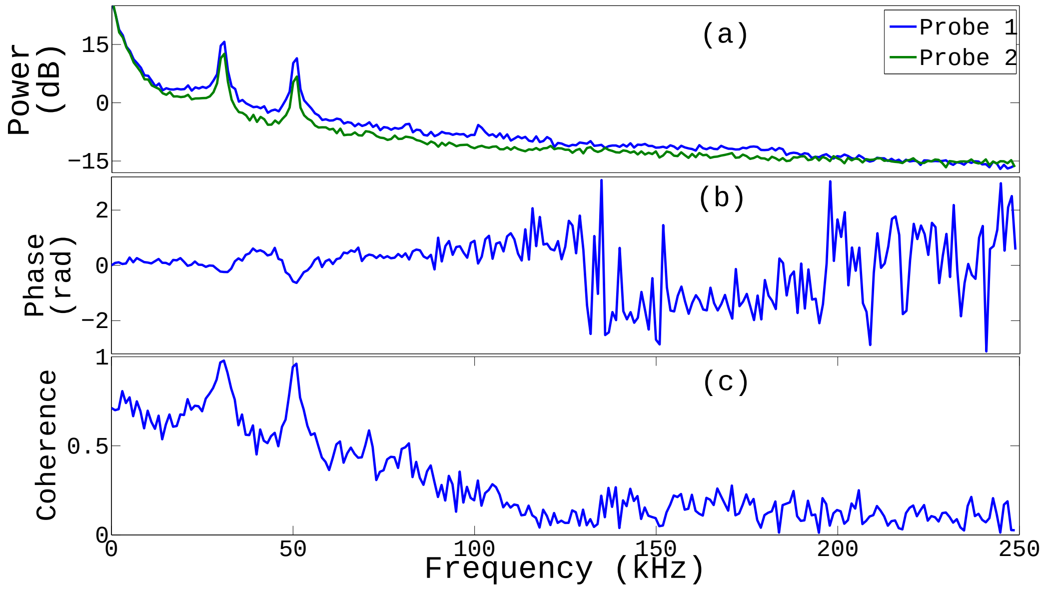

Figure 4.4: **Frequency spectra of the fluctuation power (a), the phase difference (b) between the signals from the two azimuthally separated probes and the coherence (c) between them. The two signals have been recorded at $z = 12$ cm, $r = 3.0$ cm, $p = 0.4$ mtorr, RF power $= 300$ W. The dominant peaks from the top row are 31 kHz and 52 kHz, respectively.**

4.3.2 Identification of the Instability

To identify these two simultaneous modes, we have followed the same procedures as in the previous chapter.

(i) As can be seen from Fig. 4.5, the fluctuation amplitudes for both the modes are maximum around the region where the density gradient is high. Since the electron temperature varies weakly this suggests that the modes are driven by the density gradient.

(ii) The mode numbers of the azimuthal propagation have been determined from Fig. 4.6. To obtain this figure, one LP has been fixed at $r = 3.0$

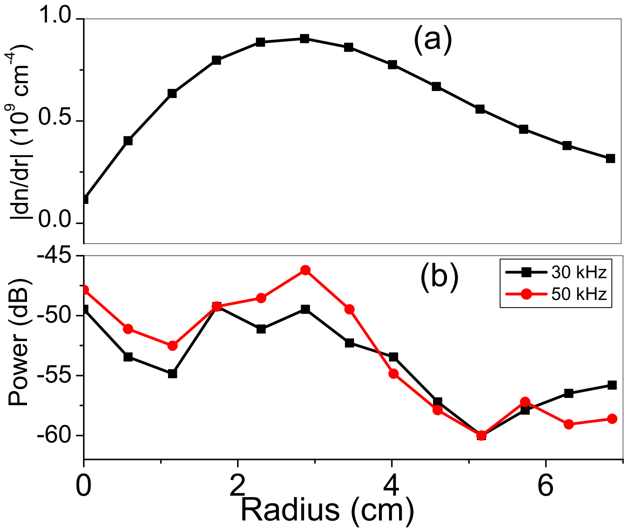

Figure 4.5: **Radial variation of (a) the density gradient $\frac{dn}{dr}$ obtained from the density profile of Fig. 4.1 and (b) the power at each frequency peak obtained from the FFT of $\tilde{\phi}_f$. Both the profiles are obtained at $p = 0.4$ mtorr, $B_z(z = 0) = 238$ G, RF power $= 300$ W and $z = 1$ cm.**

cm and another LP has been rotated azimuthally at the same radius (see Sections 2.2.2 and 3.3.2), thus varying the azimuthal separation between them. Floating potential fluctuations have been recorded simultaneously using these two LPs for each azimuthal separation. Employing the MATLAB programme, the phase difference (Φ) between the two signals has been obtained and plotted against the azimuthal separation (θ) in Fig. 4.6. We can see from this figure that the 31 kHz mode propagates with mode number $m = 1$, while the 52 kHz mode propagates with $m = 2$. The values of the azimuthal wave numbers have been calculated using equation (3.1) where the factor $\frac{\Phi}{\theta}$ has been taken as the slope of the linear fits for the respective frequencies. The typical values of k_{theta} have been shown in Table-4.1.

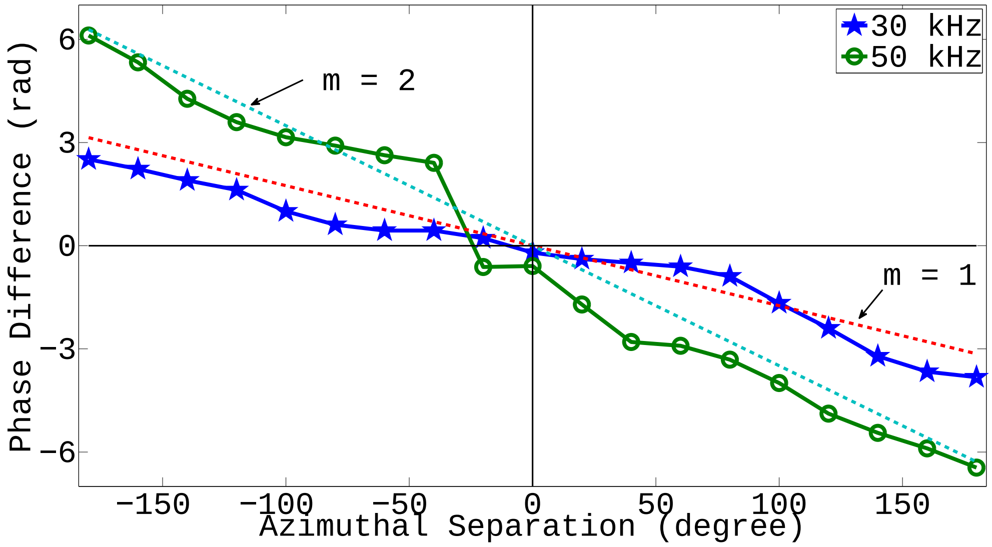

Figure 4.6: **The phase difference plotted against the azimuthal separation. The plasma conditions are the same as in Fig. 4.1. The plot for the ideal $m = 1$ and $m = 2$ lines have been shown by the dashed lines.**

(iii) The four-LP system has been employed to measure any phase difference between the density and floating potential fluctuations at the same location (see Sections 2.2.2 and 3.3.2). We have found this phase difference to be $\sim 2.3^c$ with the density fluctuations leading in phase although the theoretically predicted value under the present experimental conditions is $\sim 0.9^c$. As has been discussed in the previous chapter (see equation 3.15), this result is an indication of the dual modes being the resistive drfit type.

(iv) Figure 4.7 shows the axial propagation of both the modes. To obtain this result, two uncompensated LPs have been used after proper electric alignment (Fig. 2.8, Sec. 2.2.2) to ensure that both the LPs lie on the

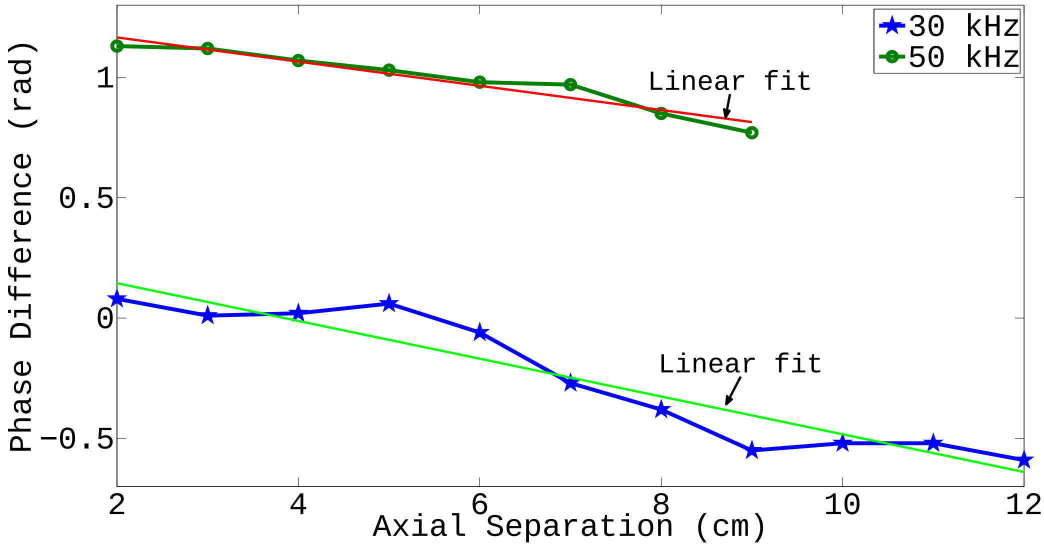

Figure 4.7: **The axial phase difference plotted against the axial separation for $r = 0$ cm and the same plasma conditions as in Fig. 4.1. The axial wave number has been calculated from the slope of the linear fits.**

same axial magnetic field line. One LP has been fixed at $z = 25$ cm, while the other LP was moved axially outwards from $z = 7$ cm in step of 1 cm. For each axial separation, floating potential fluctuations have been recorded simultaneously using the two electrically aligned LPs and using the same MATLAB programme, the phase difference ($\Delta\phi$) corresponding to each axial separation (Δz) has been obtained. The typical values of λ_z (and hence k_z) obtained from the slopes of the liner fits have been shown in Table-I. It can be seen that $\lambda_z \sim 2.0 \times L$ (where $L = 50$ cm is the length of the expansion chamber). We also find that $k_\theta \sim 3 \times k_z$ for the 31 kHz mode and $k_\theta \sim 12 \times k_z$ for the 52 kHz mode, i.e the waves are propagating predominantly along the azimuthal direction with a weak component along the axial direction.

Electron Temperature T_e	14.0 eV
Ion Temperature T_i	0.2 eV
Ion Gyrofrequency f_{ci}	94 kHz
Ion Larmor Radius ρ_i	0.42 cm
Density Gradient Scale Length L_n	$\sim$ 5.5 cm
Wave Phase Velocity (from expt.) v_{phase}	$\sim 5.0 \times 10^5$ cm/s
Ion Sound Speed	$\sim 2 \times 10^6$ cm/s
Azimuthal Wave Number k_θ for 31 kHz	0.32 cm^{-1}
Azimuthal Wave Number k_θ for 52 kHz	0.68 cm^{-1}
Axial Wave Number k_z and Axial Wavelength λ_z for 31 kHz	0.08 cm^{-1}, $\sim$ 80 cm
Axial Wave Number k_z and Axial Wavelength λ_z for 52 kHz	0.05 cm^{-1}, $\sim$ 125 cm

Table 4.1: **Parameters of the plasma for $B = 238$ G (at $z = 0$ cm), $p = 0.4$ mTorr, and RF power = 300 W.**

4.4 Theory: Excitation of Two Simultaneous Modes

Figure 4.5 shows that the mode amplitudes for both the $m = 1$ and $m = 2$ modes peak at the radial locations which coincide approximately with the location of the maximum density gradient. Also, the direction of the azimuthal propagation at all axial positions coincides with the electron diamagnetic drift direction corresponding to the peaked profile of the density. These two features suggest that the drift waves are excited close to the source region ($z \sim 0 - 3$ cm). In this region, the ion cyclotron frequency (ω_{ci}) varies from 100 kHz to 80 kHz while the two observed drift wave frequencies are always nearly at 30 and 50 kHz, respectively. A theoretical analysis of such experimental results in argon plasma (i.e. modes in the range of frequencies $\omega \sim \omega_{ci}$) has already been carried out in the previous chapter in slab geometry which led to a cubic dispersion relation. The solutions of that equation using experimentally determined parameters in helium plasma show that two distinct modes are driven unstable by the electron-neutral collisions. This last result is consistent with the observation of the phase difference between the density and potential fluctuations measured for these modes.

The characteristics observed experimentally along with the theoretical results suggest that both the upper drift and the dual upper drift modes are a new class of resistive drift modes found in the frequency regime $\omega \sim \omega_{ci}$.

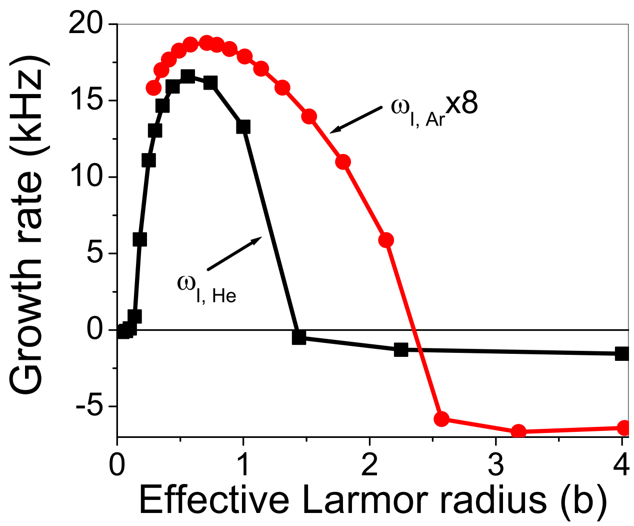

Figure 4.8: **Variation of the growth rates with the effective Larmor radius, obtained from the solutions of equation (3.22). The growth rates of Ar has been multiplied by 8. Parameters used are: (a)** $B = 180$ **G,** $L_n = 5.0$ **cm for He; and (b)** $B = 180$ **G,** $L_n = 10.0$ **cm for Ar.**

With the effective Larmor radius (b) as a parameter, equation (3.22) has been solved to obtain the growth rates for both the upper drift and the dual upper drift modes for argon and helium plasma, respectively. The results have been shown in Fig. 4.8. It can be seen that a mode is excited only at some limited values of b. This figure indicates that the growth rate (ω_I) is maximum around the same value of b for both the gases. Now, since $b = k_\perp^2 \rho^2 = \frac{m^2}{r^2}\rho^2$ and the ion Larmor radius of helium (ρ_{He}) is lower than that of argon (ρ_{Ar}), at a certain radius, only the lower mode numbers will be excited for the argon plasma. The same conclusion can be arrived at following Fig. 1 of Ellis et. al.(1980) [3].

A natural question arises that why two simultaneous modes have not been observed in the argon plasma. For helium plasma, the present experimental observation reveals the presence of two drift modes with different azimuthal mode numbers and frequencies simultaneously at the same radial location. Figure 4.9a shows the radial variation of the growth rates for two mode numbers, $m = 1$ and 2 obtained from the same cubic dispersion relation for He. Clearly, there is a region ($r \sim 5.5 - 7.0$ cm) where the growth rates of both the modes are significantly high and hence, in this region both the modes can be excited simultaneously. On the other hand, it can be seen from Fig. 9b that this overlapping region ($r > 9.0$ cm) lies at radial locations where the plasma density and its gradient are both very weak, and hence outside the region of our experimental interest. Therefore, at no radial location, simultaneous excitation of two modes is possible for argon plasma. This is in qualitative agreement with the experimental observations for both the gases. As explained earlier, the parameters of the helium plasma, particularly the small value of the ion Larmor radius seem to make it feasible for the excitation of two simultaneous azimuthal modes at the same radial location.

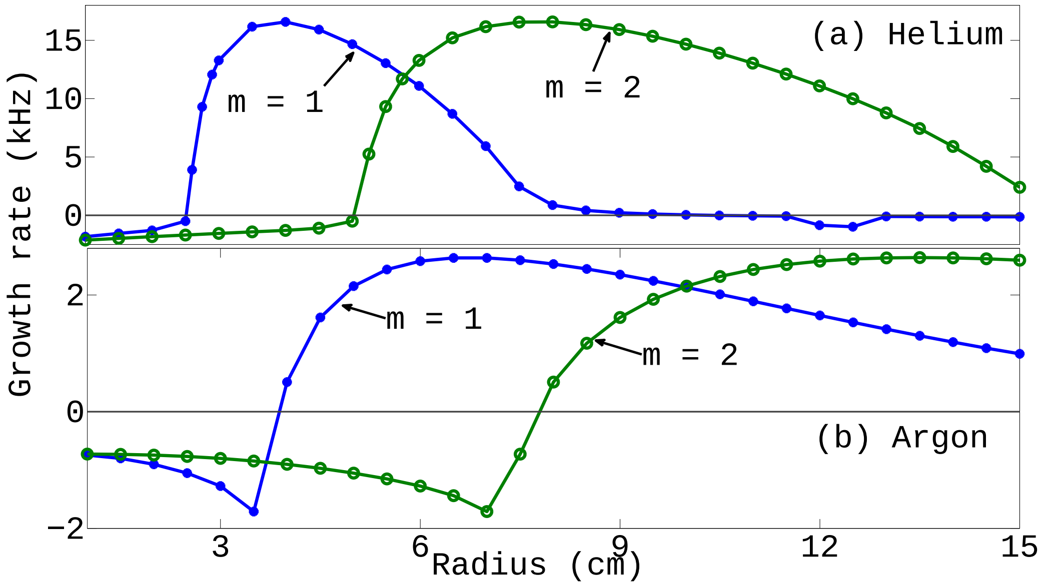

Figure 4.9: **Growth rates of the drift waves obtained at different radii by solving equation (3.22).**

4.5 Nonlinear Interaction of the Dual Drift Modes

The role played by the nonlinear interaction of multiple drift modes in the turbulence and transport phenomena in plasma has been illustrated by both theoretical and experimental works [4, 5, 6, 7, 8, 9] in the low frequency regime ($\omega << \omega_{ci}$). In earlier sections of the present chapter we have discussed the existence of self-excited resistive dual upper drift modes with observed frequencies of 31 kHz and 52 kHz (henceforth designated as primary modes **A** and **B**, respectively) in RF produced magnetized helium plasma.

Contrary to the generally reported frequency regime for the drift waves, both these modes **A** and **B** are high frequency ones (i.e. $\omega \sim \omega_{ci}$). In this section, we will discuss the existense of two other secondary modes with frequencis 62 kHz and 83 kHz (henceforth designated as secondary modes **C** and **D**, respectively), whose characteristics suggest that they have been generated via nonlinear interaction of the two primary modes **A** and **B**.

When energy transfer occurs between the waves in a three-wave coupling described by the Hasegawa-Mima equation [5], the existence of non-linear interaction can be established by the bi-spectral analysis [10, 11]. In such cases, it has been predicted that the relationships between the wavenumbers and the frequencies of the three interacting modes are: (a) $k_3 = k_1 + k_2$ or, $m_3 = m_1 + m_2$ since $k = \frac{m}{r}$ and the interaction occurs at radius r, and, (b) $\omega_3 = \omega_1 + \omega_2$. Here, the secondary mode (denoted by the subscript '3') has been generated by the non-linear interaction of the two primary modes (denoted by the subscripts '$1'$ and '$2'$). These matching conditions have been predicted for the non-linear interaction between the low frequency conventional drift waves where $\omega << \omega_{ci}$ is satisfied. We have found that the same matching conditions are satisfied in the nonlinear interaction of the dual upper drift modes (where we have $\omega \leq \omega_{ci}$). We will see that the nonlinear interactions occur in the region where the amplitudes of the primary modes are maximum.

The present experiments have been conducted in DLX under the following conditions: neutral gas pressure = 0.4 mTorr, RF power = 300 W and

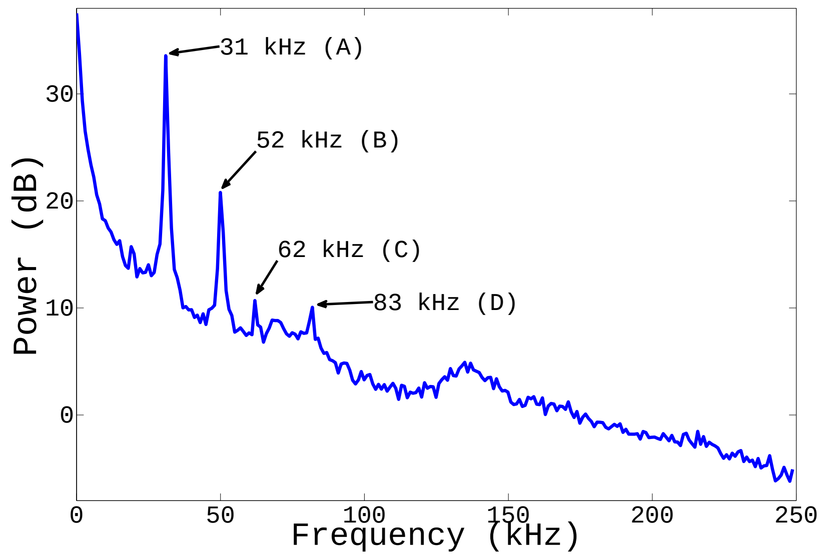

Figure 4.10: **Frequency spectrum of the floating potential fluctuations showing the simultaneous presence of two primary peaks (i.e. A and B) along with the two secondary peaks (i.e. C and D) at $z = 5$ cm, $r = 3.7$ cm. The experimental conditions are same as in Fig. 4.1.**

magnetic field $B_z = 238$ G (at $z = 0$ cm). A typical variation of the power spectrum obtained from the time series data of the floating potential fluctuations measured using an uncompensated LP, has been shown in Fig. 4.10 at $z = 5$ cm, $r = 3.7$ cm. Two large amplitude primary frequency peaks exist at 31 kHz and 52 kHz, which have already been identified as the resistive upper drift modes. It can be seen that two secondary peaks at 62 kHz and 83 kHz are also present. It is interesting to note that these two secondary peaks are detected only within a narrow radial region of $r \sim 3.2 - 4.2$ cm where the amplitudes of the primary modes are maximum (Fig. 4.5b).

To determine the azimuthal mode numbers of the two secondary modes,

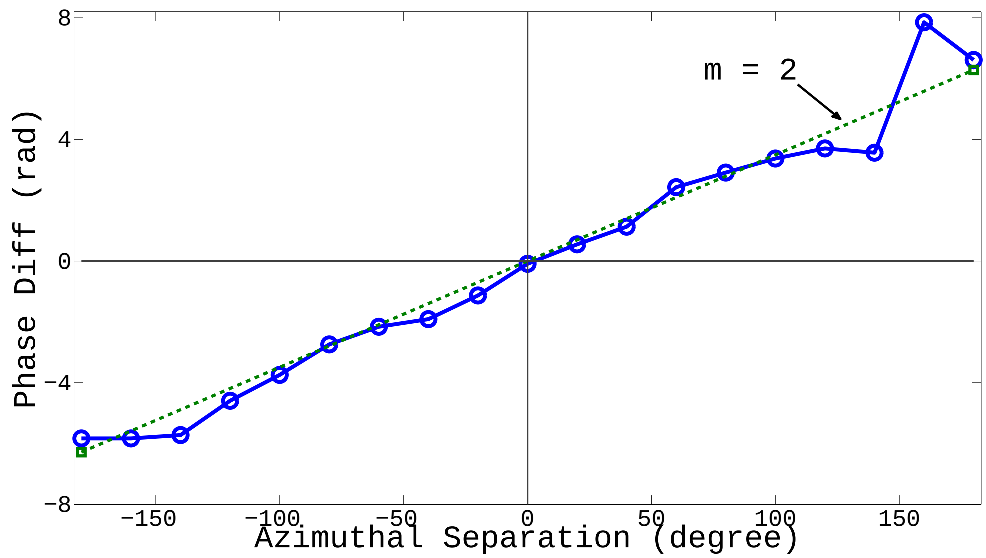

(a)

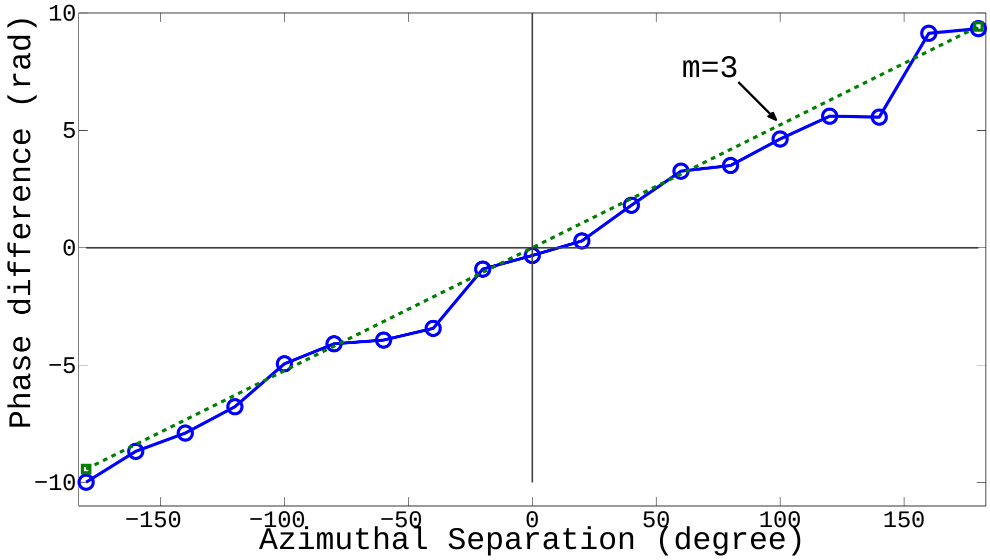

(b)

Figure 4.11: **The phase difference plotted against the azimuthal separation for (a)** 62 **kHz mode, and (b)** 83 **kHz mode. The plasma conditions are the same as in Fig. 4.1. The plots for the ideal** $m = 2$ **and** $m = 3$ **have been shown by the dashed lines.**

floating potential fluctuations have been measured simultaneously using two Langmuir probes; one probe has been fixed at a radius $r = 3.7$ cm while the second LP has been rotated azimuthally at the same radius in steps of 20^0, being kept at the same axial location. At each azimuthal separation, $\tilde{\phi}_f$s have been recorded simultaneously. From these time series data, the phase difference corresponding to each azimuthal separation has been obtained following the same method as has been described in Sec. 3.3.2. The results thus obtained have been shown in Fig. 4.11. It has already been shown in Fig. 4.6 that the primary 31 kHz mode propagates with mode no. $m = 1$ while the 52 kHz mode propagates with mode no. $m = 2$. For the secondary modes, it can been seen from Fig. 4.11a that the 62 kHz mode propagates with $m = 2$ while Fig. 4.11b shows that the 84 kHz mode propagates with $m = 3$.

Let us assign the frequency and the wave numbers to the various modes as follows: $(\mathbf{A} : 31, 1)$, $(\mathbf{B} : 52, 2)$, $(\mathbf{C} : 62, 2)$ and $(\mathbf{D} : 84, 3)$. Then it can be seen that, for the mode **C**, we have, $\omega_C = \omega_A + \omega_A$ and $m_C = m_A + m_A$. Similarly, for the mode **D**, we have, $\omega_D = \omega_A + \omega_B$ and $m_D = m_A + m_B$ i.e. the secondary peaks **C** and **D** satisfy the frequency and the wave number matching conditions stated earlier. These results suggest that the secondary mode **C** is generated by the self-interaction of the primary mode **A** and **D** is generated via the nonlinear interaction of the two primary resistive drift modes, **A** and **B**. The secondary peaks have been detected only within the narrow region $r \sim 3.2 - 4.3$ cm. It can be seen from Fig. 4.5b that the amplitudes of the primary modes are significant only in the same region.

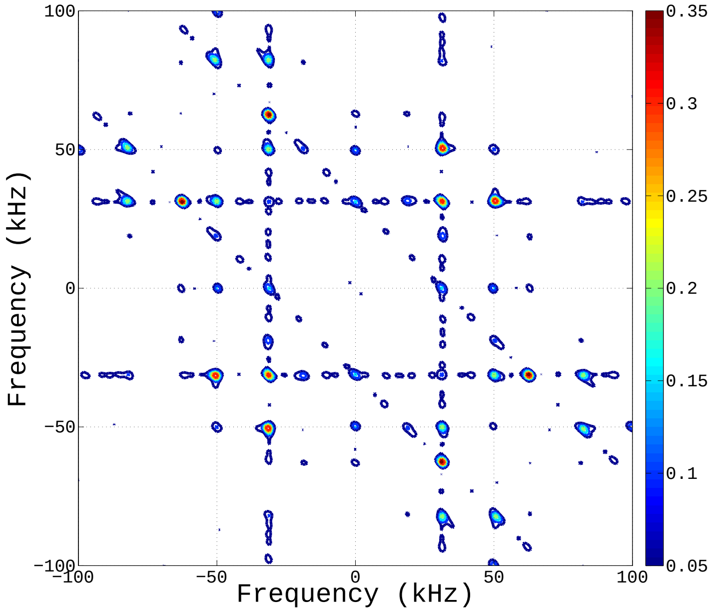

Figure 4.12: **Squared bicoherence of the signal shown in Fig. 4.10.**

Another signature of the non-linear interaction of two modes is the existence of finite bicoherence. Let us consider the interaction of three waves with frequencies ω_1, ω_2 and ω_3 which satisfy the frequency matching condition stated earlier, viz., $\omega_3 = \omega_1 + \omega_2$. If the Fourier transform of the time series signal $f(t)$ is $z(\omega)$, then the bi-spectrum B of these three waves is expressed as:

$$B =< z(\omega_1) z(\omega_2) z^*(\omega_3) >$$

If the three waves are not interacting amongst themselves, then the absolute value $|B|$ is zero; and when their phases are connected through a certain relationship, then $|B|$ assumes a finite value. Bi-coherence, b is the normalised value of B, and it is expressed mathematically as follows:

$$b^2 = \frac{|B|^2}{< |z(\omega_1)z(\omega_2)|^2 >< |z^*(\omega_3)|^2 >} \tag{4.1}$$

So, if we have finite value of b for the interaction of three waves, then we can conclude that one of three waves has been generated due to the nonlinear interaction of the other two waves.

We have shown the results of the bicoherence analysis in Fig. 4.12. In this figure, the normalised squared bicoherence has been plotted with the frequencies of the modes **A** and **B** being along the x and y axes. It can be seen that the squared bicoherence exhibits peaks at the frequency pairs $(31, 31)$ kHz and $(31, 52)$ kHz, confirming that the secondary modes at 62 and 83 kHz have indeed been generated due to the non-linear interaction of the primary modes.

4.6 Summary

In the present experiment, two self-excited modes with different frequencies (31 kHz and 52 kHz) and mode numbers ($m = 1$ and 2, respectively) have been detected simultaneously over a wide range of axial and radial distances. The modes propagate azimuthally in the direction of the electron diamagnetic drift. They have been observed to have maximum amplitudes near the locations where the radial density gradient is significantly high. The mode frequencies lie in the regime of the ion cyclotron frequency ($\omega < \omega_{ci}$) contrary to the conventional low frequency drift waves. Growth rates of the collisional drift waves are sensitive to finite ion inertia effects, with the growth rates turning negative for large values of the ion Larmor radius. For a helium plasma with the smaller values of the ion Larmor radius (compared to that of argon), the growth rates calculated from the dispersion relation (equation 3.22) yield positive values for both $m = 1$ and $m = 2$ modes with distinctly different frequencies in the region where the plasma density is significant. Such excitation of two simultaneous modes is not possible in argon plasma (with a larger ion Larmor radius) within the existing parameter range; only one mode has been observed.

The earlier results of upper drift modes in argon plasma (viz. $\omega > \omega_{ci}$) in the same device and the present results in the helium plasma (viz. $\omega \lesssim \omega_{ci}$) suggest that both belong to a different class of drift mode (termed as the upper drift mode to distinguish it from the conventional drift mode, $\omega << \omega_{ci}$) that are destabilized by collisional effects. This class of drift modes is obtained when no aprrroximation of the frequency regime is considered in the dispersion relation instead of the usual low frequency approximation $\omega << \omega_{ci}$.

Bibliography

[1] Abhijit Ghosh, S. K. Saha, S. Chowdhury, and M. S. Janaki, Phys. Plasmas 22, 122111 (2015).

[2] Abhijit Ghosh, S. K. Saha, S. Chowdhury, and M. S. Janaki, Phys. Plasmas 24, 012104 (2017).

[3] R. F. Ellis, E. Marden-Marshall, and R. Majeski, Plasma Phys. 22, 113 (1980); E. Marden-Marshall, R. F. Ellis, and J. E. Walsh, Plasma Phys. 28, 1461 (1986).

[4] A. Hasegawa and K. Mima, Phys. Rev. Lett. 39, 205 (1977).

[5] W. Horton and A. Hasegawa, Chaos 4, 227 (1994).

[6] P.H. Diamond, S-I Itoh, K. Itoh, and T.S. Hahm, Plasma Phys. Control. Fusion 47, R35 (2005).

[7] F. Brochard, T. Windisch, O. Grulke, and T. Klinger, Phys. Plasmas 13, 122305 (2006).

[8] N. Kasuya, M. Yagi, K. Itoh, and S-I Itoh, Phys. Plasmas 15, 052302 (2008).

[9] T. Yamada et al., Phys. Plasmas 17, 052313 (2010).

[10] Y. C. Kim and E. J. Powers, Phys. Fluids 21, 1452 (1978).

[11] Ch.P. Ritz et al., Rev. Sci. Instrum. 59, 1739 (1988).

Chapter 5

Summary and Conclusion

5.1 Summary

The DLX device has been developed at SINP to study the physics of DLs. The detail study of the DL in this device [1] has been reported elsewhere. The present thesis contains the detail study of the equillibrium plasma density, potential and temperature, with emphasis on the identification of the instability observed in DLX both in argon and helium plasmas. In the following, we summarize the works obtained from such studies.

- The frequency peaks observed in the density or floating potential fluctuations in DLX are $\sim \omega_{ci}$. In Chapter 1, therefore, a brief historical review of modes having $\omega \sim \omega_{ci}$ has been presented.

- Chapter 2 contains the description of the experimental device and various diagnostic tools that have been used in the studies of the equillibrium profiles and the instabilities. To minimize the effect of the RF fluctuations in the measurements of the plasma density and the electron temperature, a RF compensation circuit has been developed which gives high impedances and high-Q resonances at 13.56 MHz and its harmonics. The vacuum bellow and the guide rail system, controlled by the commands from a computer, has been used to facilitate the axial movements. The three-LP system with shaft lengths $r = 3.0, 5.9$ and 7.1 cm has been developed to measure the azimuthal propagation of the waves while the four-LP system has been used to measure the phase difference between the density and potential fluctuations. Both of these are characteristics of the resistive drift waves. To measure the axial propagations of the waves, two un-compensated LPs have been aligned electrically along the axial magnetic field line. The working principle of the hot EP which has been used to measure the plasma potential under the condition of the strong emission, has been described. The chapter has been concluded with a description of the workings of the RFEA which has been used to measure the IEDFs.

- Chapter 3 contains the experimental and theoretical results obtained from the detail study of the steady state properties of the plasma and the fluctuations with experiments performed in argon plasma. 2-D density and potential measurements have been carried out for the argon plasma diffusing through an aperture in a diverging magnetic field. The radial density profile near the source is peaked on the axis but gradually evolves into a hollow profile away from the source. We observe a slow increase of the peak density along a hollow conical surface. It is also shown that the formation of the 2-D structures with similar features are observed whenever a plasma is allowed to diffuse through a physical aperture in such diverging magnetic field configuration, with or without the presence of an electric double layer, i.e., the phenomenon is *generic* in nature.

In the same argon plasma, an electrostatic mode propagating azimuthally in the direction of the electron diamagnetic drift and frequency greater than the ion cyclotron frequency has been observed. The mode has a weak propagation along the axial direction. The mode has been detected at axial locations up to 16 cm away from the entrance aperture. For fixed values of the neutral pressure and the magnetic field, the mode frequency is found to be independent of the location at which it is measured. The amplitude of the fluctuations is maximum around the same radial location where the radial gradient in density is also maximum. By showing the relative contributions of the radial gradients of the density and the electron temperature to the pressure gradient, it has been suggested that the modes are driven by the density gradient. The modes exhibit drift wave characteristics revealing a radial structure with the azimuthal mode number $m = 1$ at the lower radial locations ($r \sim 3.0$ cm) while the $m = 2$ mode is located in the outer region. Theoretical modeling using a local dispersion relation based on the fluid equations, predicts destabilization of the modes by the electron-neutral collisions with frequency greater than the ion-cyclotron frequency.

- The important role played by the factor $k_\theta \rho_i$ for the upper drift modes has been highlighted by the theory for both kinetic and fluid models. So, the previous results in argon plasma warrant more investigations of the characteristics of such modes when the ion Larmor radius is further reduced. Hence, the same set of experiments have been repeated with helium plasma in DLX. The results have been discussed in Chapter 4. Self-excited dual upper drift modes have been observed in a magnetized helium plasma, having frequencies less than ω_{ci} but higher than that of the conventional low frequency ($\omega << \omega_{ci}$) drift waves. The modes propagate mainly in the azimuthal direction with mode numbers $m = 1$ and $m = 2$ with frequencies 31 kHz and 52 kHz, respectively and also have weak axial propagations. They coexist over a wide range of radial and axial locations and the direction of azimuthal propagation coincides with the electron diamagnetic drift for the peaked profile of the density. The same local dispersion relation obtained from the fluid description of the argon plasma predicts an instability simultaneously for both $m = 1$ and $m = 2$ modes (with different frequencies) over a range of radial locations. In a narrow radial region, $r \sim 3.2 - 4.3$ cm, where the amplitudes of these two modes are strongest, two other modes with frequencies 62 kHz and 83 kHz, respectively, have also been observed. The bi-spectral analysis confirm that these two secondary modes have been generated via the non-linear interaction of the primary modes, viz. 31 kHz and 52 kHz.

5.2 Future Scope

During the present investigation, few unanswered questions arose, which open up new possibilities for extensive works to be done in the future.

- As has been mentioned in Chapter 2, if there is an abrupt change in the diameter of the chamber containing a magnetized plasma, a DL is created at the junction between the two chambers or where the divergence of the magnetic field is maximum. It would be interesting to see whether the position of the DL changes in changing the position of the maximum divergence of the magnetic field. This can be done by controlling the magnetic field in the expansion chamber by placing Helmholtz coils around it.

- We have seen that the off-axis peaks in the 2-D structure of the plasma density are created due to the radial transport of the charged particles to the MDMFL. This transport is caused by the self-generated radial electric field. It would be interesting to see what happens to the density profile if we modify the the local radial electric field by inserting biased ring electrodes at the positions of the MDMFL.

- It has been shown [2] that the neutral gas density is depleted when the plasma pressure becomes comparable to the neutral gas pressure. Given the low neutral gas pressure in the present experiments, this effect may be significant, especially near the source and on the conical surface, where the plasma density is high. The consequent re-distribution of neutral gas may affect the plasma density profile and may need to be considered for a better understanding of the steady state profiles.

- As has been mentioned in Sec. 3.2.4, there is experimental evidence in DLX that high energy electrons (of energy up to $\sim$ 160 eV in the tail of the distribution) are present in the expansion chamber. It has also been argued there that these high energy electrons do not take part in ionizing collisions to raise the density. On the other hand, Fig. 3.8 suggests that the number of these energetic electrons decreases very rapidly with z, with a e-folding length of $\sim$ 5 cm, much less than the mean free path of ionizing collision. So, some non-classical phenomenon like instability may need to be invoked to explain this observation. Such an instability, associated with the dynamics of the electrons, would be a high-frequency mode appropriate for a proper investigation.

- It has been suggested in Sec. 3.4.3 that the mismatch between the theoretically predicted frequencies with the experimentally observed ones (Fig. 3.17) is due to the use of the local slab model, as has been shown by R.F. Ellis and co-workers [3] for the low frequency drift modes ($\omega << \omega_{ci}$). Also, we presented the non-linear interaction of the upper drift modes in Chapter 4. The existing theories for this type of non-linear interaction has been developed for the same low frequency drift modes. So, it would be interesting to see what happens if we do not assume the low frequency approximation in developing the non-local cyclindrical model for the upper drift modes or to the Hasegawa-Mima equation which describes the energy transfer occuring between the waves in a three-wave coupling.

Bibliography

[1] S.K. Saha, S. Raychaudhuri, S. Chowdhury, M.S. Janaki, and A.K. Hui, Phys. Plasmas 19, 092502 (2012).

[2] A. Aanesland, L. Liard, G. Leray, J. Jolly, and P. Chabert, Appl. Phys. Lett. 91, 121502 (2007).

[3] R. F. Ellis, E. Marden-Marshall, and R. Majeski, Plasma Phys. 22, 113 (1980).